1-1-2012

Axial Load Behaviour of Double Skin Composite Walls Subjected to Elevated Temperatures

Antonio Taormina
Ryerson University

Axial Load Behaviour of Double Skin Composite Walls Subjected to Elevated Temperatures

By

Antonio Taormina

Bachelor of Engineering in Civil Engineering,

Ryerson University, Toronto, Ontario, 2010

M.A.Sc. Thesis

Presented to Ryerson University

In Partial Fulfillment of the Requirements for the

Masters of Applied Science in the Program of Civil Engineering

Toronto, Ontario, Canada, 2012

AUTHOR'S DECLARATION

I hereby declare that I am the sole author of this dissertation.

I authorize Ryerson University to lend this dissertation to other institution or individuals for the purpose of scholarly research.

SIGNATURE

I further authorize Ryerson University to reproduce this dissertation by photocopying or by other means, in total or in part, at the request of other institutions or individuals for the purpose of scholarly research.

SIGNATURE

Axial Load Behaviour of Double Skin Composite Walls Subjected to Elevated Temperatures

Antonio Taormina, Masters of Applied Science, 2012

Department of Civil Engineering

Ryerson University

ABSTRACT

Double skin composite walls (DSCWs) consist of two skins of profiled steel sheeting and in-fill of concrete. DSCWs are proposed to act as axial and lateral load resisting elements in buildings. This research concentrates on the structural performance of DSCWs made of high performance concretes (HPCs) subjected to elevated temperatures of up to 800^{o}C maintained for steady state duration of two hours. Performance of DSCWs subjected to elevated temperatures is evaluated in terms of physical changes, residual axial load capacity/stiffness, axial load-deformation response, ductility, strain characteristics, steel-concrete interaction, and overall failure modes. Analytical models for the residual axial load capacity of DSCWs are developed based on experimental results. The recommendations of this research will be useful for the development of guidelines for the post-fire axial strength/ductility/stiffness of DSCWs and will aid in the development of fire protection measures.

ACKNOWLEDGMENTS

I would like to express my sincere gratitude to my supervisor Dr. Khandaker M. Anwar Hossain, without whom this research could not be accomplished. His persistent support, encouragement and valuable suggestions have guided me through all the steps from the beginning to completion of my graduate study. My knowledge on the specialized subject of the research study has enhanced significantly from his vast experience, and sophisticated understanding for which I am deeply indebted to him. His countless proof readings, corrections and support made this document possible.

I would like to thank Mr. Nidal Jaalouk, Mr. Min Yao, Mr. Mohammad Aldardari, Mr. Dan Peneff, Mr. Alan Machin, and all other lab staffs who assisted me in fabrication and performing physical tests in the Structures and Concrete Labs. Their assistance and brilliant ideas made it possible to carry out successfully the complex experimental tests.

Thanks are extended to the post-doctoral fellows of the Civil Engineering Department notably, Dr. Erdogan Ozbay, and Dr. Okan Karahan for their great help in casting concrete and test specimens.

I would like to acknowledge the financial support from the National Science and Engineering Research Council (NSERC) of Canada.

I am thankful to the Canam Group for providing the profiled steel sheets. In addition, I would like to thank Bekaert Corporation for providing the steel fibers and Grace Construction Products for providing concrete admixtures.

I also extend my special thanks to examining committee members: Dr. Medhat Shehata and Dr. Arnold Yuan.

Finally, I am deeply and forever indebted to my parents, Mr. Agostinio Taormina and Mrs. Anna Taormina for their love, encouragement and supports throughout my entire life.

TABLE OF CONTENTS

LIST OF SYMBOLS AND ABBREVIATIONS

A_c	area of the concrete core
A_s	area of the steel sheeting
A_{cp}	cross-section area of the concrete in one pitch of the concrete core wall
b	smallest flange thickness presented in the profiled steel sheeting
C_c	coefficient of gradation of the fine sand
C_u	uniformity coefficient of the fine sand
D	overall thickness of the concrete core wall
$E_{c20,}$ E_c	modulus of elasticity of the concrete at 20°C
E_{ct}	modulus of elasticity of the concrete at a given temperature due to fire degradation of concrete
$E_{s20,}$ E_s	modulus of elasticity of the steel sheeting at 20°C
E_{st}	modulus of elasticity of the steel sheeting at a given temperature due to fire degradation of steel sheeting
$f'_{c20,}$ f'_c	maximum compressive cylinder strength of concrete at 20°C
f'_{ct}	maximum compressive cylinder strength of concrete at a given temperature due to fire degradation of concrete
f'_{cst}	maximum compressive cylinder strength of concrete at a given temperature due to softening of concrete
f_{cu}	maximum compressive cube strength of concrete at 20°C
$f_{y20,}$ f_y	yield strength of the steel sheeting at 20°C
f_{yt}	yield strength of the steel sheeting at a given temperature due to fire degradation of steel
K_e	experimental initial stiffness of the double skin composite wall, steel sheeting wall, or concrete core wall

K_{e20}	experimental initial stiffness of the double skin composite wall, steel sheeting wall, or concrete core wall at 20°C
K_{et}	experimental initial stiffness of the double skin composite wall, steel sheeting wall, or concrete core wall at a given temperature
K'_{e}	experimental post-peak stiffness of the double skin composite wall, steel sheeting wall, or concrete core wall
K'_{e20}	experimental post-peak stiffness of the double skin composite wall, steel sheeting wall, or concrete core wall at 20°C
K'_{et}	experimental post-peak stiffness of the double skin composite wall, steel sheeting wall, or concrete core wall at a given temperature
N_w	axial load capacity of the double skin composite wall
N_{wm}	modified axial load capacity of the double skin composite wall
N_c	axial load capacity of the profiled concrete wall
N_e	experimental load capacity of the double skin composite wall, steel sheeting wall, or concrete core wall
N_{e20}	experimental axial load capacity of the double skin composite wall, steel sheeting wall, or concrete core wall at 20°C
N_{et}	experimental axial load capacity of the double skin composite wall, steel sheeting wall, or concrete core wall at a given temperature
N_s	axial load capacity of the steel sheeting wall
P	pitch of the profiles in the concrete core wall
T	thickness of the steel sheeting
t	temperature in Celsius
α	correction factor for voids present in profiled concrete wall or infill concrete
ß	correction factor for ratio between buckling stress to yield stress of steel
$ß_c$	fire degradation/reduction factor for maximum compressive strength of the concrete

$ß_{ce}$	fire degradation/reduction factor for modulus of elasticity of the concrete
$ß_{cs}$	softening/ reduction factor for maximum allowable compressive strength of the concrete due to fire degradation
$ß_{s}$	fire degradation/reduction factor for yield strength of steel sheeting
$ß_{se}$	fire degradation/reduction factor for modulus of elasticity of steel sheeting
$ß_{i}$	interaction reduction factor for the double skin composite walls exposed to elevated temperatures
$\Delta_{\text{peak load}}$	experimental axial deformation of the double skin composite wall, steel sheeting wall, or concrete core wall at peak load
$\Delta_{0.75\text{ peak load}}$	experimental axial deformation of the double skin composite wall, steel sheeting wall, or concrete core wall at 75% peak load after peak load has been reached
DSCW	double skin composite wall
ECC	engineered cementitious composite
HSC/HPC	high strength / high performance concrete
NSC	normal strength concrete
PCW	profiled concrete wall
SSW	steel sheeting wall
SCC	self-consolidating concrete
UHPC	ultra high performance concrete

LIST OF FIGURES

LIST OF TABLES

CHAPTER 1

Introduction

1.1 General

Profiled steel sheeting is widely used in composite construction and composite slabs known as "fast-track construction" (Wright et al. 1987). The use of composite slabs has grown rapidly since early 1980's, replacing traditional reinforced concrete flooring system. More recently, a novel form of composite walling system which comprises vertically aligned profiled steel sheeting and an infill of concrete as shown in Fig.1.1 was proposed (Wright et al. 1992; Wright et al. 1994; Wright and Gallocher 1995; Hossain and Wright 1995). Such composite walling system has many advantages and is thought to be applicable as axial and lateral load resisting elements in building. Such walls have also potential in basements and blast resisting structures.

The advantages of this system arise from many aspects. First, during construction, profiled steel sheeting acts as a formwork for in-fill concrete (Wright and Gallocher 1995). Second, the steel sheet acts as a bracing system to the building frame against wind and destabilizing forces in the construction stage (Hossain and Wright 1995). Third, in the service stage, profiled steel sheets act as reinforcement. Finally, the added confinement of the concrete by the steel sheeting will both increase the load resistance as well as the potential to increase fire durability compared to traditional reinforced concrete (RC) structures.

In such construction, the shear bond and interaction between sheeting and concrete plays an important role in the composite action of the system and will govern the type of failure of the wall. The interface shear bond failure may be limiting criteria for the design of such system (Hossain and Wright 2004a,b). The bond between steel and concrete can be improved by embossments installed in the commercial profiled steel sheets available in North America or by

installing other forms of connectors such as fasteners and other mechanical devices to connect pair of sheeting as shown in Fig. 1.1. The mechanical interlock at the sheet-concrete interface may govern the ductile and brittle failure of such composite walls.

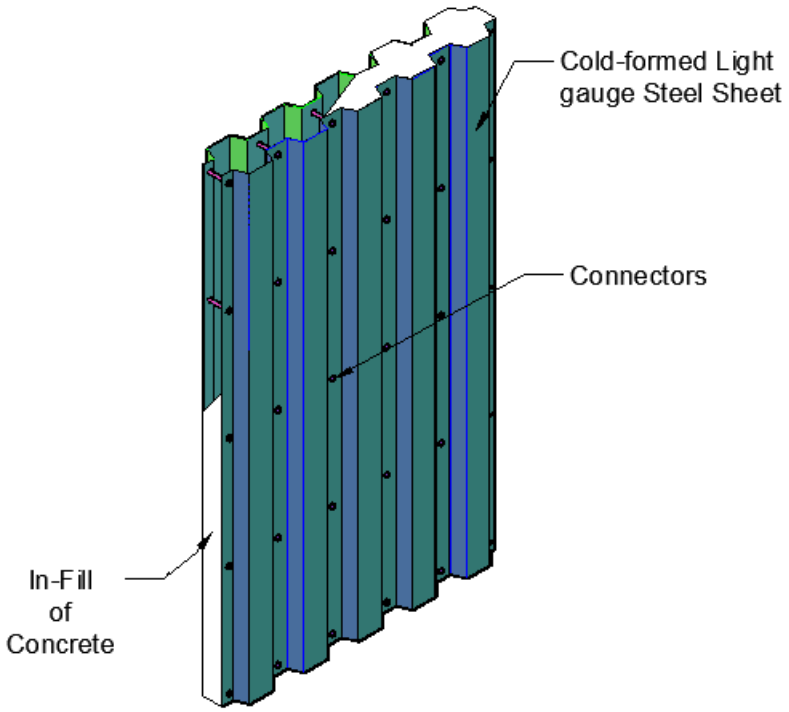

Figure 1.1- Double skin composite wall (DSCW)

The behaviour of the DSCWs under axial and in-plane shear loading was associated with the difficulty in the transfer of load between the steel sheeting and the in-fill concrete and the buckling of the steel sheeting (Bradford et al. 1998; Wright 1998a,b; Hossain 2000; Hossain and Wright 2004c). The problem of load transfer between steel and concrete can be overcome by providing additional shear connection devices at the head and foot of the wall in case of wall under axial load or by providing adequate connections between sheeting and concrete at the boundaries (Hossain and Wright 2004c). The general behaviour of the DSCWs subjected to compressive axial load and the model for the axial load capacity were presented by Wright et al. (1994), Wright (1998a,b), and Hossain (2000). Hossain (2000) also conducted research on pierced and non-pierced composite walls subjected to axial loading.

The behaviour of DSCWs subjected to in-plane shear loading was investigated and analytical models for the shear strength and stiffness were developed (Wright and Hossain 1997; Hossain and Wright 1998a; Hossain and Wright 2004 a-e). The behaviour of profiled steel sheeting and profiled concrete panels was also investigated by Wright and Hossain (1997) and Hossain and Wright (1998b), respectively. Further investigation on the behaviour of DSCWs under in-plane cyclic and impact loadings was conducted by Hossain et al. (2004a), Rafiei et al. (2009), and Rafiei (2011).

The sheet-concrete interface behavior in a composite wall is complex as profiled ribs play an important role in providing mechanical bond when steel tends to slide over the concrete after the failure of chemical bond. In this case, the transverse shear bond perpendicular to the profiles (derived mainly from friction) plays an important role and mobilization of such bond will provide high in-plane shear resistance of composite walls (Hossain and Wright 1998a).

Over the last few years new generation of high performance concrete (HPC) such as Self-Consolidating Concrete (SCC), Engineered Cementitious Composites (ECC), and Ultra High Performance Concrete (UHPC) with improved strength, durability, ductility and energy absorbing capacity has been developed. SCC is very flowable (Khayat 1999; Hossain and Lachemi 2010), achieves good consolidation, and can flow into place between two profiled steel sheets without vibration and without defects due to bleeding or segregation.

Self-consolidating ECC was reported to have superior workability, ductility and durability, which translates to speedy construction, reduced maintenance and a longer life span for the structure (Li and Kanda 1998; Wang et al. 2006; Şahmaran et al. 2009). Micromechanical design allows optimization of ECC for high performance, resulting in extreme tensile strain capacity while minimizing the amount of reinforcing fibres, typically less than 2% by volume. Unlike ordinary cement-based materials, ECC strain hardens after first cracking and demonstrates a strain capacity 300 to 500 times greater than normal concrete through the use of incorporating fibers. Even at large imposed deformation, crack widths of ECC remain small, less than 60 μm. UHPC is also flowable and a durable concrete which exhibits high compressive strength capacity (more than 100 MPa) compared to SCC, ECC, and normal strength concrete (Hossain et

al. 2012). It demonstrates increased energy absorption capacity and strain hardening behaviour through the addition of steel fibers which control crack propagation and width (Koksal et al. 2008).

The use of such HPC in DCSWs can significantly improve the structural performance. In addition, the knowledge of the behavior of DSCW systems incorporating new generation of HPC being exposed to elevated temperatures is an important aspect of the implementation of this system in a building.

1.2 Significance of the Research

Previous research has been conducted on DSCWs subjected to axial loading as well as in-plane monotonic, cyclic and impact loading. Experimental, analytical, and numerical investigations were conducted to develop design equations/guidelines for strength and stiffness of DSCWs under these loading conditions. However little or no research has been conducted on the behavior of DSCWs incorporating HPCs as well as on the effect of elevated temperatures on the strength, stiffness and ductility of these walls. There are also no guidelines currently available for the post-fire behaviour and performance of DSCWs made with HPC. Current research has focused on these aspects and the research outcomes will contribute significantly to the understanding of the behaviour of DSCWs and will aid in the evaluation of the structural performance after exposure to elevated temperatures as well as in the development of fire protection measures for the walling system (Taormina and Hossain 2012).

1.3 Scope of the Research

The primary focus of this research was to study the behaviour and performance of DSCWs (made of HPCs) and components subjected to elevated temperatures. In addition, the research was also focused on the evaluation of the post-fire material properties of the steel sheeting and the in-fill HPCs.

1.4 Objectives of the Research

The main objectives of this research were to:

- Perform experimental tests on cold formed light-gauge steel sheeting under tensile axial load after being subjected to elevated temperatures of up to 800^{o}C and gain comprehensive information on post-fire residual yield strength and modulus of elasticity.
- Perform experimental investigation on SCC/ECC/UHPC, under compressive axial load after being exposed to elevated temperatures of up to 800^{o}C and gain comprehensive information on post-fire residual compressive strength and modulus of elasticity.
- Perform experimental investigation on DSCWs and its components, profiled concrete walls (PCWs) and steel sheeting walls (SSWs) under compressive axial load after being exposed to elevated temperatures of up to 800^{o}C and gain comprehensive information on post-fire axial load capacity, axial load - deformation response, stiffness/ductility, load-strain behavior, steel sheet-concrete interaction, and modes of failure. Twelve tests were conducted on the scaled-down DSCWs at four different temperatures for each concrete types- SCC/ECC/UHPC. Nine tests were conducted on PCWs at three temperatures for each concrete type. In addition, four tests were conducted on SSWs at four temperatures.
- Carry out analytical and design oriented analyses to develop:
    - Empirical models for determining the post-fire residual yield strength/modulus of elasticity of cold formed light-gauge steel sheeting as well as residual compressive strength of SCC/ECC/UHPC as a function of temperature.
    - Analytical models for post-fire residual axial strength of DSCWs and its components at elevated temperatures.
    - Validate and analyze the performance of analytical models based on experimental results and make guideline recommendations.

1.5 Outline of the Thesis

This thesis consists of seven chapters which are outlined as follows:

Chapter 1 presents brief introduction about the novel form of the double skin composite wall, research significance and objective of the study.

Chapter 2 presents a comprehensive literature review on double skin composite walls, the three different types of HPCs (SCC/ECC/UHPC), cold formed light-gauge steel sheeting and concrete filled steel tubular columns at ambient/elevated temperatures.

Chapter 3 presents the experimental test results and analysis on cold formed light-gauge steel sheeting coupon samples and concrete cylinders for each HPC types after exposure to elevated temperatures. This chapter also presents developed empirical models for post-fire strength and modulus of elasticity of steel and HPCs subjected to elevated temperatures.

Chapter 4 presents the experimental test results and analysis on all specimens for two types of walls, steel sheeting wall and profiled concrete wall, under compressive axial loading after exposure to elevated temperatures. The post-fire axial load behavior is described and compared based on strength, stiffness, ductility, stress-strain characteristics and failure modes.

Chapter 5 presents the experimental test results, discussion and analysis of for double skin composite walls under compressive axial loading after exposure to elevated temperatures. The post-fire axial load behavior is described and compared based on strength, stiffness, ductility, stress-strain characteristics and failure modes.

Chapter 6 presents analytical models for the residual post-fire axial load capacity of DSCW and its components, PCWs and SSWs after exposure to elevated temperatures. The fire degradation factors for materials (steel and concrete) and sheet-concrete interaction degradation factors incorporated in the analytical models are described. The performance of analytical models described based experimental results

Chapter 7 presents the main conclusions of the study along with recommendations for future research on DSCWs.

CHAPTER 2

Literature Review

2.1 Introduction

Traditionally reinforced concrete walls are used in reinforced concrete building structures for many years to resist gravity loads. The proposed novel form of double skin composite walls (DSCW) consists of two vertically aligned profiled steel sheeting with an in-fill of concrete. In this chapter, a review of the development and recent investigations on this innovative DSCW system; the three different types of high performance concretes (HPCs): Self-Consolidating Concrete (SCC), Engineered Cementitious Composites (ECC), and Ultra High Performance Concrete (UHPC), and other composite elements subjected to both ambient and elevated temperatures is presented.

2.2 Double Skin Composite Wall (DSCW)

The DSCW has additional stiffness provided by the in-fill concrete to prevent buckling of the steel sheeting and the confinement of the steel sheeting to increase concrete carrying capacity of the wall even after the concrete has cracked (Wright et al. 1994; Wright and Gallocher 1995; Wright and Hossain 1997; Wright 1998a,b; Hossain 1998b; Hossain 2000; Hossain and Wright 2004a-e; Rafiei et al. 2009; Rafiei 2011). The advantages of this walling system arise from the type of construction where profiled steel sheeting acts as a formwork for in-fill concrete in the construction stage. However, due to the lateral pressure from the wet concrete, which is higher in the wall than in composite flooring, temporary lateral supports as shown in Fig. 2.1 may be needed to restrain the pressure (Wright and Gallocher 1995). In the service stage, after the concrete has hardened, loading will be resisted by both the steel sheeting and concrete core, where the profiled steel sheets also act as reinforcement. The composite wall can resist axial

loading, axial-bending forces due to eccentric loads, and in-plane shear loads caused by either wind or earthquake (Wright and Gallocher 1995; Hossain et al. 2005). The strength and stiffness of the wall will be dependent upon the material properties of the steel and concrete, the geometry of the profiling, and the bond at the steel/concrete interface (Wright and Gallocher 1995; Hossain et al. 2005).

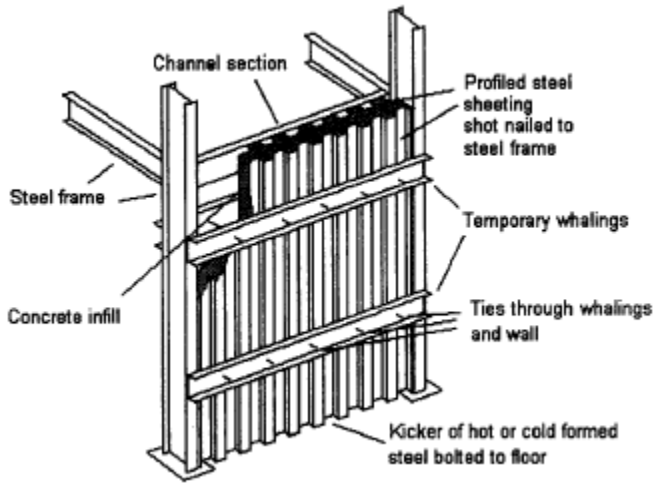

Figure 2.1- Double skin composite walls during construction stage (Wright and Gallocher 1995; Wright 1998a)

2.2.1 Axial Load Behaviour of DSCWs

Research has been conducted on the axial load behaviour of DSCWs (Wright and Gallocher 1995; Wright 1998a,b; Hossain 2000). Axial load behaviour of composite wall is described based on the maximum load capacity or strength, the load-axial deformation response, the load-strain behavior, the steel sheet-concrete interaction, and failure modes.

Previous researches on the axial load behaviour of DSCWs (Wright and Gallocher 1995; Hossain and Wright 1998a) have shown that there was little mobilization of the ductile bond strength between steel and concrete surfaces produced by the embossments. Commercial profiled steel deck embossments are of insufficient size to produce a large ductile transfer of load. The transfer of load under axial compression from the concrete core to the steel decking should be rapid, to prevent concrete crushing at the loading point of the wall, which is not required in composite

slabs as the maximum force in the steel sheeting produced through bending occurs near the centre and may be spaced over less highly-stressed regions closer to the supports. As a result, the embossments provided on steel decking profiles tend to be small and unsuitable for composite walling. Therefore it was shown that axial load capacity of the wall is influenced by the bond between the steel and concrete, especially in the area close to the point of application of load.

In case of DSCWs, it has been observed that the steel sheeting is likely to debond from the concrete (Wright 1998a,b). In order to prevent sheet-concrete separation and optimize sheet-concrete interaction, wire mesh fabric was welded to the steel sheeting at the top and bottom of the wall specimens in order to improve the load transfer from the concrete to the steel. The debonding of the steel sheets from the concrete was clearly a major factor in the axial load carrying capacity of such walling system. In later tests, special connection devices at the top and bottom of the wall were also installed in the form of steel hooks, as shown in Fig.2.2, to ensure steel-concrete composite action (Wright 1998a,b). In addition, intermediate fasteners or bolts can be placed throughout the wall to increase the interaction between steel sheeting and in-fill concrete through decreasing the buckling effective length of the steel sheeting and thus preventing global steel sheet buckling (Hossain 2000). This will ensure that the profiled steel sheet reaches its yield stress under compressive axial loading before failure. The concrete core provides bracing to the profiled steel sheet and acts as a stiffener and prevents buckling (increases buckling capacity of steel sheet) of the sheet prior to its yielding capacity.

Based on the tests results from previous research studies on the pierced and non-pierced DSCW system under axial loading, the following findings can be summarized on overall behavior and failure modes (Wright and Gallocher 1995; Wright 1998a,b; Hossain 2000):

1. Steel-concrete interface bond failure produced interface slip and an accompanying drop in steel strain before failure.
2. Failure occurred due to concrete crushing at the top of the wall.

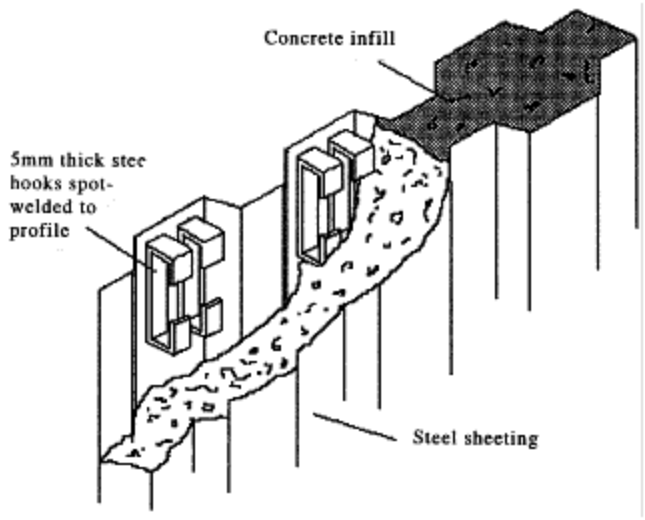

Figure 2.2- Detail of load transfer device (Wright 1998a)

3. Local buckling of the profiled steel sheeting was observed at the top.
4. Cracking of the concrete occurred along the troughs of the walls. In pierced walls localized cracking occurred at the corner of the opening due to increased stress concentration (Hossain 2000).
5. Tearing and peeling of the steel sheeting at the location of the spacers.
6. For pierced walls, the unsupported weak concrete at the top of the hole was crushed and the overall load-carrying capacity was reduced compared with non-pierced walls. The use of strengthening system around the perforation was necessary to ensure uniform transfer of loads and increase axial load capacity (Hossain 2000).

The maximum load capacity of the wall (N_w) can be then calculated based on the contributions from steel sheeting and the concrete in-fill as per Eq.2.1. This equation is based on the assumption that the interaction between the steel sheet-concrete in-fill will ensure full composite action (Wright and Gallocher 1995, Hossain 2000).

$$N_w = 0.67 f_{cu} A_c + A_s f_y \qquad \text{[Eq. 2.1]}$$

where N_w is the maximum load capacity of the profiled DSCW, f_y is the yield strength of the steel sheeting, f_{cu} is the maximum compressive cube strength of the different concrete, and A_s, A_c are the cross-sectional area of the wall steel sheeting and concrete core, respectively.

The axial capacity (N_w) is reduced by 10% to account for eccentric loading and imperfections in the walls as shown in Eq. 2.2 (Wright 1998b, Hossain 2000):

$$N_w = 0.6 f_{cu} A_c + 0.87 A_s f_y \qquad \text{[Eq. 2.2]}$$

If the bond between steel and concrete is less than complete (partial steel-concrete interaction), a reduction factor representing the loss of bond must be introduced into the Eq.2.1. If the load can be applied in the correct proportions to both steel and concrete, connection between the two is not critical and the full axial load capacity should be achievable (Wright and Gallocher 1995). Compression buckling of the steel sheeting is another possible constraint on axial load resistance for such walls. Unlike conventional reinforced concrete structures, where the longitudinal bars are constrained by the surrounding until crushing of the surrounding concrete matrix occurs, local buckling of the steel sheeting can occur and will considerably reduce the axial load capacity of walls (Wright and Gallocher, Hossain 2000).

After experimentation conducted by Wright and Gallocher (1995) and Hossain (2000), it was concluded that the ultimate axial load resistance of the walls was considerably less than the calculated fully-composite failure load. The two main factors affecting the performance of the walls are the steel-concrete interface bond strength and the local buckling capacity of the external steel sheeting.

During experimentation, it was observed that the local crushing had occurred at the extreme edges of the walls. It is important to consider this action in the case of the DSCW. The extreme edges of the wall do not present a solid mass of concrete. As a result, extra bending stresses must be carried on only that concrete in the ribs of the profile. Consequently, a profiled wall of the same overall width as a solid wall will be less able to carry bending moments caused by

eccentric load application and imperfections in the wall. An empirical correction to the assumed concrete capacity was derived (Wright 1998a, Hossain 2000).

The reduction in axial load capacity was assumed to be directly proportional to the extent of void created by the profiling on the compressed edge of the wall. A reduction factor α, must be applied to the strength of the concrete in the wall, which can be calculated by using Eq. 2.3 (Wright 1998a; Hossain 2000):

$$\alpha = 1 - ((D * p) - A_{cp})/2A_{cp} \qquad \text{[Eq. 2.3]}$$

where D is the overall thickness of the wall, P is the pitch of the profiles in the wall and A_{cp} is the cross-section area of the concrete in one pitch of the wall (Fig.2.3). This reduction factor α is also applicable to eccentric loading cases and loading with bending moments (Wright 1998b, Hossain 2000).

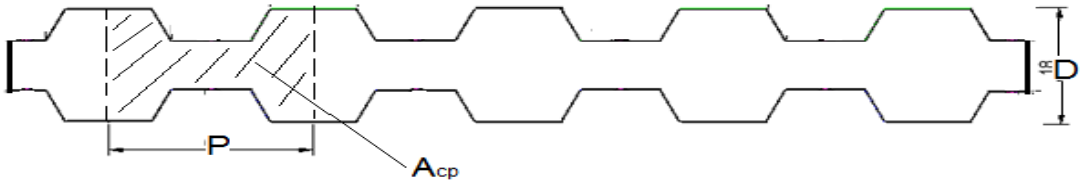

Figure 2.3- Geometric dimensions of the cross-section of the in-fill concrete core in the DSCW

A reduction factor ß, the ratio of sheet buckling stress to yield stress, which may be applied to the strength of the steel sheeting in the wall can be calculated by using Eq.2.4 to take into account the buckling of the steel sheeting in contact with the concrete (Hossain 2000):

$$\beta = 3.9846(10)^{-0.01(b/T)} \qquad \text{[Eq. 2.4]}$$

where b is the length of end plate of the steel sheeting and T is the thickness of the steel sheeting, as shown in Figure 2.4.

This reduction factor ß is also applicable to eccentric loading cases and loading with bending moments (Wright 1998b, Hossain 2000). The reduction factor ß may also be calculated using Eq.2.4 which was derived for steel sheeting having a yield stress of 350 MPa. For steel sheeting with yield stress of f_y (MPa), the value of ß from Equation 2.3 should be multiplied by the factor, $f_y/350$ (Hossain 2000).

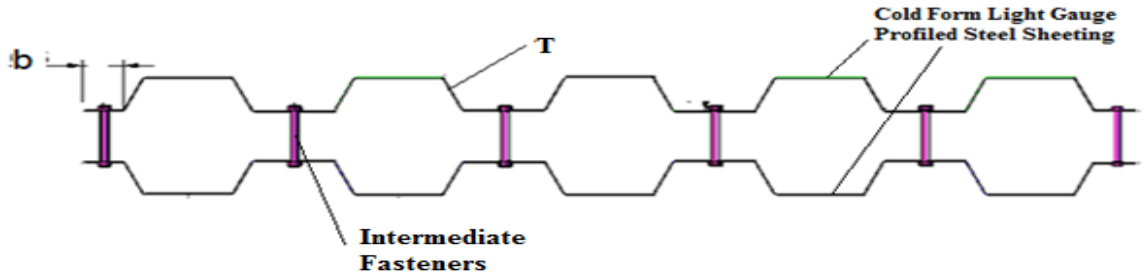

Figure 2.4- Geometric dimensions of the cross-section of the steel sheeting in the DSCW

The model for the maximum load capacity of the DSCWs, as shown in Eq. 2.3, was modified to include the factors α and ß, as shown in Eq.2.5. This model was further modified in order to take in to account concrete cylinder compressive strength (f'_c) instead of cube compressive strength (f_{cu}), as shown in Eq.2.6 (Hossain 2000).

$$N_w = 0.4 f_{cu} A_c \alpha + 0.75 A_s f_y \beta \quad \text{[Eq. 2.5]}$$

$$N_w = 0.63 f_c' A_c \alpha + 0.75 A_s f_y \beta \quad \text{[Eq. 2.6]}$$

where f'_c is the cylinder compressive strength of the concrete, α is a reduction factor to take into account the extent of void created by the profiling on the compressed edge of the wall (Eq.2.3) and ß is the ratio between the buckling stress and yield stress of the wall (Eq.2.4).

The effect of holes/perforations (location, geometry, size) as well as strength enhancement around perforations in DSCW were studied and necessary modifications to Eq.2.6 is suggested for axial load capacity (Hossain 2000) The presence of holes in the walls was found to reduce the axial capacity in the range of 10 to 24% depending on the location and dimensions (Hossain 2000).

2.2.2 Behaviour of DSCW under In-plane Monotonic, Cyclic and Impact Shear Loading

Research has been conducted on of DSCWs under in-plane monotonic, cyclic, and impact shear loading (Wright et al. 1997; Hossain and Wright 2004a-e; Rafiei et al. 2009; Rafiei 2011). The behaviour was described based on the maximum shear load capacity or strength, shear stiffness, the load-deflection response, the load-strain behavior, the steel sheet-concrete interaction, energy absorbing capacity, residual strength and the failure modes.

The general model for the shear strength and shear stiffness of profiled steel sheet panel wall was presented and was validated by experimentation and finite element analysis (Hossain and Wright 2004b-e). The stiffness and strength of the profiled sheeting was found to be dependent on the manner of attachment of the sheeting to the boundary frame. It was observed that the strength and stiffness of the spot welded panel is reduced to half and one third, respectively of the clamped panel. Analytical models for stiffness and strength of the profiled sheeting with different boundary conditions were developed. The failure of the sheeting is associated with the formation of local buckling and extended tension fields with subsequent bending and twisting of the profile which leads to the loss of profile geometry. Unstable and very rapid post-buckling behaviour was observed and therefore the generalized buckling formula for strength should not include any post-buckling shear loads. Profiled steel sheeting exhibited much better structural performance under shear than its equivalent plain steel sheet panels.

The in-plane shear strength and shear stiffness of the profiled concrete core walls was investigated by Hossain and Wright (1998b) through experimentation and finite element analysis. It was observed that the strain behaviour of the profiled concrete walls was different in comparison to plain concrete walls due to its profiled geometry. The development of diagonal tension and compression was observed and was confirmed by both experimental and numerical investigations. Analytical models for stiffness and strength of the profiled concrete shear walls were developed. The failure of the profiled concrete shear wall is associated with the formation of cracking along the diagonal of the wall.

Extensive experimental investigations couple with numerical (finite element) and design oriented analyses were conducted by Hossain and Wright (2004 b,c,e) to study the load-deformation response, strength, stiffness, strain condition, sheet-concrete interaction and failure modes of the DSCW system under in-plane shear. Diagonal tension failure was observed in the walls, which was confirmed by the strain conditions and cracking patterns in concrete core. Debonding of steel sheeting from the concrete, propagation of cracking in the concrete, and buckling of profiled steel sheeting, with development and extension of tension fields supported the strain conditions. If boundary connections between sheeting and concrete are adequate, the DSCWs can provide high shear resistance. DSCWs were found to provide shear strength and shear stiffness higher than the summation of the individual contributions from the pair of sheeting and concrete core. Analytical models for shear strength and stiffness were derived. The performance of design equations was validated through experimental results. Design guidelines are developed for the double skin composite framed shear wall system for tall building (Hossain and Wright 2004b).

Experimental and numerical investigations were also conducted by Rafiei et al. (2009) and Rafiei (2011) on DSCWs subjected to in-plane monotonic and cyclic shear loading with high performance concrete materials such as ECC and SCC. It was observed that ECC exhibited more ductile behaviour than SCC, with better crack development characteristics. The DSCWs composed of ECC when subjected to cyclic loading had its stiffness reduced by 47.8% which was lower than SCC. The displacement ductility of the ECC wall was also the higher than the SCC wall by 13%. In general, the ultimate cyclic shear load capacity of wall specimens was not less than 12% of their monotonic load capacity, which indicated the superior strength retaining capacity of the DSCWs under cyclic shear and demonstrated their potential to be used as shear resisting elements in buildings. In general, the failure of composite walls was due to yielding of steel sheet associated with post-yield buckling. Sufficient steel-concrete composite action was provided by the intermediate fasteners along the height and width, which prevented early elastic buckling of the profiled steel sheets and initiated failure due to steel yielding. Finite element models were developed to model DSCW behaviour and found to be reasonably simulate the strength, stiffness, stress development, failure modes and sheet-concrete interaction.

Rafiei et al. (2009) and Rafiei (2011) developed analytical models for the shear resistance of the profiled steel sheet, profiled concrete core and composite wall based on existing theoretical models. For the steel sheet, the model was developed based on the assumption of failure due to shear yielding of steel before buckling as a result of increased steel buckling capacity due to steel-concrete interaction, the presence of sheet-concrete interface connections and composite confinement. The shear resistance of the profiled concrete core was derived based on the simplified modified compression field theory (MCFT). The analytical model for the shear resistance of the composite wall was derived based on the combined strength of profiled concrete core and double skins of profiled steel sheets. The difference between the experimental and analytical shear resistance was found to be less than 10%. The proposed analytical was suggested to be used for the prediction of shear resistance of composite walls with reasonable accuracy.

Rafiei (2011) studied the behaviour of DSCWs subjected to in-plane impact shear loading condition. The post impact shear strength of the composite wall did not reduce (compared to control wall tested under static monotonic loading without impact) after the application of about 3100 J impact energy which was more than six times of impact energy capacity of the wall at elastic range. This can be associated with the localized nature of the concrete damage in the proximity of the impact load as observed during the test. Such localized concrete damage was not able to degrade the overall integrity of the steel-concrete composite system in resisting monotonic loading besides the degradation of wall stiffness. Stiffness degradation of the wall after impact was around 8% compared to the equivalent wall specimen tested purely under monotonic loading without impact. This was an indication of better strength retaining capacity of the wall at impact and its suitability as impact resisting element in a building frame.

Rafiei (2011) also developed finite element models to simulate DSCW behavior under in-plane impact loading. The developed finite element model was capable of simulating the behaviour of the composite shear wall under impact loading reasonably well. The maximum horizontal displacement of the wall at impact was about 20% higher than the experimental value, showing a good agreement considering the high complexity of the problem. The fundamental period of the

wall obtained from the FE model which was 10% higher than the experimental value. It was found that the finite element results for acceleration were very sensitive to the location of the accelerometers and the difference between FE and experimental results was more in concrete (55%) compared to steel (25%).

2.3 Properties of the In-fill Concrete

The in-fill concrete core plays an important role in load carrying capacity of DSCWs. Research (experimental and theoretical) has been conducted on the behaviour concrete core in composite wall under both axial and in-plane loading conditions (Hossain and Wright 1998b). Both normal weight and lightweight concrete have been used in composite walls and their performance has been investigated as concrete wall alone and as core in composite wall (Hossain and Wright 2004c). The pressure of fresh concrete on profiled steel sheet acting as formwork was also investigated (Wright and Gallocher 1995). The proposed use of high performance concretes (HPCs) such as self-consolidating concrete (SCC), engineered cementitious composite (ECC) and ultra-high strength/performance concrete (UHSC/UHPC) will significantly improve the process of casting through self-consolidation as well as improve the strength, ductility and durability of DSCW systems.

2.3.1 Self-Consolidating Concrete (SCC)

Self-Consolidating Concrete (SCC) is a highly flowable concrete that can flow into place under its own weight. SCC achieves good consolidation without external or internal vibration and also without defects due to bleeding or segregation (Ozawa et al. 1989; Li 1995; Yurugi 1998; Petersson 1998; Khayat et al. 2001; Lachemi et al. 2003; Poon and Ho 2004b; Khatib 2008). SCC typically has a higher content of fine particles and improved flow properties compared to the conventional concrete. SCC can be used to improve the productivity of casting congested sections and also to insure the proper filling of restricted areas with minimum or no consolidation (Khayat 1999). SCC showed greater homogeneity of distribution of in-place compressive strength than conventionally vibration-compacted concrete. SCC can improve the

working environment by eliminating the noise and pollution caused by vibrators and also reduces labour cost. SCC was developed in Japan in the early 1980's (Hayakawa et al. 1993; Hossain and Lachemi 2010).

High-strength SCC usually has a low water/cementitious material ratio which requires high binder content, but results in the addition of high range water reducers or superplastizer (Behnood and Ziari 2008). But it is important to do mix proportioning in a manner that prevents segregation of the concrete. Previous investigation by Yahia et al. (1999) has shown that the amount of superplastizer can be reduced by the addition of fly ash and blast furnace slag to have the similar slump flow compared to concrete made with Portland cement only.

Several different approaches can be used to develop SCC. One approach is to replace the coarse aggregates by sand at a ratio of 5% to 4%, which in turn requires a high volume of cement (Lachemi et al. 2003). Another method is to design SCC by incorporating viscosity modifying admixture (VMA) to improve the stability. Commercial VMA currently available in the market is costly and may increase the price of such a concrete (Lachemi et al. 2003). VMAs are water soluble polymers which enhance the ability of cement paste to retain its constituents in suspension and also increase the viscosity of the mixture. Using VMA with super-plasticizers can ensure adequate workability without segregation. The last technique is to increase significantly the amount of fine materials such as fly ash, volcanic ash and slag cement without changing the water content compared to common concrete. This method is the least expensive of the three mentioned above and these supplementary cementing materials help create highly flowable cohesive mixtures at a lower cost with high durability (Lachemi et al. 2003; Hossain and Lachemi 2010).

2.3.2 Engineered Cementitious Composite (ECC)

Engineered Cementitious Composite (ECC) is a class of ultra-ductile fiber reinforced composites originally invented at the University of Michigan in the early 1990s (Li 1993). ECC is characterized by high ductility under uniaxial tensile loading in the range of 3–7%. It has a tight

crack width of around 60-100 μm, which improves durability (Wang and Li 2007; Sahmaran and Li 2010; Sahmaran et al. 2011). The sequential development of multiple cracks, instead of continuous increase of crack opening contributes to larger tensile strength capacity in the range of 3 to 5% (Wang and Li 2007). When cracking begins in ECC, it undergoes strain-hardening and has a 300–500 times higher strain capacity than normal concrete. Cracks in ECC do not widen any further after the initial cracks are formed, which allow for additional tensile deformation to occur through the propagation of micro cracks, with spacing about 1–2 mm (Sahmaran et al. 2011). Under compressive loads, ECC exhibits compressive strength of 60MPa, similar to high strength concretes. Under compressive loading, ECC reaches its compressive strength at higher strain due to the exclusion of aggregates and as a consequence has a lower modulus of elasticity than conventional concrete (Fischer and Li 2003). It has relatively low fiber content of 2% or less by volume (Li 1998; Li et al. 2001; Li 2003; Sahmaran and Li 2010; Sahmaran et al. 2011).

The addition of fibers in ECC increases tensile strength, ductility and toughness and improves durability. The efficiency of the fiber reinforcement is affected by the properties of the concrete mix, as well as the fiber geometry, size, type, volume and dispersion. The typical fibres used in ECC are polypropylene (PP), glass (GF), carbon (CF) and polyvinyl alcoholic (PVA) (Cavdar 2012). The most common fiber used in ECC is the polyvinyl alcohol (PVA) fiber with a diameter of 39 μm and a length of 6–12 mm (Li et al. 2001; Kunieda and Rokugo 2006).

ECC contains higher cement content, when compared with conventional concrete. This high cement content is used to promote better fiber dispersion, rheology control or workability, and most importantly to promote strain hardening behavior. The exclusion of aggregates in ECC explains the increased cement content. In order to reduce the amount of cement used in ECC, supplementary cementing materials such as fly ash or blast furnace slag can be incorporated into the mix design. In order to have adequate workability, while maintaining a water-to-cementitious material ratio of around 0.25 to 0.3, a high range water reducer or superplastizer must be employed (Wang and Li 2007). In general the aggregates in ECC are either silica sand (usually

with an average particle size of a 100-200 micrometres), crushed sand or gravel sand of nominal sizes of around one or two millimetres.

It was observed that ECC with silica sand yielded slightly higher compressive strength than those with gravel sand and crushed sand, with crushed sand having higher compressive strength than gravel sand (Sahmaran and Li 2009). Large aggregates are not used in ECC because the large aggregates would hinder micro-scale interactions between fiber and the concrete matrix. These interactions are important for promoting the strain-hardening behavior of ECC. Eliminating large aggregates also promotes low matrix fracture toughness (Lepech et al. 2008).

In order to have tight micro crack width and high tensile ductility while keeping the fiber content low (2% or less by volume), ECC has been optimized through the use of micromechanics (Li 1993, Sahmaran and Li 2009). Micromechanics is a branch of mechanics applied at the material constituent level that captures the mechanical interactions among the fiber, mortar matrix, and fiber matrix interface. Usually, fibers are of the order of millimeters in length and tens of microns in diameter, and they may have a surface coating on the nanometer scale (Nawy 2008).

2.3.3 High Performance/ High Strength Concrete (HPC/HSC)

High performance / high strength concrete (HPC/HSC) is highly durable and has compressive strength greater than 80 MPa. Recently, comprehensive research has been conducted to develop ultra high performance concrete (UHPC) having a compressive strength of over 130 MPa. Fresh, mechanical and durability properties including bond strength of developed UHPC have been investigated (Ametrano 2010, Mak 2011).

In order to have high strength, HPC/HSC usually has low water-to-cementitious material ratio, which is accompanied with higher cement content compared with conventional concrete (Behnood and Ziari 2008). In order to have adequate workability, while maintaining a water-to-cementitious material ratio of around 0.25 to 0.35, a high range water reducer or superplastizer must be employed, usually in large dosages. This is done to achieve deflocculation of cement

particles to allow the mix to be sufficiently flowable and for the solids to be dispersed in a way that dense packing of the solids can occur (Behnood and Ziari 2008; Neville, 2010). This high cement content is used to promote better fiber dispersion and workability, and most importantly to promote strain hardening behavior. In order to decrease pores, aggregates used in UHPC can be very fine, such as silica sand (average size 100 to 200 micrometers), crushed sand, or gravel sand of nominal sizes of around one or two millimeters. In order to reduce the amount of cement in HPC/HSC, supplementary cementing materials such as silica fume is incorporated into the mix design.

Silica fume is produced as a by-product from electric arc furnaces from the manufacturing of ferro-silicon alloys and silicon metal. It is used today to improve the mechanical properties and durability of HPC/HSC (Behnood and Ziari 2008). It serves as excellent filler between cement and the aggregates and improves the cement paste-aggregate interface in concrete, which is the weakest zone in a concrete matrix (Koksal et al. 2008). Silica fume increases the water demand of concrete because it acts as an addition to concrete mix and not just as a supplementary cementing material. Silica fume is generally used in tandem with superplasticizer to control the workability. It is used to produce high strength concrete, but as a side effect it causes the ductility of the concrete to decrease and become more brittle (Koksal et al. 2008). The pozzolanic reactions found in silica fume form very dense microstructures in concretes. The high pozzolanic activity found in silica fume is a result of the very high content of amorphous silicon dioxide and very fine spherical particles (Behnood and Ziari 2008).

Tests conducted by Poon et al. (2004a), Behnood and Ziari (2008), and Koksal et al. (2008) have shown that the addition of silica fume as a replacement for a certain portion of cement in concretes such as HPC/HSC has increased the initial compressive strength in comparison to concretes using only cement. Analysis of stress-strain curves from previous tests have shown that the addition of silica fume resulted in higher strains at the peak stresses, with steeper descending branch in stress-strain curves.

Fibers are used in concrete to increase energy absorption capacity of concrete and increase ductility of the concrete. Steel fibers limit crack propagation and delay crack formation by behaving as crack arresters or bridging mechanism in the concrete. This is best observed after the cracking begins in the concrete (Koksal et al. 2008). Analysis of stress-strain curves from previous tests conducted by Poon et al. (2004a) has shown that the addition of steel fibres significantly changed the stress-strain curves by flattening the descending paths. The steel fibres also increased the strain at the peak stresses in concretes with normal cement, but did not do so in concretes containing silica fume.

Experimentation conducted by Koksal et al. (2008) has shown that the compressive strength of concrete increased with the addition of silica fume due to increased bond strength of cement paste-aggregate interface. The modulus of elasticity of concrete increased with the addition of silica fume, but decreased with the addition of steel fibers to concretes containing silica fume.

2.4 Fire Resistance of In-fill Concrete

Concrete exposed to high temperatures is non combustible and continues to perform satisfactorily without the release of toxic fumes. The characteristics of good performance for concrete exposed to high temperatures and used as a protective material for steel are: load-carrying capacity, resistance to flame penetration, and resistance to heat transfer. In practice, concrete should maintain structural integrity over the desired length of time when exposed to high temperatures such as two-hours, which is known in the industry as a fire rating. This is not to be confused with fire resistance (Neville, 2010).

Moisture content is a factor when it comes to concrete exposed to high temperatures. Excessive moisture in concrete can lead to spalling when exposed to high temperatures (Chan et al. 1999a; Neville 2000; Hossain 2006). Moisture content is affected by the water to cementitious material ratio (w/c). The higher the w/c, the higher the moisture content and permeability of the concrete will be, which is known to have a negative effect on the behavior of concrete at high temperatures (Khoury et al. 2000). Chan et al. (1999) observed that the concrete with a w/c of

0.22 heated to 200°C and 300°C has higher residual compressive strength than concrete with a w/c of 0.33. However, concrete with a w/c of 0.33 had shown a decrease in compressive strength at 450°C, but at the same temperature exploded when w/c was reduced to 0.22. As the moisture content increases the amount of evaporable water also increases, which will lead to increased pore pressure in the concrete and increased temperature gradient during heating. On the other hand, the higher the w/c is, the higher the permeability of the concrete will be, which is known to have a positive effect on behavior of concrete at high temperatures. Tests have shown that the positive effect of increased permeability is more dominant than the increased moisture content in concretes with higher w/c (Behnood and Ziari 2008). It has also been observed that concretes that are more saturated have suffered greater loss in strength compared to dryer concretes. When concrete is exposed to high temperatures, high temperature gradients between hot surface layers spall from the cooler interior core layers (Neville, 2010).

2.4.1 Fire Resistance of Normal Concrete (NSC) and Self Consolidating Concrete (SCC)

Research has been conducted in the past on concrete exposed to elevated temperatures (Hossain and Wright 1999a-b; Chan et al. 1999a-b; Bouzoubaa and Lachemi 2001; Tolentino et al. 2002; Poon et al. 2000b; Persson 2004; Hossain 2006; Peng et al. 2006; Hossain and Lachemi 2007; Annerel et al.2007; Fares et al. 2009; Chan et al. 2008a; Behnood and Ziari 2008; Behnood and Ghandehari 2009; Hossain and Lachemi 2010; Bastami et al. 2011). When concrete is exposed to elevated temperatures, the reduction in compressive strength between ambient temperature and 150°C is caused by expansion of the unbounded water which reduces cohesion between the layers of calcium silicate hydrate. The reduction the bond between the layers is caused by the Van der Waal forces. The unbounded water also evaporates and escapes through the pores of the concrete. Between 150°C and 300°C, evaporation of the bounded water occurs, which dehydrates the cement paste in the concrete and reduces compressive strength even further. This loss of water will result in overall mass loss of the concrete in this temperature range (Fares et al. 2009; Bastami et al. 2011).

At temperatures greater than 400°C, decomposition of calcium hydroxide and dehydration of the calcium silicate hydrate is another factor that leads to a decrease in compressive strength (Chan et al. 1999a). Pozzolans, such as silica fume, fly ash, volcanic ash and other supplementary cementing materials (SCM), which uses calcium hydroxide in their chemical reaction, should be used to reduce this effect (Neville 2010). The decomposition of calcium hydroxide and dehydrated cementing materials/ aggregates can result in further mass loss (Bastami et al. 2011). At higher temperatures of 800°C, there is a further reduction in strength caused by the complete breakdown of the cement paste from the sand and coarse aggregates. At high temperatures, the bond between the aggregate and the paste is weakened due to the contraction of the paste, decrease in moisture and the expansion of the aggregate (Hossain and Lachemi 2007; Behnood and Ziari 2008; Behnood and Ghandehari 2009; Bastami et al. 2011). There is also an observed loss of integrity of the coarse aggregate itself. This can result in additional mass loss in this temperature range (Bastami et al. 2011).

As the temperature of the concrete increases, the total porosity also increases due to the decomposition of the hydration products. Porosity may also increase due to the formation of micro-cracks in the concrete (Hossain 1999a; Hossain 2006; Hossain and Lachemi 2007) and or evaporation of bounded and unbounded water (Fares et al. 2009; Bastami et al. 2011).

Cracking at elevated temperatures which can also be associated with explosive spalling, is caused by the decomposition of hydration products and can occur in both the cement paste and around the aggregate particles. Rapid heating of the concrete can also lead to internal cracks when a temperature difference occurs between the cooler core and a warmer surface (Peng et al. 2006). The addition of supplementary cementing materials such as fly ash and glass furnace blast slag can reduce thermal cracking of the hardened concrete (Hossain and Lachemi 2010).

2.4.2 Fire Resistance of Engineered Cementitious Composite (ECC)

Research has been conducted in the past on engineered cementitious composite exposed to elevated temperatures (Sahmaran and Li 2010; Sahmaran et al. 2011; Cavdar 2012), and on

concretes made with blast furnace slag (Grainger 1980; Sarshar and Khoury 1993; Poon et al. 2001). When ECC is exposed to elevated temperatures, the reduction in compressive strength between ambient temperature and 150°C is the same as SCC as the unbounded water cannot escape as of yet due to the low porosity of ECC (Sahmaran and Li 2010). Between 150°C and 300°C, the behaviour of ECC is similar to SCC as the bonded water still cannot escape due to low porosity. The addition of low melting-point synthetic fibres, such as polyvinyl alcoholic (PVA) and polypropylene (PP), in ECC can reduce spalling by allowing the water vapour produced at high temperatures to travel through the voids created by the melted fibers. This may relieve high internal vapor pressures, and reduce the probability of spalling (Sarvaranta and Mikkola 1994a,b; Nishida et al. 1995; Sahmaran and Li 2010; Sahmaran et al. 2011). However, the additional porosity due to the melting of PP and PVA may lead to a decrease of the residual mechanical performance of concretes (Cavdar, 2012). This loss of water and loss of the material attributed to the melted fibers will result in overall mass loss of ECC in this temperature range (Sahmaran and Li 2010).

At temperatures higher than 400°C, the behaviour of ECC is similar to SCC. The decomposition of calcium hydroxide and dehydration of the calcium silicate hydrate (Sahmaran and Li 2010) lead to a decrease in compressive strength. Cracking can occur at this temperature, and is caused by the decomposition of hydration products. Cracking can occur in both the cement paste, unhydrated supplementary cementing material, and around the aggregate particles (Sahmaran and Li 2010; Sahmaran et al. 2011). This leads to decrease in strength and stiffness of ECC. The decomposition of calcium hydroxide and dehydration of the calcium silicate hydrate results in overall mass loss of the concrete in this temperature range (Sahmaran and Li 2010).

As the temperature of the concrete increases, the total porosity also increases in the same manner as SCC. Porosity is also increased by the melting of synthetic fibers such as PVA and PP. It was observed by Sahmaran et al. (2010) that the higher the temperature of ECC, the coarser the pore structure had become. This coarsening can lead to significant strength and stiffness losses in the concrete. However it has been shown by Poon et al. (2001) that concretes made with slag have

lower porosity and smaller pore diameter when exposed to elevated temperatures in comparison to conventional concrete.

Research conducted by Grainger (1980) showed that the cement-based specimens made with blast furnace slag had an overall higher residual strength after being exposed to elevated temperatures compared to the pure cement paste specimen. Experimentation conducted by Sarshar et al. (1993) gave similar results for both cement-based and concrete specimens. Research conducted by Poon et al. (2001) showed that concretes made with slag had higher residual strength after exposure to elevated temperatures than normal concrete. The concretes made with slag also had no signs of explosive spalling or cracking except the development of hairline cracks, and performed better than normal concrete and HPC/HSC made with silica fume.

2.4.3 Fire Resistance of High Performance / High Strength Concrete (HPC/HSC)

Research has been conducted in the past on high performance / high strength concrete exposed to elevated temperatures (Hertz 1984, Hertz 1992, Sarshar and Khoury 1993; Hammer 1995; Felicetti and Gambarova 1998; Chan et al. 1999b; Chan et al. 2000a,b; Poon et al. 2001; Reis et al. 2001; Phan et al. 2002; Chen and Young 2004; Poon et al. 2004a; Peng et al. 2006; Behnood and Ziari 2008; El-Dieb 2009 and Tai et al. 2011).

Up to 300°C, the behaviour of HPC/HSC is different from that observed in SCC and ECC. The bonded and unbounded water that evaporates cannot escape due to low HPC/RSC permeability. It was observed by Tai et al. (2011) that HPC/HSC heated between 200°C and 300°C has an increase in compressive strength compared to ambient temperature. This increase in compressive strength is attributed to the fact that high temperatures accelerate the pozzolanic reaction of supplementary cementing materials incorporated in HPC which in turn increases the hydration products, and reduces the pore size.

At temperatures higher than 400°C, the behaviour of HPC/HSC is similar to SCC and ECC where the decomposition of calcium hydroxide and dehydration of the calcium silicate hydrate

lead to a decrease in compressive strength. Further reduction in compressive strength can occur due to cracking caused by thermal stresses as seen in SCC and ECC, as well as due to the vapour pressure build up in the concrete caused by the low permeability. In some cases these stresses lead to explosive spalling in HPC/HSC (Chan et al. 2000a; Poon et al. 2001; Peng et al. 2006; Neville 2010; Tai et al. 2011).

At 800°C, there is a further reduction of strength in HPC/HSC. This reduction occurs due to the contraction of the paste and expansion of the aggregate, similar to SCC. However, due to the very dense structure in the zone between aggregates and paste, which is caused by the presence ultra-fine silica fume particles and their pozzolanic reactions, higher stress concentrations are produced in this zone. This results in greater strength losses in HPC/HSC containing silica fume compared to conventional concretes, SCC, and ECC (Behnood and Ziari 2008).

Tests conducted by Chan et al. (2000a) have shown that the addition of silica fume in concretes such as HPC/HSC increased the residual compressive strength after exposure to high temperatures in comparison to concretes with no silica fume. The increased compressive strength is due to the pozzolanic reaction where silica fume reacts with calcium hydroxide to form calcium silicate hydrate (CSH). However, the addition of silica fume creates highly dense pore structure with a very low permeability, which in turn lead to explosive spalling as a result of vapour pressure build up and thermal stresses. This causes silica fume HPC/HSC to have lower residual compressive strength compared to conventional concretes at elevated temperatures. Porosity in silica fume HPC/HSC s is higher with larger pore diameter after being exposed to elevated temperatures than concretes made with slag and conventional concrete. This was due to internal cracking caused by very dense structure (Hertz 1984; Hertz 1992; Sarshar and Khoury 1993; Hammer 1995; Felicetti and Gambarova 1998; Poon et al. 2001).

In HPC/HSC, steel fibers are used to constrain a change in volume due to rapid temperature change which helps control the initiation and propagation of microscopic defects in the concrete (Chan et al. 2000a). Steel fibers have been used to improve the ductility of concrete. Steel fibers can also improve the residual strength properties of concrete after exposure to high temperatures.

At high temperatures, steel fibers prevent crack formation in cement paste and subsequent crack expansion and help to strengthen the specimens to a certain extent. The steel fibers at the surface of specimen undergo oxidation after being exposed to high temperatures, which produced black carbon particles that were absorbed by the concrete (Tai et al. 2011). Tests conducted by Poon et al. (2004) have shown that HPC with steel fibres had the highest strength but had the highest reduction of strength after being exposed to a temperature of 800^{o}C for 1 hour, followed by HPC with polymer fibres, HPC with no fibres, and normal strength concrete (NSC).

2.5 Fire Resistance of Steel

Research has been conducted in the past on cold formed light gauge steel sheeting exposed to elevated temperatures (Outinen 1999; Lee et al. 2003; Chen and Young. 2004; Mecozzi and Zhao. 2005; Kolarkar 2006; Ranawaka and Mahendran 2009a; Bandula Heva 2009; Kankanamge and Mahendran 2011). Cold formed light-gauge steel sheeting exposed to elevated temperatures experiences degradation in both yield strength and modulus of elasticity. The deterioration of the mechanical properties of light gauge steel, such as the yield strength and modulus of elasticity is considered as the primary element affecting the performance of steel structures under fire. Eurocode 4 (2005) provides reduction factors for yield strength and modulus of elasticity of both hot-rolled steel and cold-formed steel exposed to high temperatures. But such factors are based on hot-rolled steels. The steel design standards set in Eurocode 4 (2005) overestimate the yield strength and modulus of elasticity of light gauge steel (Lee et al. 2003). This was also observed by Kolarkar (2006), Ranawaka and Mahendran (2009a), Bandula Heva (2009), and Kankanamge and Mahendran (2011) as shown in Figs. 2.5-2.6.

The strength degradation of light gauge steel occurs at lower temperatures when compared to hot-rolled sections. Light gauge steel has higher thermal conductivity and a high ratio of perimeter to the cross-sectional area (shape factor). These factors promote the degradation of the mechanical properties of this material. The cold-forming process does increase the yield strength at ambient temperature, but at high temperatures this strength gain is lost (Lee et al. 2003; Ranawaka and Mahendran 2009a).

Hot rolled steels have less reduction (by 10–20%) in mechanical properties compared to cold-formed steels due to the metallurgical composition and molecular surface effects of cold formed steels (Sidey and Teague 1988). The yield strength of the steel sheeting had very little effect on the reduction of both yield strength and modulus of elasticity (Lee at al. 2003; Ranawaka and Mahendran 2009a) and the difference in thickness of the steel sheeting also had very little influence on the reduction of both yield strength and modulus of elasticity (Ranawaka and Mahendran 2009a).

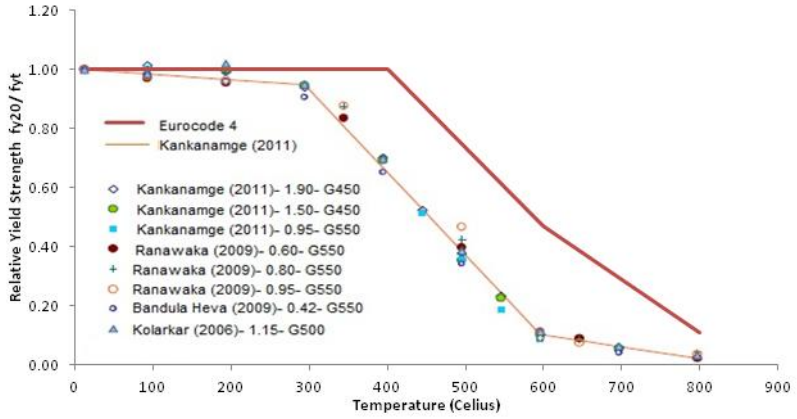

Figure 2.5- Relative yield strength of steel sheeting at elevated temperatures **(**Kankanamge and Mahendran 2011; Ranawaka and Mahendran 2009a; Bandula Heva 2009; and Kolarkar 2006)

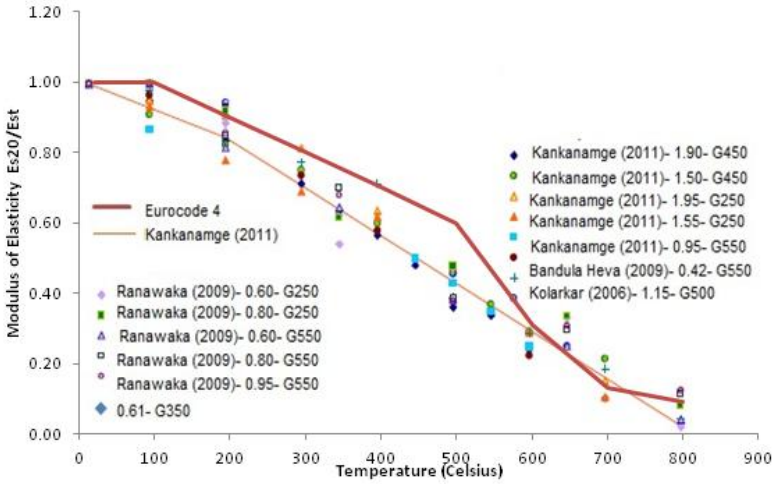

Figure 2.6- Relative modulus of elasticity of steel sheeting at elevated temperatures **(**Kankanamge and Mahendran 2011; Ranawaka and Mahendran 2009a; Bandula Heva 2009; and Kolarkar 2006)

2.6 Fire Resistance of Axially Loaded Composite Structural Elements

Concrete filled steel tube columns (CFSTs) are composed of steel tube with an in-fill of concrete. Similar to DSCWs, CFSTs use the steel as permanent formwork during the construction stage and as reinforcement in the service stage (Hossain 1999b; Hossain 2001; Hossain 2003b; Hossain et al. 2003a,b; Lachemi et al. 2006a,b). The CFSTs can be used to eliminate the need for external fire protection to the steel (Kodur 1999).

Hossain (2003b) observed that there were two types of failures depending on the slenderness of the rectangular CFST columns. The failure of columns was caused by initial debonding of the steel and concrete, which was followed by local or global buckling. The failure mode for short columns was due to the formation of successive local buckles with plastic yielding and bending of columns as shown in Fig.2.7. Bending failure of the column was initiated in the zone of plastic yielding, which was located between two adjacent buckles on the steel, as shown in Fig.2.7a. Concrete was crushed locally in short columns, which pushed the steel wall outward leading to buckling caused by the increase of lateral pressure in the steel. The failure mode for slender columns was due to global buckling. Bending failure of the column was initiated in the zone of plastic yielding, which was located between two adjacent buckles on the steel, located near the mid-span as shown in Fig.2.7b.

Confinement of concrete in CFSTs improved the overall performance and the failure load was dictated by the performance of steel section. The maximum load capacity should be based upon the increased confined strength of the concrete, as well as the increased plate buckling capacity of the steel due to composite action. Analytical models for the maximum load capacity were proposed by taking into account the effect of confinement on both steel and concrete.

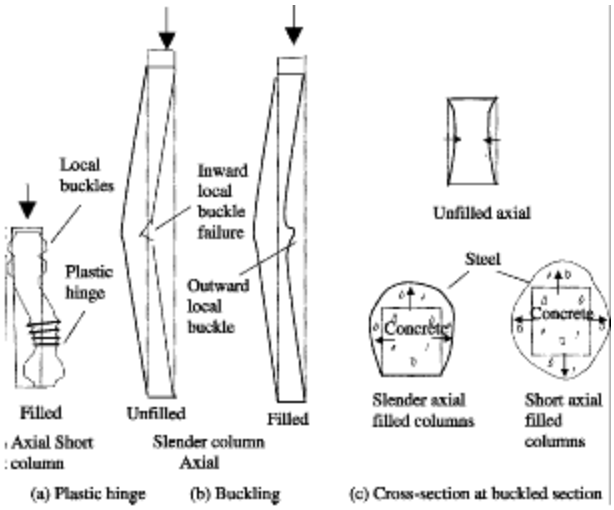

Figure 2.7- Failure modes of the CFSTs (Hossain 2003a,b)

It was observed that the failure modes of short and slender CFST columns were same at elevated temperatures (Hossain 1999b; Hossain and Lachemi 2003a). The maximum load capacity of the columns decreased with the increase of duration of fire as well as with the increase of temperature. Analytical models for the maximum load capacity were proposed for CFSTS which took into account the confinement on both steel and concrete, as well as the effect of elevated temperatures

CFSTs have much better endurance characteristics than conventional reinforced concrete columns under fire conditions as the steel protects concrete against fire and prevents spalling. Infill concrete provides stability to the steel tube, and the steel tube in turn provides confinement to the concrete (Romero et al. 2011). In fire conditions, the steel section acts as a barrier to the concrete core and a steam layer in the steel–concrete boundary appears (Romero et al. 2011). During fire exposure, there is a load transfer between the steel and concrete in the CFST short columns. Ultimate compressive strength of the inner core concrete degrades slowly due to the slow temperature elevation. The core concrete can continuously take compressive loads transferred from the steel section until the outer concrete reaches its compressive strength.

The interaction between the steel and concrete in the composite columns is an important factor responsible for performance of CFST short columns exposed to fire. When the steel section

begins to yield, the core concrete resists the deformation no longer carried by the steel and share the load from the steel section. Due to the fact that the compressive stress of concrete is not even because of the non-uniform temperature distribution, the outer part of the concrete is the most vulnerable in the whole concrete. The outer part of the concrete, which has higher temperature/compressive stress and lower strength, now carries the load transferred from the steel. When outer concrete t reaches its compressive strength, which is now reduced due to exposure to the fire, it begins to crush. While this is happening, the inner part of the concrete alone is resisting the load. Buckling of the steel section and crushing of the outer part of the concrete reduces the confinement on the inner part of concrete, which leads to a reduction in the capacity of the inner part of the concrete. In the end, the CFST short column will fail when the core concrete can no longer resist the load transmitted from the steel section (Lu et al. 2009).

When CFST short columns are exposed to high temperatures and then tested under axial compressive loading, the primary failure mode was outward bulges of the steel section with no lateral deflection. The ultimate failure of short columns was caused by compressive failure rather than overall buckling which is attributed to the presence of infill concrete that alter the buckling mode and behaviour of the steel section. It was also observed that the CFST short columns retained integrity, showing no separation between the concrete and steel sections after the test. Therefore, there was an interaction between the steel and concrete in the CFST short columns subjected to elevated temperatures during the entire test. It was observed that the outer concrete at the middle height of the CFST short column was crushed, which corresponded to the outward bulge observed in the steel section. There was also longitudinal cracking on the surface of the concrete. There was no observed spalling of the concrete or tangential slipping between the concrete and steel section (Lu et al. 2009).

Lu et al. (2009) observed that the local buckling of the steel section of CFST short columns at elevated temperatures occured before the columns reached the maximum load capacity under fire conditions. The buckling of the steel section did not have much effect on the behaviour of the columns. Outward bulging in the steel section developed from one bulge to several bulges

gradually. In between the bulges, where the steel section was still in contact with the concrete, the concrete provided support to the steel section, as shown in Fig.2.8.

When CFST slender columns were exposed to high temperatures and then tested under axial compressive loading, the primary failure mode was associated with overall buckling associated with lateral deflection, as shown in Fig.2.9 (Romero et al. 2011). It was also observed that the CFST slender columns lost integrity and there was separation between the concrete and steel sections after test. The steel section heated up faster than concrete core, since it was directly exposed to fire and had a higher thermal conductivity. This promoted slip at the steel–concrete interface due to the faster axial elongation of the steel section (Romero et al. 2011).

Figure 2.8- Failure mode of short CFST columns (Lu et al. 2009)

Figure 2.9 - Failure mode of slender CFST columns (Romero et al. 2011)

2.7 Review Conclusion

Research has been conducted in the past on the DSCWs subjected to axial, and lateral including monotonic, cyclic, and impact loading conditions. To date, however, no research has been conducted on the effect of elevated temperatures on the strength, stiffness and ductility of the DSCWs. Also very little research has been conducted on DSCWs using HPCs such as SCC, ECC or UHPC. The knowledge of the structural behaviour of such walls with HPCs subjected to elevated temperatures is very important in developing analytical models to predict post-fire strength, stiffness and ductility. Such models can be useful to develop design guidelines for

DSCW system used in practical construction applications. Proposed research on the axial load behaviour of DSCWs incorporating HPCs subjected to elevated temperatures is a timely initiative and is warranted.

CHAPTER 3

Behaviour of Steel and Concrete at Elevated Temperatures

3.1 Introduction

In this chapter, experimental results are presented on the individual materials that make up the composition of the double skin composite walls (DSCWs). The objective of this investigation was to determine the effect of elevated temperatures on the post-fire material properties of both cold-formed light-gauge steel sheeting and three different types of high performance concrete (HPC): Self-Consolidating Concrete (SCC), Engineered Cementitious Composite (ECC), and Ultra High Performance Concrete (UHPC). Investigation was conducted on steel sheeting coupon samples and concrete cylinders made from each concrete subjected to elevated temperatures maintained for two hours, and sequential cooling. The steel sheeting samples were tested using a tensile testing machine, and the concrete cylinders were tested using a compressive testing machine before and after subjected to elevated temperatures. The observations during the testing and the test results for tensile and compressive axial loading are presented in terms of yield strength and modulus of elasticity for steel sheeting, and compressive strength and modulus of elasticity for concrete. Stress-strain behaviour was also modeled for the steel sheeting and the different concrete types. All tests, except the unheated samples, were tested after being exposed to elevated temperatures of up to 800°C (500°C for ECC).

3.2 Behavior of Steel Sheeting Exposed to Elevated Temperatures

3.2.1 Sample Preparations and Testing Methodology

Tests were conducted on the steel sheeting coupon samples, a component of the DSCWs. For each temperature range, steel sheet coupon samples as shown in Fig. 3.1, were cut from the profiled cold-formed light gauge steel sheeting of thickness of 0.61 mm. These samples were

heated at a rate of 2.5°C/min (Fig. 3.2) in a kiln until specified steady state temperature was achieved and sustained for two hours at temperatures of 400°C, 600°C and 800°C. Then the samples were allowed to cool down naturally before being tested. After exposure, samples were visually inspected for any physical changes. These heated samples along with the non-heated samples, were then tested by applying axial tensile force, in accordance with ASTM E8 (2011), to determine the yield strength (f_y) and modulus of elasticity (E_s) and stress-strain characteristics (Fig.3.3). Due to lab constraint, it was not possible to test the steel sheeting samples under axial load at the same time as the samples were being heated. Therefore, the results presented here are the post-fire residual yield strength and modulus of elasticity of the steel sheeting. Stress-strain curves for steel sheet were produced for each given exposed temperature.

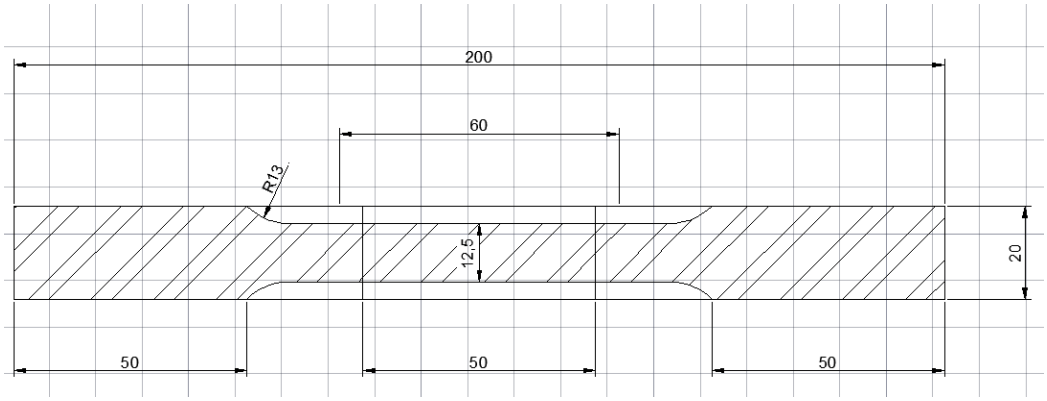

Figure 3.1- Steel sheet coupon sample (dimensions in mm)

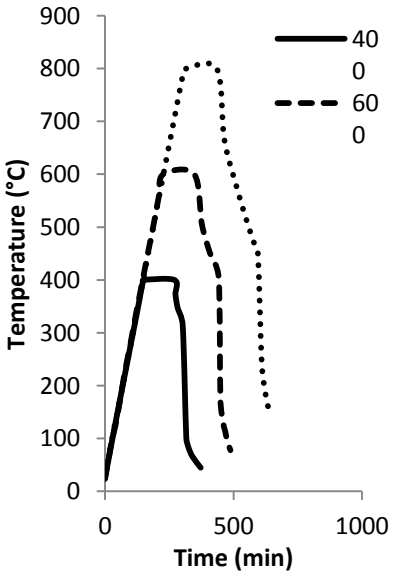

Figure 3.2- Heating-cooling curves for steel sheeting , SCC and UHPC

Figure 3.3- Test setup for tensile testing of steel sheeting coupon samples

3.2.2 Fire Degradation of Yield Strength and Modulus of Elasticity of the Steel Sheeting

It was observed that the steel sheeting behaved differently based on the reduction factors (ratio of property at any given temperature "t' to property at 20°C termed as relative property) presented in Eurocode 4 (2005) and observed by Kankanamge and Mahendran (2011), Ranawaka and Mahendran (2009a), Bandula Heva (2009), and Kolarkar (2006). The reduction factors used in Eurocode 4 (2005) are used for both hot-rolled steel and cold-formed steel exposed to elevated temperatures, but the research behind the reduction factors is based on hot-rolled steel. These reduction factors are shown to overestimate the yield strength and modulus of elasticity of light gauge cold formed steel exposed to elevated temperatures research conducted by Kankanamge and Mahendran (2011) as shown in Figs.3.4-3.5. However, all these models represent the properties of the steel sheeting at elevated temperatures while the heat is being maintained. The reduction in the residual yield strength and modulus of elasticity of the steel sheeting obtained from current experimentation are the post-fire properties based on the samples being heated to a given temperature, sustained for two hours, and then allowed to cool before being tested.

At temperatures of 400°C, 600°C, and 800°C, the yield strength of the steel sheeting was higher than the strength observed in Kankanamge and Mahendran (2011) by a factor of 1.42, 7.01, and 12.64, respectively; and the modulus of elasticity of the steel sheeting was higher by a factor of 1.62, 2.86, and 20.94, respectively (Figs.3.4 and 3.5). Therefore, cooling down to ambient temperature after heating before it was loaded, allowed the steel sheeting to regain some of its strength and stiffness. As a result lower reduction factors were observed in the current study compares with those observed in both Eurocode 4 (2005) and Kankanamge and Mahendran (2011).

.

The relative yield strength (f_{yt}/f_{y20}) was calculated for each temperature by determining the ratio of the yield strength at a given temperature (f_{yt}) to the yield strength at ambient temperature (f_{y20}), as shown in Table 3.1. Using the relative yield strength (termed as fire degradation factor for yield strength of steel, β_s), analytical models were developed to determine the yield strength (f_{yt}) of steel sheeting after exposure to elevated temperatures (t) relative to ambient temperature (20^oC) and presented as Eqs. 3.1:

$ß_s = f_{yt}/f_{y20} = -0.00012t + 1.0024$ for 20 °C $\leq t \leq$ 400 °C ($r^2 = 1.0$) [Eq.3.1a]

$ß_s = f_{yt}/f_{y20} = -2.605(10)^{-6}t^2 + 1.688(10)^{-3}t + 0.696$ for 400°C< t < 800 °C ($r^2 = 1.0$) [Eq.3.1b]

Table 3.1- Yield strength of steel sheeting samples at elevated temperatures

Temperature (°C)	20	400	600	800
	Yield Strength (MPa)			
STEEl-1	392.8	375.1	305.9	146.7
STEEL-2	393.3	376.0	301.0	149.6
STEEL-3	394.4	375.5	303.2	151.6
Mean	393.5	375.6	303.4	149.3
Standard Deviation	0.82	0.47	2.41	2.45
Relative Yield Strength ($ß_s = f_{yt}/f_{y20}$)	1.00	0.95	0.77	0.38

f_{y20}- yield strength at 20°C, f_{yt}- yield strength at t°C

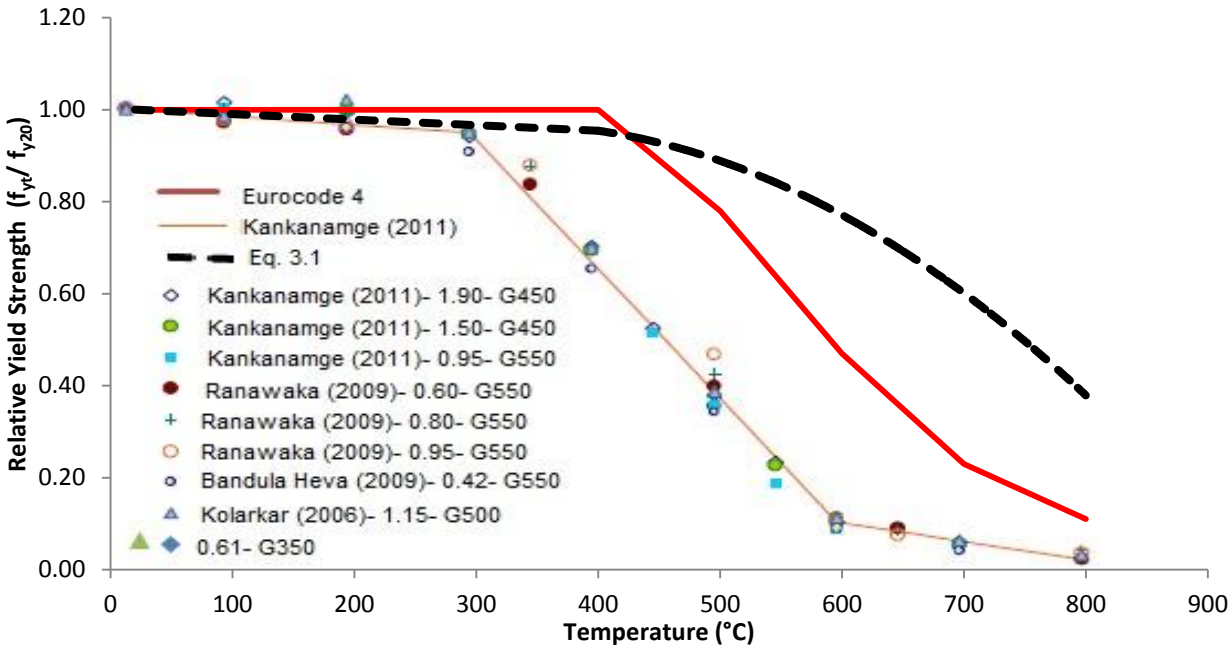

Figure 3.4- Relative yield strength of steel sheeting at elevated temperatures

The relative modulus of elasticity (E_{st}/E_{s20}) was calculated for each temperature by determining the ratio between the modulus of elasticity at a given temperature (E_{st}) to the modulus of elasticity at ambient temperature (E_{s20}) (Table 3.2). Using the relative modulus of elasticity (termed as fire degradation factor for elasticity, β_{se}), theoretical models were developed to

determine the modulus of elasticity (E_{st}) of steel sheeting after exposure to elevated temperatures (t) relative to 20°C and presented as Eqs. 3.2:

$$ß_{se} = E_{st}/E_{s20} = -0.0000000952t^2 - 0.000131t + 1.00 \text{ for } 20\ °C \leq t \leq 800\ °C \ (r^2 = 0.99) \qquad [Eq.3.2]$$

Table 3.2- Modulus of elasticity of steel sheeting samples at elevated temperatures

Temperature (°C)	20	400	600	800
	Modulus of Elasticity (GPa)			
STEEl-1	207.6	190.8	183.7	172.4
STEEL-2	199.3	199.3	188.6	189.2
STEEL-3	215.9	195.1	179.4	161.5
Mean	207.6	195.1	183.9	174.3
Standard Deviation	8.32	4.27	4.59	14.0
Relative modulus of elasticity ($ß_{se} = E_{st}/E_{s20}$)	1.00	0.94	0.89	0.84
Yield Strain (Microstrain)	2860	1950	1540	1727

E_{s20}- Modulus of elasticity at 20°C, E_{st}-: Modulus of elasticity at t°C

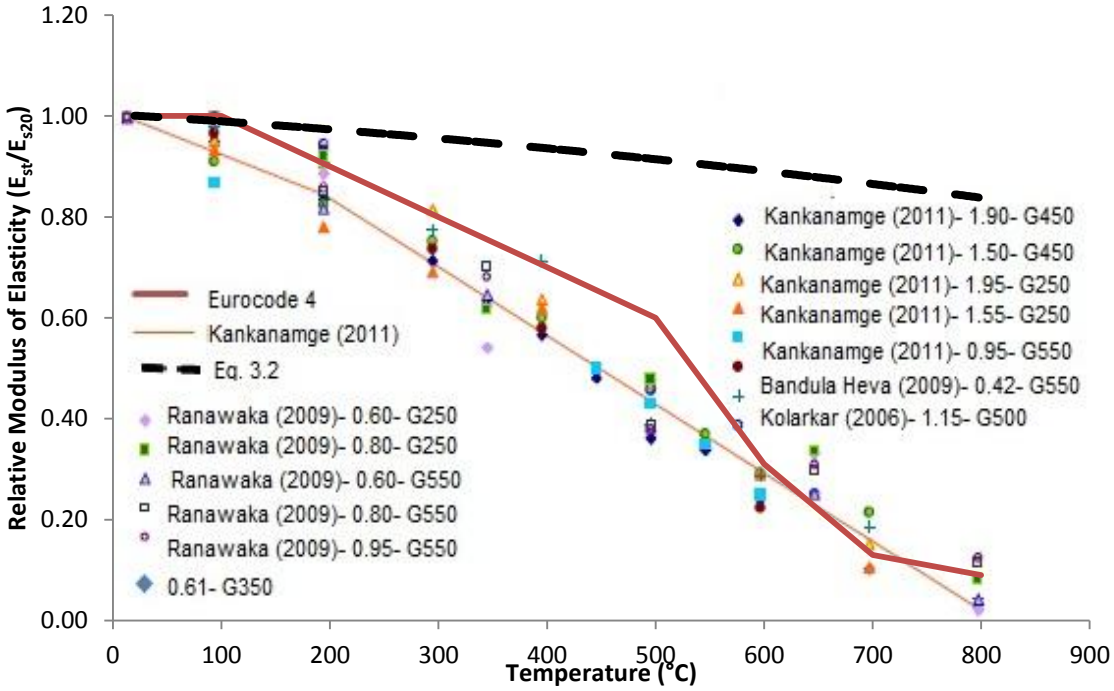

Figure 3.5- Relative modulus of elasticity of the steel sheeting at elevated temperatures

3.2.3 Stress-Strain Behaviour of Steel Sheeting at Elevated Temperatures

The stress-strain curves for the steel sheeting are shown in Fig.3.6. It is observed that the stress-strain behaviour matches very closely to that of conventional steel used as per current standards. The stress-strain curve was also similar to those observed in Kankanamge and Mahendran (2011), with the expectation of higher yield strength observed in the yielding plateaus and higher slope of the ascending braches due to higher modulus of elasticity.

At 20°C, the 0.2% offset yield strength, modulus of elasticity and yield strain of the material were about 394 MPa, 207 GPa and 2860 microstrain, respectively. Both the yield strength and modulus of elasticity of the steel sheeting decreased with the increase of temperatures from 20°C to 800°C. The steel sheet lost 62% and 16% of its yield strength and modulus of elasticity, respectively after exposure to 800°C for 2 hours.

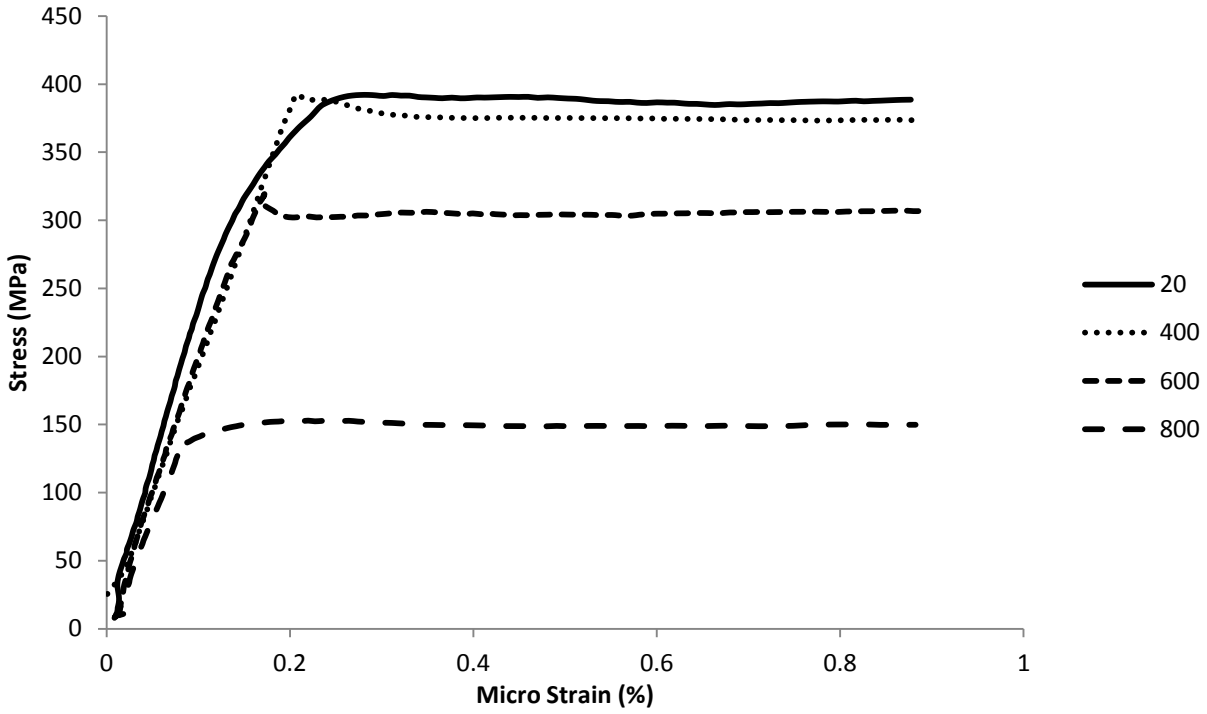

Figure 3.6- Stress-strain behavior for steel sheeting at elevated temperatures (°C)

3.2.4 Physical Changes and Failure Modes of Steel Sheeting Coupon Samples

The steel sheeting samples failed at the center of the coupon in a diagonal manner, which was expected in this type of test, similar to the failure mode observed in Kankanamge and Mahendran (2011). The failure pattern of all three samples, at control and at elevated temperatures was observed to be the same (Fig.3.7).

Figure 3.7- Failure Mode in Steel Sheeting Coupon Samples (20°C to 800°C)

No discolouration or damage of the exterior surface of the steel was observed up to 400^{o}C (Fig.3.7). At 600^{o}C, minor greyish discoloration was observed only on the very top layer as a form of dust or powder. At 800^{o}C, the discoloration was a mixture of black and brown, and instead of being a fine dust or powder, the burnt portions of the steel peeled or flaked off, indicating a greater extent of damage compared to those samples heated at 600^{o}C.

3.3 Behaviour of In-fill Concrete Exposed to Elevated to Temperatures

3.3.1 Sample Preparations and Testing Methodology

Experiments were conducted on three different high performance concretes (HPC): Self-Consolidating Concrete (SCC), Engineered Cementitious Composite (ECC), and Ultra High Performance Concrete (UHPC). These HPCs were used as concrete in-fill in DSCWs.

The SCC is a concrete mix, with a water/cementious ratio of 0.35, consisting of general purpose cement (CSA A3001, 2008) and white slag as the cementing material, water, 8 mm maximum size crushed limestone from Munroe quarry, fine edgar sand (having fineness modulus of 3.57) and a polycarboxylate-based high range water reducer Type A and F as per ASTM C494 (2011). Gradation of fine aggregates is presented in Fig.3.9. The superplasticizer is designed to help produce high strength concrete with enhanced strength development and high early strength, low water/cementious ratios, enhanced concrete cohesiveness with low viscosity for rapid placement, and superior finish on cast surfaces.

The ECC has a water/cementious ratio of 0.30, PVA fiber content of 1% fibers/kg of dry material. It consists of general purpose cement and white slag as the cementing material, water, natural grain silica sand with 110 micrometer nominal size, Polyvinyl Alcohol (PVA) fibers (ASTM C1116, 2010*),* and the same superplasticizer used in SCC. Gradation of silica sand is presented in Fig.3.10. The PVA fibers are 39 microns in diameter, 8 mm in length, a tensile strength of 1620 MPa, modulus of elasticity of 42.8 GPa, and has a melting point of 225°C, as shown in Fig.3.11.

The UHPC mix has water to cementitious material ratio of 0.22 and a steel fiber content of 9% by mass of dry material. It consists of general purpose cement and silica fume (Undensified Microsilica Grade 971**)** as the cementing material, water, natural grain silica sand of 110 micrometer nominal size, steel fibers (ASTM A820, 2011), and the same superplasticizer used in SCC. The steel fibers used are 0.2 mm in diameter and 13 mm in length with a tensile strength of 2160 MPa, modulus of elasticity of 210 GPa, and melting point higher than 800°C, as shown in Fig.3.11.

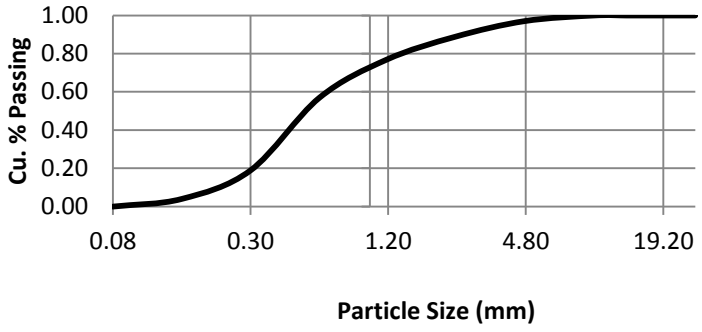

Figure 3.9- Particle size distribution of fine sand

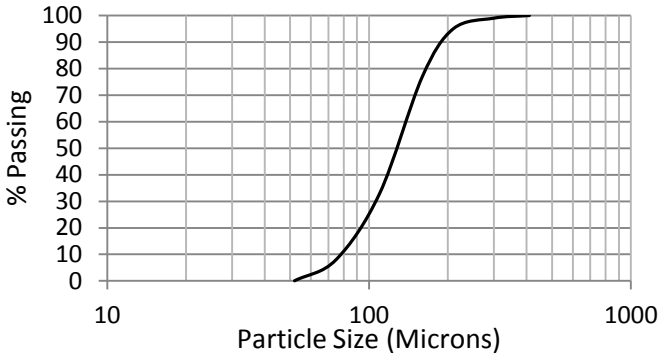

Figure 3.10- Particle size distribution of silica sand

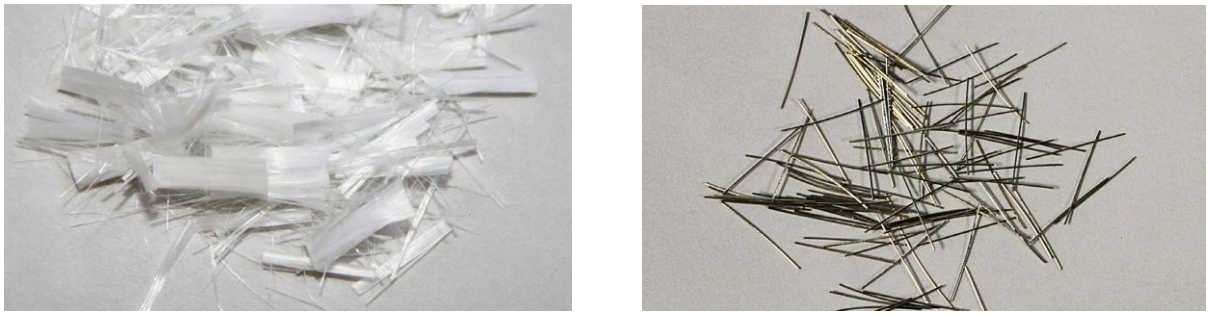

Figure 3.11- Polyvinyl alcohol fibers (left) and steel fibers (right)

For each temperature range, concrete cylinder samples of dimensions 100mm x 200mm were cast as per ASTM C192 (2007) and cured in the laboratory under similar conditions as the profiled concrete walls. At the age of 28 days, these cylinder samples were heated at a rate of 2.5°C/min, similar to Chan et. al. (1999a), in a kiln up to the specified steady state temperature was achieved and sustained for two hours (ranging from 20°C to 800°C) and then the samples were allowed to cool down before being tested. However, the rate of heating is significantly lower than the standard fire rate of temperature rise specified by ASTM E 119a (2000), which is about 600°C in the first 6.7 min. This was due to the limitations of the kiln. ECC specimens were heated to 500°C and for steady state duration of 1 hour due to some laboratory problems. Fig.3.2 shows the heating curves for SCC and UHPC and Fig.3.12 shows those for ECC. Due to lab constraint it was not possible to test the concrete cylinder samples under axial load at the same time as the samples were being heated. Therefore, the results presented hereafter are the post-fire residual compressive strength and modulus of elasticity of the each concrete type after exposure to elevated temperatures and then cooled. After exposure, samples were visually inspected for any physical changes.

These heated samples along with the non-heated samples, were tested by applying axial compressive force, corresponding to ASTM C39 (2012), to determine the compressive strength (f'_c), and the modulus of elasticity (E_c,) as shown in Fig.3.13. Three strain gauges were installed on selected cylinders of each concrete type and for each tested temperature to obtain the stress-strain behaviour of each concrete. Stress-strain curves were produced for each given temperature. From the data obtained from the stress-strain curves, the modulus of elasticity at various temperatures for each concrete type was determined.

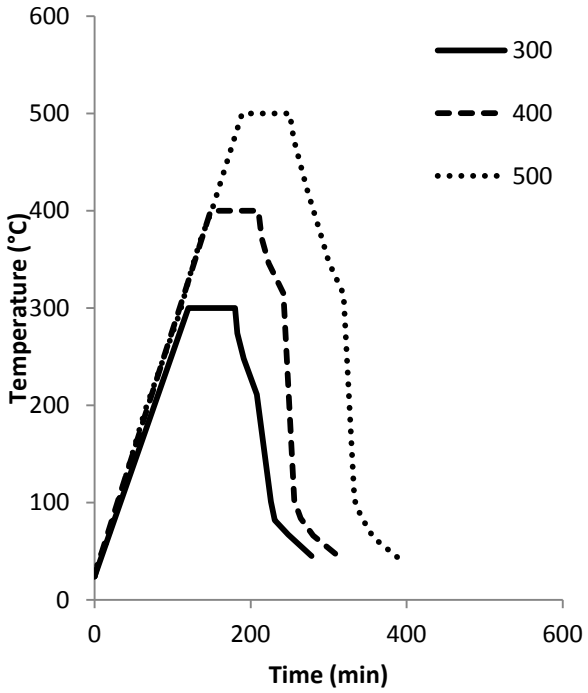

Figure 3.12- Heating-cooling curves for ECC specimens

Figure 3.13- Test setup for compressive strength of concrete cylinders

3.3.2 Properties of In-Fill Concrete at Ambient Temperature

Table 3.3 compares properties of SCC, ECC and UHPC. The 28-day compressive strengths of SCC and ECC were 61.47 and 60.30 MPa, respectively, while the compressive strength for UHPC was 119.51 MPa. The modulus of that elasticity for SCC was similar to that of normal strength concrete, which has a modulus of that elasticity 33.59 GPa, but has a higher modulus of elasticity than observed in the ECC, which was 24.98 GPa. This observation makes sense considering that ECC is designed to be more flexible than SCC as described in Li (1993), Fischer and Li (2003), Wang and Li (2007), and Sahmaran et al. (2010). On the other hand, UHPC had a modulus of elasticity of 42.42 GPa - the highest modulus of elasticity of all the concrete types due to the presence of steel fibers embedded in the highly-dense concrete matrix.

The maximum compressive strain for SCC was 1828 microstrain, which was found to be less than the assumed values for normal concrete, which are 2500, 3000, and 3500 microstrain for Eurocode 4 (2005), ACI 318 (2011), and CSA A23.3 (2004), respectively, and less than the maximum compressive strain for UHPC and ECC, which were 2655 and 2779 microstrain, respectively. This observation makes sense considering that ECC is designed so that a series of micro-cracks would form after loading in generalized area as described in Sahmaran et al. (2010). Similarly UHPC has steel fibers which control crack width and propagation throughout the concrete, as opposed to SCC where one or more larger cracks would form after loading in a localized area and has no fibers to aid in crack control. that The maximum compressive strain for ECC is higher than that of SCC also proves that ECC is a more flexible than SCC and failure at the same strength occurs in higher strain in ECC compared to SCC. However, even though the maximum compressive strain of UHPC is similar to ECC, UHPC (due to its high strength at the same strain) has higher stiffness and less flexibility than ECC.

Table 3.3- Comparison of properties of different concrete types

	SCC	ECC	UHPC
Maximum Compressive Strength (f'_c) (MPa)	61.5	60.3	119.6
Modulus of Elasticity (E_c) (GPa)	33.6	25.0	42.4
Maximum Compressive Strain (microstrain)	1828	2779	2655

3.3.3 Fire Degradation of Compressive Strength

The relative compressive strength (f'_{ct}/f'_{c20}) also termed as fire degradation factor for concrete compressive strength ($ß_c$) was calculated for each temperature by determining the ratio between the compressive strength at a given temperature (f'_{ct}) to the compressive strength at ambient temperature (f'_{c20}), as shown in Table 3.4. The degradation of compressive strength of each of the concrete types and the reduction factors proposed by Eurocode 4 (2005) for normal strength concrete are presented as a function of temperature (t) in Fig.3.14.

At 400°C, it was observed that the compressive strength of SCC was reduced by 8%, followed by ECC at 13%, and UHPC at 21%. The reduction in compressive strength for SCC was initially (between ambient temperature and 150°C) caused by expansion of the unbounded water which reduces cohesion between the layers of calcium silicate hydrate by reducing the bond between the layers caused by the Van der Waal forces (Fares et al. 2009). The unbounded water also evaporates and escapes through the pores of the concrete. Between 150°C and 300°C, evaporation of the bounded water occurs, which dehydrates the cement paste in the concrete and reduces compressive strength even further (Fares et al. 2009).

At 400°C, ECC behaves in a similar manner as SCC with the exception that it would experience a greater increase in porosity and a decrease in strength due to the melting of the PVA fibers as was observed by Sahmaran et al. (2010). This reduced strength causes cracking due to thermal stresses, which was not observed in SCC at this temperature. This causes the reduction of compressive strength in ECC to be higher than SCC.

At 400°C, UHPC experiences the greatest reduction of compressive strength due to explosive nature of this type of concrete caused by vapour pressure buildup within the concrete. Unlike SCC and ECC which has pores for the water vapour to escape through, the low permeability restrains the vapour pressure until it breaks through the concrete in the form of explosive spalling or cracking (Chan et al. 2000a). The steel fibers restrict the crack growth and propagation by holding the cracked portions of concrete together. But the cracks gradually form throughout the concrete due to water pressure build up and thermal stresses. The steel fibers hold these cracked

portions in place until the bond between the cracked portions and the fiber breaks. This failure is more sudden and not gradual which causes the strength of the concrete to be reduced significantly.

Between 400°C to 600°C, decomposition of calcium hydroxide in the concrete occurs. This reduces the compressive strength of the concrete considerably. The reduction is experienced by all three concrete types where compressive strength of SCC and UHPC were reduced by 35% and 54% respectively at 600°C; and for ECC was reduced by 26% at 500°C. Once again the reduction in compressive strength is the highest in UHPC due to the volatile nature of this concrete. This trend continues into 800°C where strength is further reduced to 18% of ambient temperature strength. The reduction in strength is higher in ECC than in SCC at 500°C, which is due to the increased porosity of the ECC due to melting of the PVA fibers. At 800°C, the compressive strength of SCC is further reduced to 41% of the ambient temperature strength. This reduction in strength is caused by the complete breakdown of the cement paste with the sand and coarse aggregates, as well as the loss of integrity of the coarse aggregate itself (Bastami et al. 2011).

Analytical models (Eqs.3.3 to 3.5) are formulated to model the effect of fire degradation on the compressive strength of all three concrete types expressed in the form of fire degradation factor for concrete compressive strength ($ß_c$) as function of temperature (t):

SCC

$$ß_c = f'_{ct}/f'_{c20} = -0.0000012t^2 + 0.000196t + 1.002 \leq 1.00 \text{ for } 20\ °C \leq t \leq 800\ °C \ (r^2 = 0.99) \quad \text{[Eq.3.3]}$$

ECC

$$ß_c = f'_{ct}/f'_{c20} = -0.00000206t^2 + 0.000525t + 0.99 \leq 1.00 \text{ for } 20\ °C \leq t \leq 500\ °C \ (r^2 = 0.99) \quad \text{[Eq.3.4]}$$

UHPC

$$ß_c = f'_{ct}/f'_{c20} = -0.000000963t^2 - 0.0002581t + 0.996 \text{ for } 20\ °C \leq t \leq 800\ °C \ (r^2 = 0.99) \quad \text{[Eq.3.5]}$$

Eurocode 4 (2005) has higher fire degradation for normal strength concrete (NSC) than both SCC and ECC in compressive strength. This result is in line with previous research indicating that concretes containing blast furnace slag have higher compressive strength than NSC (Poon et

al. 2001). The behaviour of UHPC is close to Eurocode 4 (2005) due to the cracking induced by vapour pressure.

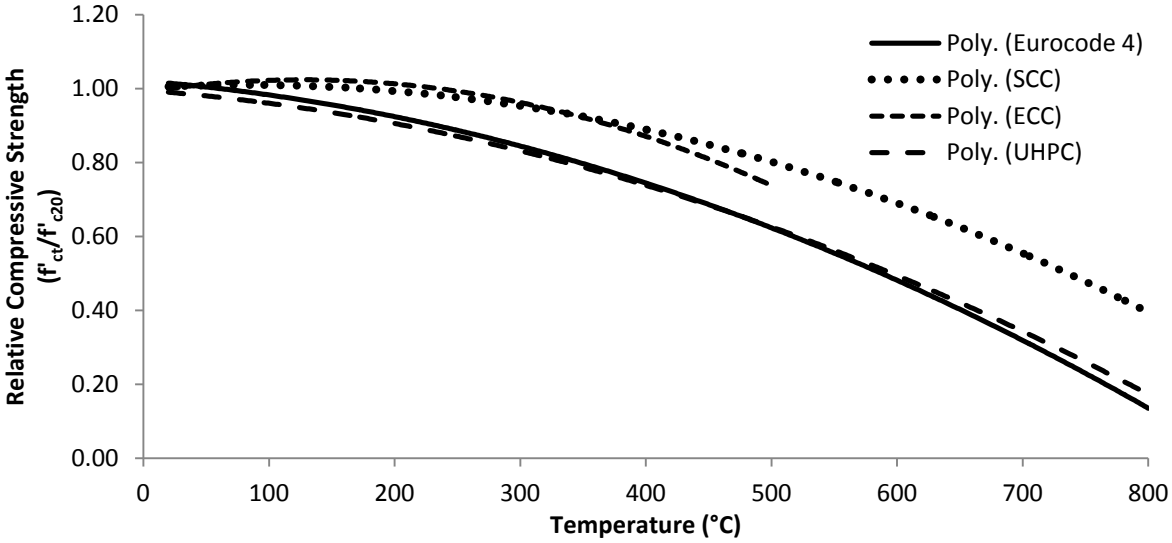

Figure 3.14- Relative compressive strength of concretes at elevated temperatures

Table 3.4- Compressive strength of concretes exposed to elevated temperatures

MPa	SCC				ECC				UHPC				
Temp. (°C)	20	400	600	800	20	300	400	500	20	200	400	600	800
CY-1	62.3	58.8	36	10.6	60.6	63.8	57.7	42.3	113.3	103.6	94.1	44.2	16.1
CY-2	56.9	54.3	40.4	18.4	56.6	52.4	46.1	46.5	109.3	104.7	95.7	65.7	27.8
CY-3	62	56.2	34.3	18.1	66.8	58.1	56	44.4	124	105.9	93.1	54.5	22
CY-4	64.1	55.2	35.7	13.2	61.3	56.2	50.4	45.9	131.4	102	94.3	50.3	24.6
CY-5	62	57.5	37.6	15.1	56.3	59.7	52.5	43.3	119.7	103.6	95.4	59.9	18.2
Mean	61.5	56.4	36.8	15.2	60.3	58.1	52.5	44.5	119.6	104	94.5	55	21.7
S.D.	2.7	1.8	2.3	3.3	4.3	4.2	4.6	1.8	8.7	1.5	1.1	8.3	4.7
f'_{ct} / f'_{c20}	1.00	0.92	0.65	0.41	1.00	0.96	0.87	0.74	1.00	0.87	0.79	0.46	0.18

f'_{c20}- maximum compressive cylinder strength of concrete at a 20°C, f'_{ct} - maximum compressive cylinder strength of concrete at a given temperature due to fire degradation of concrete, S.D.- the standard deviation.

3.3.4 Effect of Fire Degradation on Modulus of Elasticity and Stress-Strain Behaviour

The relative modulus of elasticity (E_{ct}/E_{c20}) termed as fire degradation factor for modulus of elasticity ($ß_{ce}$**)** was calculated for each temperature by determining the ratio between the modulus of elasticity at a given temperature (E_{ct}) to the modulus of elasticity at ambient temperature (E_{c20}), as shown in Table 3.5. The fire degradation of modulus of elasticity of each of the

concrete types and the reduction factors proposed by Eurocode 4 (2005) for normal strength concrete are presented as a function of temperature in Fig.3.15. Eurocode 4 (2005) over predicted the fire degradation of both SCC and ECC by showing more degradation of modulus of elasticity. The stress-strain behaviour of SCC and ECC at various elevated temperatures is presented in Figs.3.16 and 3.17, respectively. Stress-strain behaviour of UHPC at elevated temperatures could not be determined due to explosive failure of the cylinder specimens.

In general, modulus of elasticity decreased with the increase temperature (Fig.3.15). At 400°C, it was observed that the modulus of elasticity of SCC was reduced by 37% and ECC was reduced by around 23% (interpolation between values of 300°C and 500°C). The reduction in modulus of elasticity for SCC was due to evaporation of water that would have caused the porosity of the concrete to be higher, thus making the concrete more compressible and thereby reducing the modulus of elasticity. The same actions occur in ECC, except for the fact that the remaining fiber material left would have retarded the decrease in modulus of elasticity. At 500°C, the modulus of elasticity of ECC was reduced by 36% whereas SCC modulus was reduced by 88% at 800°C.

Analytical models (Eqs.3.6 to 3.7) are formulated to model the effect of fire degradation on the modulus of elasticity of SCC and ECC expressed in the form of fire degradation factor for modulus of elasticity ($ß_{ce}$) as function of temperature (t):

SCC

$$ß_{ce} = E_{ct}/E_{c20} = 0.000000032t^2 - 0.00122t + 1.04 \text{ for } 20\ °C \leq t \leq 800\ °C \ (r^2 = 0.96) \quad [Eq.3.6]$$

ECC

$$ß_{ce} = E_{ct}/E_{c20} = -0.00000151t^2 + 0.0000365t + 1.00 \text{ for } 20\ °C \leq t \leq 500\ °C \ (r^2 = 1.00) \quad [Eq.3.7]$$

Table 3.5- Modulus of elasticity of SCC and ECC exposed to elevated temperatures

	SCC				ECC		
Temperature (°C)	20	400	600	800	20	300	500
Modulus of Elasticity (E_{ct}) (GPa)	33.6	21.3	7.2	4.0	25.0	21.9	16.0
Fire degradation factor (E_{ct}/E_{c20})	1.00	0.63	0.21	0.12	1.00	0.88	0.64

E_{c20}- modulus of elasticity of concrete at a 20°C, E_{ct} - modulus of elasticity of concrete at a given temperature due to fire degradation of concrete

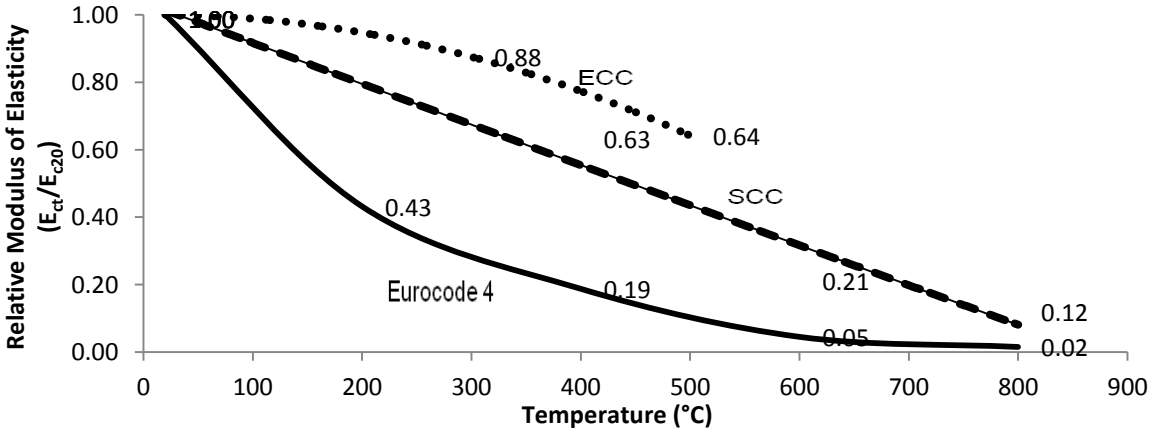

Figure 3.15- Relative modulus of elasticity for SCC and ECC at elevated temperatures (°C)

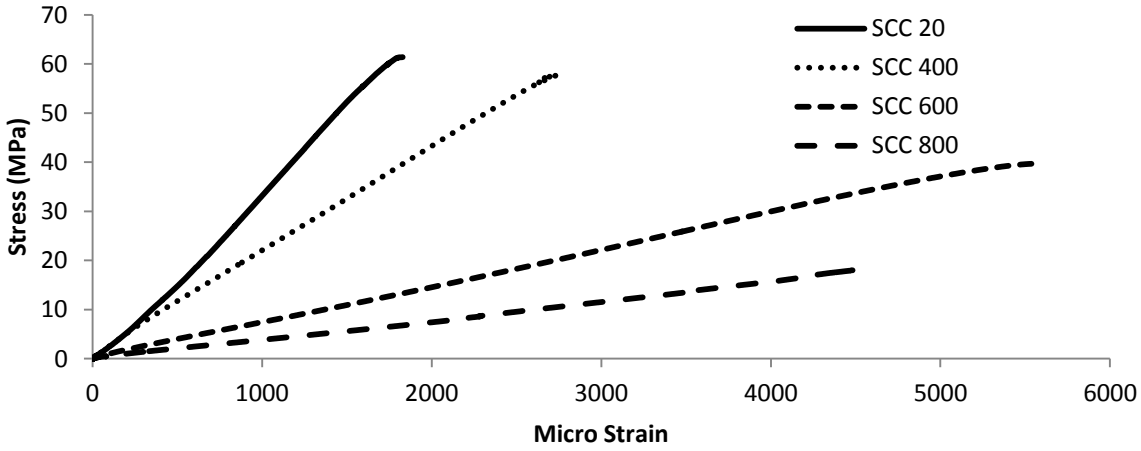

Figure 3.16- Stress-strain behaviour of self consolidating concrete at elevated temperatures (°C)

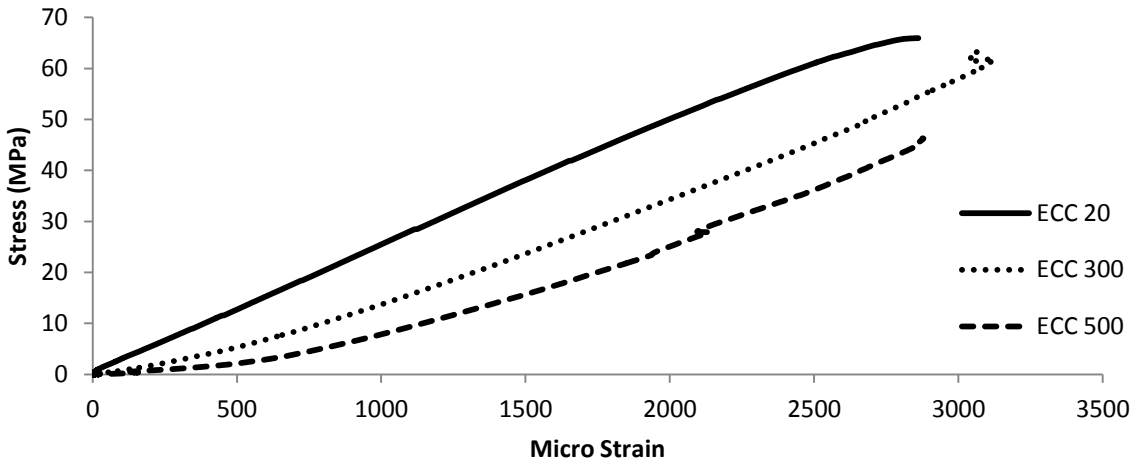

Figure 3.17- Stress-strain behaviour of engineered cementious composite at elevated temperatures (°C)

3.3.5 Softening of Compressive Strength due to Elevated Temperatures

The maximum compressive strain allowed in the design of NSC in Eurocode 4 (2005) is 2500 μm/m at 20°C. But when the concrete is heated to elevated temperatures, the maximum allowable compressive strain is still the same, but occurs at a lower compressive stress than the maximum compressive stress at that temperature. This behaviour is known as softening of the concrete due to exposure to elevated temperatures. Therefore, the compressive stress of NSC to be used in design at different temperatures is equal to the compressive stress observed in that concrete at a strain level equal to 2500 μm/m, for any given temperature. The same is also true for SCC and ECC exposed to elevated temperatures except that at 20°C, the maximum compressive strain is approximately 1828 μm/m for SCC and 2779 μm/m for ECC which are lower and higher, respectively than the maximum compressive strain of NSC.

The relative compressive strength after softening of the concrete (f'_{cst} / f'_{c20}) also termed as softening factor for concrete due to fire degradation ($ß_{cs}$) was calculated for each temperature by determining the ratio between the compressive strength at a given temperature due to softening (f'_{cst}) to the compressive strength at ambient temperature (f'_{c20}), as shown in Table 3.6. The degradation of compressive strength due to softening of each of the concrete type and the reduction factors based on Eurocode 4 (2005) for normal strength concrete due to softening are presented in Fig.3.18.

It was observed that overall effect of softening on the compressive strength of ECC was not as high as observed in SCC. The modulus of elasticity of each concrete at each given temperature, affects the stress reached by each concrete at each temperature, based on comparison to the maximum strain at ambient temperature. A direct comparison was made between the behaviour of the modulus of elasticity (shown in Fig.3.15) and the reduction in compressive strength due to softening (shown in Fig.3.18), which indicated that the behaviour of both properties is exactly the same. Therefore, the behaviour of the reduction in compressive strength due to softening is explained by the behaviour of the reduction of the modulus of elasticity as explained in the previous section.

At 500°C, the effect of softening of the concrete has reduced the compressive stress observed at maximum compressive strain by 30% in ECC, and at 800°C, the effect of softening of the concrete has reduced the compressive stress observed at maximum compressive strain by 89% in SCC (Fig.3.18).

Analytical models (Eqs.3.8 to 3.9) are formulated to model the effect of softening on the maximum compressive strength of SCC and ECC due to exposure to elevated temperatures in the form of fire softening factors for concrete due to fire degradation ($ß_{cs}$) as function of temperature (t):

SCC

$$ß_{cs} = f'_{cst} / f'_{c20} = -0.000000102t^2 - 0.00111t + 1.03 \text{ for } 20\ °C \leq t \leq 800\ °C \ (r^2 = 0.98) \qquad [Eq.3.8]$$

ECC

$$ß_{cs} = f'_{cst} / f'_{c20} = -0.00000062t^2 - 0.000316t + 1.01 \text{ for } 20\ °C \leq t \leq 500\ °C \ (r^2 = 1.00) \qquad [Eq.3.9]$$

Table 3.6- Compressive stress to reach maximum strain after exposure to elevated temperatures

	SCC				ECC		
Temperature (°C)	20	400	600	800	20	300	500
Stress at Maximum Strain (MPa)	63.0	39.7	16.1	6.8	61.4	52.8	42.8
Relative compressive stress/softening factor (f'_{cst}/f'_{c20})	1.00	0.63	0.26	0.11	1.00	0.86	0.70

f'_{cst} - maximum compressive cylinder strength of concrete at a given temperature due to softening of concrete,
f'_{c20} - maximum compressive cylinder strength of concrete at a 20°C

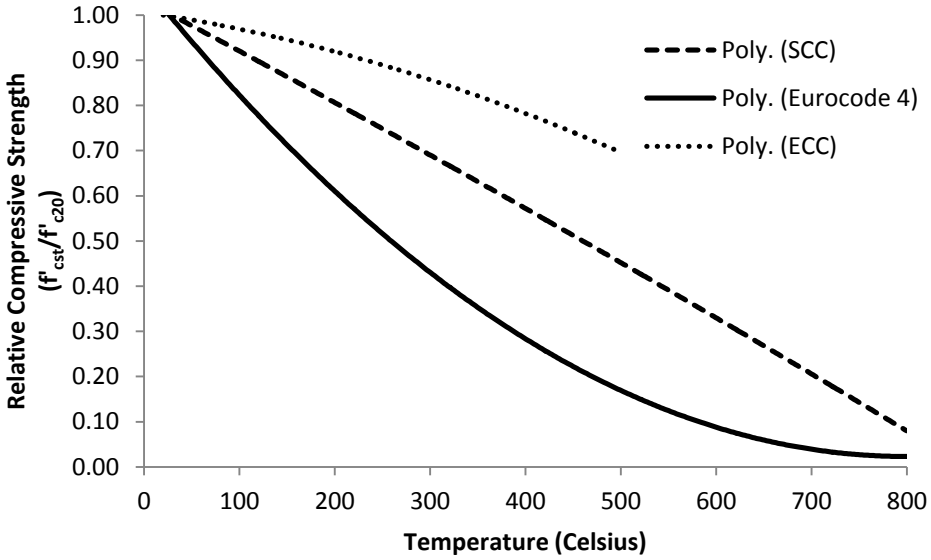

Figure 3.18- Relative compressive stress/softening factor after exposure to elevated temperatures

3.3.6 Failure Modes and Durability of Concrete Specimens at Elevated Temperatures

The failure of SCC cylinders tested after exposure to elevated temperatures is shown in Fig.3.18. Failure at 20^{o}C occurred at the top in a cone and shear pattern while between 400°C and 600°C, pure shear failure occurred from side to side. This behaviour is similar to conventional concrete where failure occurred along the bond between mortar and aggregate. At 800^{o}C, a pure columnar failure occurred from the top to the bottom (Fig.3.19) due to weakened condition of the concrete at the top and bottom of the cylinder. ECC concrete cylinders tested at control and at elevated temperatures failed from the top to the bottom showing a pure columnar failure as depicted in

Fig.3.20. This was due to the PVA fibers and the highly-dense concrete matrix which prevent shear failure. All heated and unheated UHPC concrete cylinders showed similar cone type failure (Fig.3.21) when not exploded. This was due to the steel fibers and the highly-dense concrete matrix which prevent shear failure of the concrete by controlling the crack width and limiting the cracks.

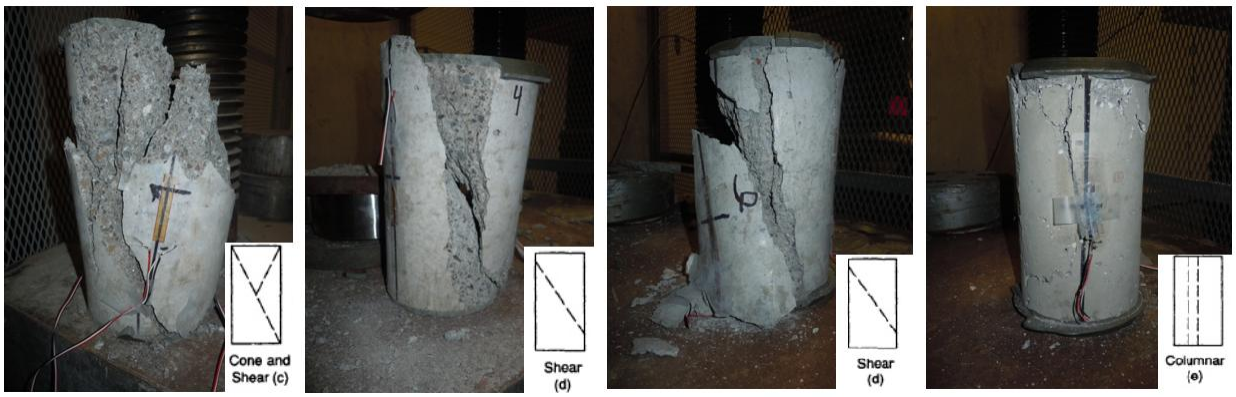

Figure 3.19- Failure Mode of SCC Cylinder at Control, 400°C, 600°C, and 800°C

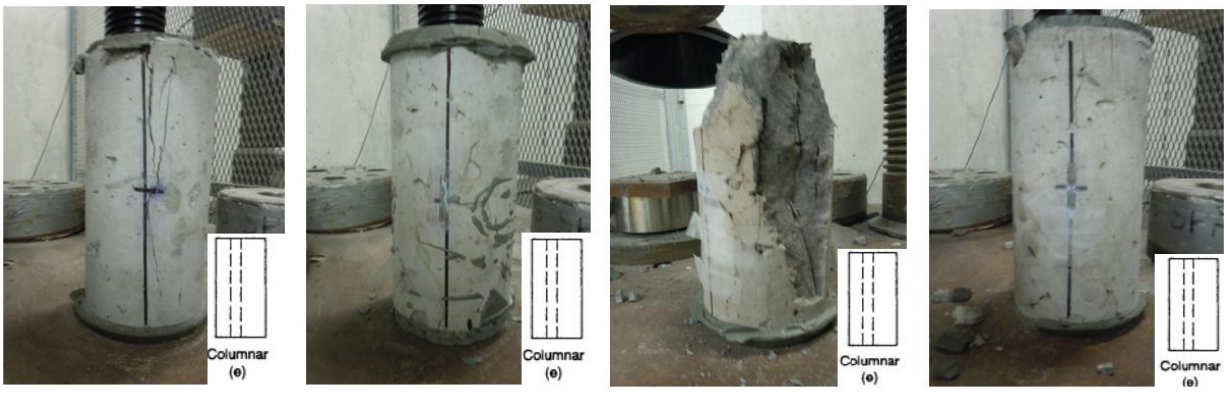

Figure 3.20- Failure Mode of ECC Cylinder at Control, 300°C, 400°C, and 500°C

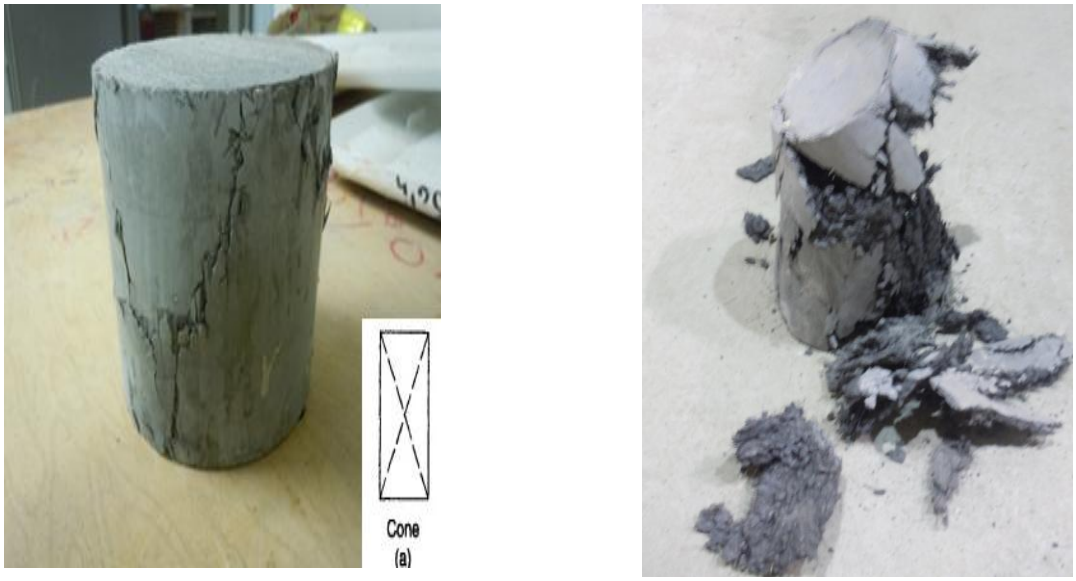

Figure 3.21- Failure mode of UHPC unheated cylinder (left) and heated cylinder to 400°C (right)

It was observed that when UHPC was heated to temperatures higher or equal to 400°C, explosive spalling of the concrete would occur, as shown in Fig.3.21. The explosive spalling occurred from the middle towards the top or about one-third from the top. This spalling was due to excessive water vapour pressure from unbounded water that built up in the concrete when heated that was unable to escape due to the very low permeability of this type of concrete, similar to the behaviour of HPC observed by Peng et al. (2006). It should be noted that explosive spalling did not occur in all cylinder samples heated past 400°C. Some cylinders had minor to extensive cracking only, depending on the temperature.

It was observed that when ECC was heated to elevated temperatures, that PVA fibers would begin to melt inside the concrete, as shown in Fig.3.26. As the fibers melted, the volume occupied by the fibers decreased, forming or increasing the porosity of the concrete. This increase in porosity which allowed portions of the unbounded water that became vapor during heating the ability to expand into these voids and help relieve pressure. There was no evidence of explosive spalling with ECC. This behaviour of ECC was also observed by Sahmaran et al. (2010).

Figure 3.22- Voids present in ECC after melting of PVA fibers

3.3.7 Physical changes after Exposure to Elevated Temperatures

Spalling of the concrete was not observed in any of concrete cylinders composed of SCC, when exposed up to temperatures of 800°C. Minor discolouration was observed up to 400° C with no indication of externally visible cracks or damage. At 600° C, minor discolouration and damage in the form of cracking was evident throughout the cylinder. At 800° C, minor discolouration with exterior surface coated with dust or powder was observed. Damage in the form of cracking was evident throughout the cylinder after heating. (Fig.3.23)

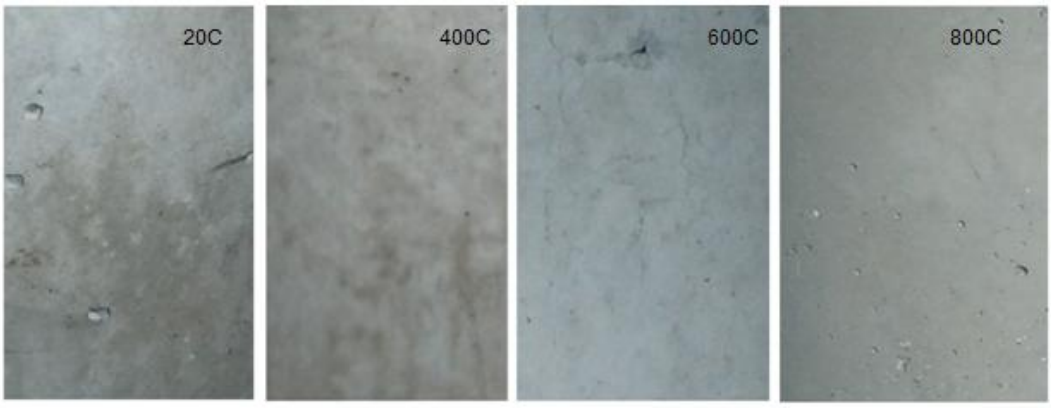

Figure 3.23- Physical changes of SCC cylinder at Control, 400°C, 600°C, and 800°C

For ECC cylinders, minor discolouration was observed up to 300^{o}C with no indication of externally visible cracks or damage. At 400°C, concrete cylinders also had minor discolouration with damage in the form of cracking throughout the specimens. Similar to SCC, ECC specimens at 500°C showed minor discolouration with exterior surface coated dust or powder. Damage in the form of cracking was evident throughout the cylinder at 400°C. However, cracks were quite larger and contain large portions of discolouration in and around the cracks (Fig.3.24).

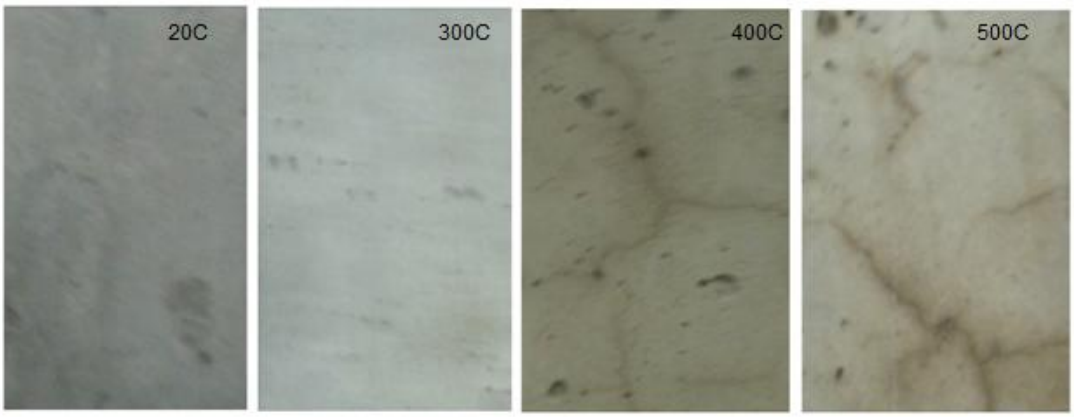

Figure 3.24- Physical changes of ECC Cylinders at control, 300°C, 400°C, and 500°C

UHPC cylinders did minor discolouration at 400°C with damage in the form of cracking. At 600° C, cylinders had minor discolouration with damage in the form of cracking throughout the cylinders to a greater degree than the observed at the previous temperature. At 800°C, cylinders minor discolouration with pinkish colour was still observed. Damage in the form of extensive cracking was evident throughout the cylinder after heating to 600° C and above with larger cracks (Fig.3.25).

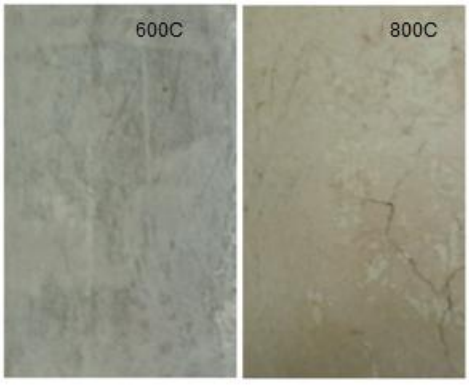

Figure 3.25- Physical changes of UHPC Cylinder at 600°C and 800°C

3.3.8 Mass Loss Elevated Temperatures at and its effect on Compressive Strength and Modulus of Elasticity

The mass loss of all concrete types is presented in Fig.3.26. Fig.3.27 and Fig.3.28 show the effect of mass loss on compressive strength and modulus of elasticity of SCC, ECC and UHPC mixtures.

When concrete is heated to elevated temperatures, the mass of the concrete decreased. This decrease in mass was attributed to the loss of unbounded water in the early stages (ambient to 150°C) and bound water between 150°C and 300°C as it evaporates into water vapour at elevated temperatures (Fares et al. 2009). The majority of the mass loss of SCC observed at 400°C, which was a loss of 5.35%, was attributed to evaporation of the unbounded and later bounded water. Based on the behaviour of SCC observed in Fares et al. (2009), it is assumed that the majority of the loss occurred before 300°C. Between 400°C and 600°C there was less change in mass, which was 7.54%, indicating that the majority of the water has evaporated. The change in mass in this temperature range is explained by the cracking observed at 600°C, which released small amount of dehydrated sand, slag and cement paste (including decomposed calcium hydroxide). After the SCC was exposed to 800°C, there was a larger mass loss observed, which was 15.67%, which was around two times more than the mass loss observed at 600°C. This additional mass is caused by the weakening of the bond between the aggregate and the paste due to the contraction of the paste and expanding of the aggregate as observed in Behnood and Ghandehari (2009), and the breakdown of the integrity of the aggregates, similar to the behaviour observed in Bastami et al. (2011). It was observed in the cylinders composed of SCC that were heated to 800°C that the aggregates now appeared white and some of them were loose from the cement paste and sand, which was also severely damaged. The dust and powder observed along the surface of the concrete was produced as a result of this breakdown and some of it must have fell from the surface before weighing of the concrete sample, thus reducing the weight.

The behaviour of ECC up to 225°C is assumed to be the same as SCC expect for the fact that ECC has a much denser and has a lower permeability than SCC (Lepech and Li 2008b). Therefore the amount of mass loss would be less than SCC. The same is true for UHPC, but to

an even greater extent given that this concrete is denser and has lower permeability than ECC (Chan et al. 2008a). At 200°C it is observed in UHPC that less than a percent of mass loss has occurred at this point, which is a result of the low permeability of this type of concrete.

It is assumed that up to 225°C, the mass loss of ECC is less than the mass loss of SCC due to the low permeability of ECC, but at both 300°C and 400°C it is observed that the mass loss of ECC, which was 9.61% and 11.91%, respectively, was higher than the mass loss observed in SCC (2.2 times greater at 400°C). The reason for this difference in mass loss is the fact that at 225°C, the PVA fibers present in ECC begin to melt and by 300°C, it was observed that the melted fibers had evaporated, thus causing an overall decrease of mass due to less polyvinyl alcohol being present in the concrete. The effect of melted fibers on the mass loss of this concrete was also observed by Sahmaran et al. (2010). In addition, the melting of PVA fibers creates pores in which some of the water vapour from unbounded and bounded water that couldn't escape before due to low permeability is now free to do so. This is why explosive spalling is not observed in ECC, even though it has a low permeability, which also occurred in ECC observed by Sahmaran et al. (2010). Between 400°C and 500°C cracks were formed, which similar to SCC and observed in ECC by Sahmaran et al. (2010). During this time, small amounts of dehydrated sand, slag and cement paste might have been released during the cracking. The mass loss at 500°C, which was 14.41%, is still higher than SCC due to the accumulated mass loss that occurred at earlier temperatures due to the melting of the PVA fibers.

It is assumed that up to 400°C, the mass loss of UHPC is less than the mass loss of SCC due to the low permeability of UHPC, but at 400°C it is observed that the mass loss of UHPC, which was only 8.87%, was higher than the mass loss observed in SCC (1.7 times greater at 400°C).

UHPC does not have PVA fibers, instead they have steel fibers, which do not melt or evaporate at these tested temperatures. The reason for this difference in mass loss is the fact that at 400°C, the water vapour pressure from both the unbounded and bounded water that was unable to escape before due to the low permeability of this type of concrete, now escapes through cracks that form due to the thermal stresses on the concrete and the stresses induced by the water vapor pressure itself (Chan et al. 2008a). If explosive spalling does not occur, portions of the concrete may be

realised, similar to SCC, but with greater amount due to larger cracks. This explains why the mass loss is higher in UHPC than SCC.

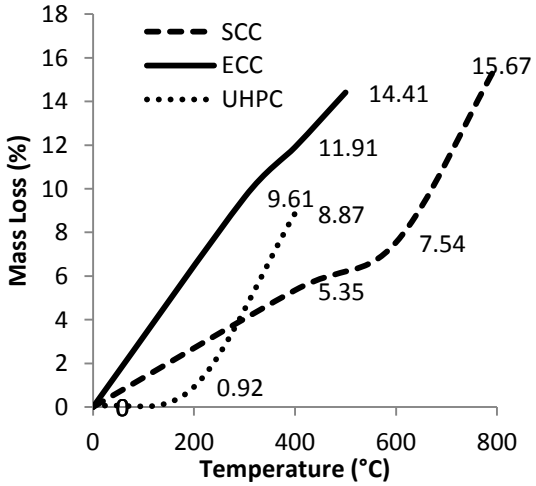

Figure 3.26- Mass loss in all concrete types after heating

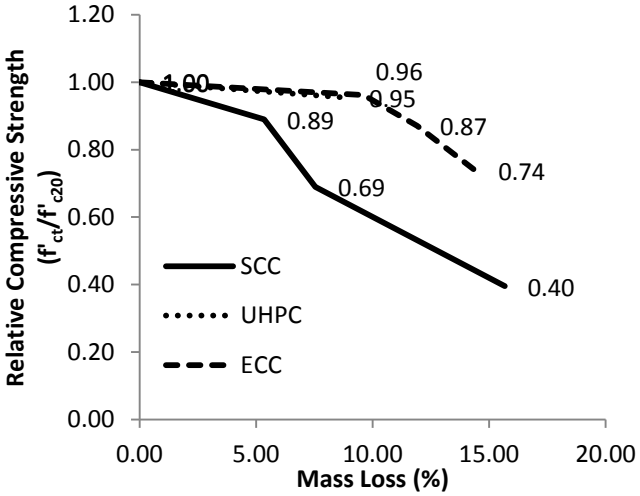

Figure 3.27- The effect of mass loss on the residual compressive strength of all concretes

All concrete types have the general trend of increased mass loss as the temperature increases, which is to be expected. The greatest decrease in compressive strength for SCC occurs between 600°C and 800°C, which also is the same temperature range in which the greatest reduction in mass is observed. This result makes senses given that the greatest mass loss is caused by the loss of integrity of the aggregates and the cement paste in this temperature range, which would decrease compressive strength considerably.

The greatest decrease in compressive strength for ECC occurs between 300°C and 500°C, which occurs after the melting of the PVA fibers. Along with the loss of strength due to degradation of the PVA fibers, the melting of these fibers is increasing the porosity of the concrete and thus reducing the compressive strength. Since the melting of the PVA fibers occurs before 300°C, the majority of mass loss should be before that temperature is reached, which is what was observed. The behaviour of UHPC closely matches that of ECC (Fig.3.27).

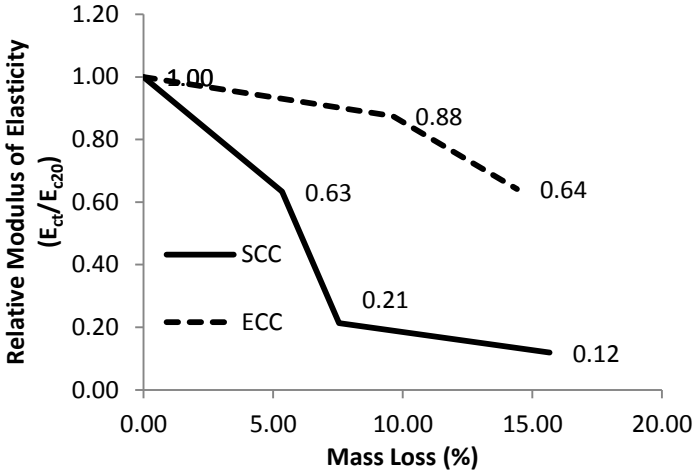

Figure 3.28- The effect of mass loss on the residual modulus of elasticity of SCC and ECC

The modulus of elasticity of SCC decreased by 37% up to 400°C and by 79% up to 600°C. This reduction in modulus of elasticity, which is the highest, is observed to occur in the temperature ranges between ambient temperature and 400°C and between 400°C and 600°C, where the mass loss is the second and third largest reduction of mass. This behaviour is the opposite of what is observed in the reduction of compressive strength for SCC, indicating that the increase in porosity of the concrete in this temperature range has a greater effect of the modulus of elasticity than on compressive strength. The greatest decrease in modulus of elasticity for ECC occurs between 300°C and 500°C, which was 12% and 36%, respectively, which occurs after the melting of the PVA fibers. This behaviour is the same as what was observed in the reduction of compressive strength for ECC, due to the fact that the PVA fibers due not melt until 225°C and evaporated around 300°C which causes the porosity to not significantly change until the temperature range of 300°C to 500°C, a later temperature than observed in SCC as shown in Fig.3.28.

3.4 Chapter Conclusion

In this chapter, experimentation was conducted on the individual materials that make up the composition of the DSCWs. The effect of elevated temperatures on the post-fire material properties of both the steel sheeting and the three different high performance concretes (HPCs);

Self-Consolidating Concrete “SCC”, Engineered Cementitious Composite “ECC”, and Ultra High Performance Concrete “UHPC” were investigated.

The steel sheeting during post-fire conditions performed better, up to 800°C, than the steel illustrated in Eurocode 4 (2005), Kankanamge and Mahendran (2011), and other previous research studies, in which the results were based on the steel being tested in a fire setting. The steel sheeting in the current study performed better because it was able to regain a portion of its strength and modulus of elasticity (that was reduced during the fire) during the post-fire cooling period.

Both SCC and ECC performed better at elevated temperatures of up to 800°C (500°C for ECC) than normal strength concrete illustrated in Eurocode 4 (2005) in terms of residual maximum compressive strength and modulus of elasticity. The behaviour of both SCC and ECC before 225°C regarding the compressive strength is the same. Due to the melting of PVA fibers which occurs at this temperature, the porosity of ECC increases at a faster rate than SCC and therefore the compressive strength of ECC begins to fall below SCC around 300°C (which is the approximate temperature of the evaporation of the PVA fibers). UHPC performed very close to that of normal strength concrete with lower reduction before 400°C and higher reduction after 400°C.

Regarding the modulus of elasticity, the reduction found in ECC was less than the reduction observed in SCC. The lower reduction in ECC, when compared to SCC, is due to the remaining PVA fibers in the concrete that have solidified after cooling and are able to help deter the reduction in modulus of elasticity, through the added flexibility they provide.

Analytical models are derived as function of temperature for the residual yield strength (f_y) and the modulus of elasticity (E_s) of the steel sheeting as well as (residual compressive strength (f'_c) and the modulus of elasticity (E_c) of different concretes. These models can be applied to develop models for the strength of DSCWs or other composite structures (made with these materials) exposed to elevated temperatures.

CHAPTER 4

Steel Sheeting Walls and Profiled Concrete Walls Exposed to Elevated Temperatures

4.1 Introduction

In this chapter, experimental results on the axial load behaviour of steel sheeting walls (SSWs) and profiled concrete walls (PCWs), which are components of double skin composite walls (DSCWs) subjected to elevated temperatures are presented and discussed. The SSWs are composed of a pair of profiled light-gauge cold-formed steel sheets having a thickness of 0.61mm and PCWs are composed of three types of high performance concrete (HPC): Self-Consolidating Concrete (SCC), Engineered Cementitious Composite (ECC), and Ultra High Performance Concrete (UHPC). The performance of the walls is described based on post-fire residual axial load capacity or strength, axial load-deformation response, stiffness/ductility, load-strain characteristics and failure modes. The walls were tested after being exposed to elevated temperatures of up to 800°C (500°C for ECC).

4.2 Behavior of Steel Sheeting Walls

4.2.1 Specimen Preparations and Testing Methodology

Steel Sheeting Walls (SSWs) having an overall dimensions of 540 mm x 320 mm containing no concrete in-fill, were constructed by attaching two profiled light-gauge cold-formed steel sheets of thickness 0.61 mm by using intermediate fasteners at each trough, in five rows at spacing of 110 mm at the top and bottom and 140 mm at the center (Figs.4.1-4.3).

The SSW specimens were heated at a rate of 2.5°C/min in a kiln up to the given temperatures of 400°C, 600°C and 800°C and sustained at the respective steady state temperatures for two hours before being allowed to cool down naturally to ambient temperature. This rate was chosen to

correspond to the rate used in the material testing of steel sheeting samples described in Chapter 3. However, the rate of heating is significantly lower than the standard fire rate of temperature rise specified by ASTM E 119a (2000), which is about 600°C in the first 6.7 min. This was due to the limitations of the kiln. The heating and cooling curves for each temperature are presented in Fig.4.4. Heated wall specimens along with the un-heated walls were then tested in an axial compression testing machine until failure, as shown in Fig.4.5. Strain gauges were installed at key locations on the crests at the top (65 mm from the top) and at the middle of the wall as shown in Fig.4.2. During testing axial load- deformation response and strain development were obtained using data-acquisition system. The SSWs were loaded at a loading rate of 50 kN/ min until failure.

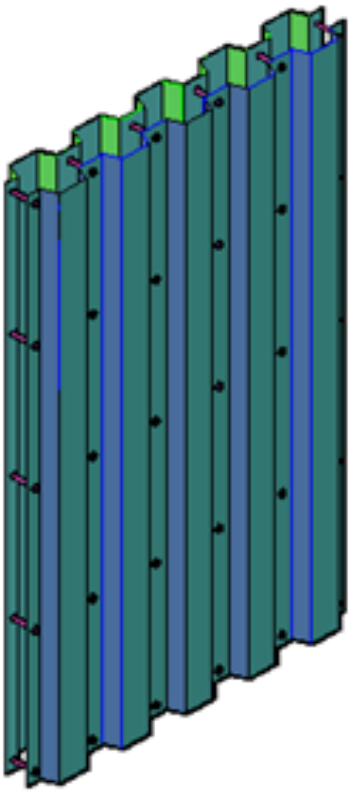

Figure 4.1- Steel sheeting wall

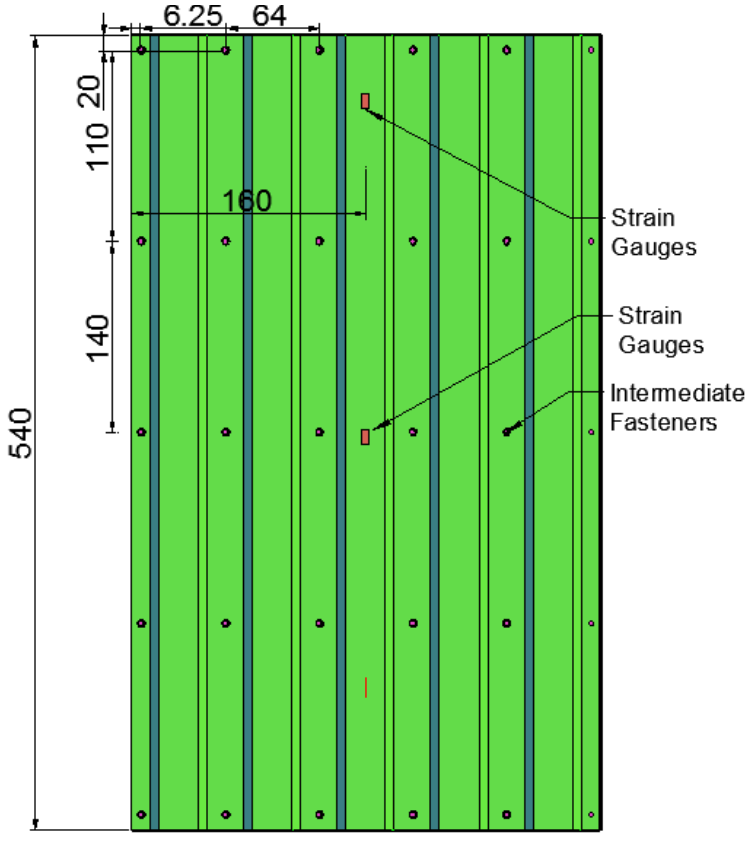

Figure 4.2- Dimensions of steel sheeting wall (dimensions in mm)

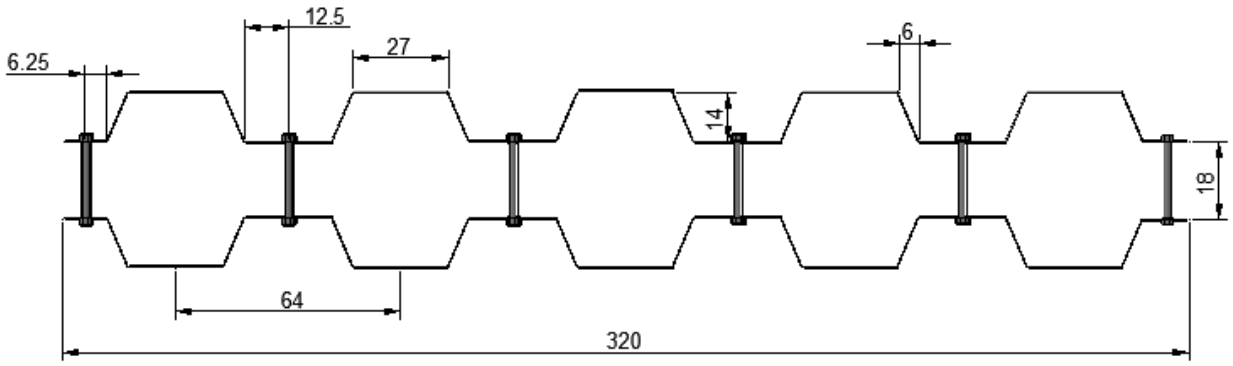

Figure 4.3- Cross section of steel sheeting wall (dimensions in mm)

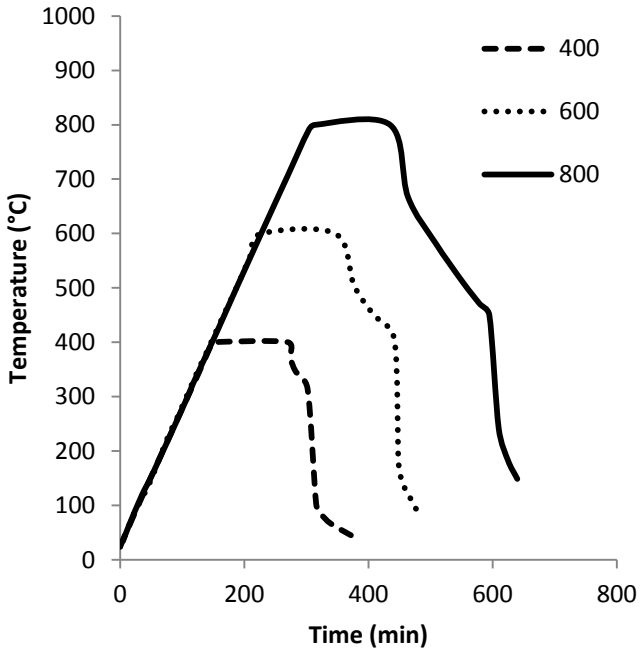

Figure 4.4 – Heating-cooling curves for steel sheet and profiled concrete walls composed of SCC and UHPC

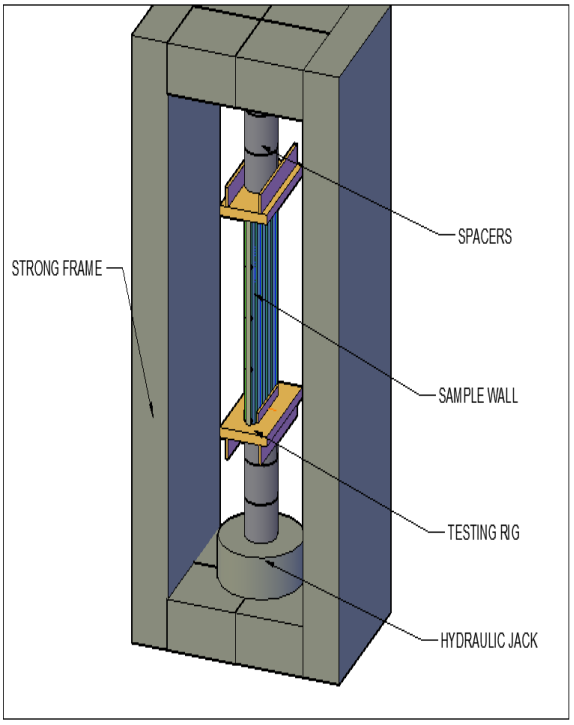

Figure 4.5- Axial loading test setup for steel sheet and profiled concrete walls

4.2.2 Physical Changes of Steel Sheeting Walls

At temperatures up to 400°C, there was no discolouration or damage of the exterior surface of the steel (Figs.4.6-4.7). Minor greyish discoloration was observed at 600^{o}C, as a form of dust or powder. At 800°C, the discoloration was a mixture of black and brown, and instead of being a fine dust or powder, the burnt portions of the steel peeled or flaked off, indicating a greater extent of damage compared to those specimens heated at 600°C. No physical damage was observed on any of the steel sheeting walls heated to elevated temperatures. This behaviour was similar to what was observed in light gauge cold-form steel columns exposed to temperatures up to 800°C observed by Ranawaka & Mahendran (2009b).

4.2.3 Axial Load Capacity and Failure Modes of the Steel Sheet Walls

The failure modes of the SSWs at all temperatures (400°C, 600°C and 800^{o}C) including ambient temperature subjected to post-fire axial loading, are presented in Figs.4.6-4.8. The failure of the un-heated (control) SSWs was due to global buckling at the mid section around the middle line of bolts on one side of the wall. The buckling in this region was sudden, and observed when the ultimate load capacity was reached. The formation of plastic hinges at areas of local buckling in the troughs around the middle section of the wall was evident. First buckling occurred on one side and the intermediate fasteners of the wall remained attached to both sheets during this time. This caused the middle of the wall to lean away from the side (steel sheet) of first observed buckling. Since both sides (steel sheets) were still interacting with one another, the other side was forced to buckle in the same direction causing the wall to experience eccentric loading that gradually increased until the test was concluded. This resulted in tension in one sheet and compression in the opposite sheet. This additional bending stress from the eccentric loading decreased the load capacity of the wall, in comparison to a steel wall that did not buckle and reached full yield load capacity.

Due to the unstable nature of this failure, the SSWs were unable to carry any additional load after the buckling load was reached and post-buckling load level decreased rapidly. Therefore, the steel sheet walls were unable to reach the ultimate yield load capacity. The SSWs exhibited

unstable post-buckling behaviour and the walls should not be considered to carry any post-buckling loads.

This post-buckling behaviour differs from the behaviour observed in light gauge cold-form steel columns observed by Ranawaka and Mahendran (2009b). The steel columns were able to reach the yield load capacity, even though it was only about 9% higher than the buckling load capacity. The reason for this dissimilarity lies in the difference of configuration. The steel sheets in these experimental SSWs were tied together with intermediate fasteners but in columns tested by Ranawaka and Mahendran (2009b), the steel sections were only attached together on one side in an enclosed c-shape. When load was applied to the steel columns, the columns deflected laterally outwards or inwards, on the open side, in the opposite direction. Since the steel on each side of the opening deformed independently of each other, no eccentric loading occurred.

The failure behaviour of SSWs heated to 400°C was approximately the same as unheated wall with slightly varying axial vertical displacement and maximum load capacity. There was also a shift of the buckling from around the middle line of bolts to the second line of bolts (Figs.4.6-4.8). This observation makes sense due to the fact that steel sheeting has relatively the same properties for the yield strength and modulus of elasticity at both temperatures.

The failure behaviour of the SSWs heated to 600°C and 800°C was different than those tested at lower temperatures. These walls failed more gradually at failure than the other walls, but these walls still exhibited unstable post-buckling behaviour. In the case of the 600°C wall, there was also a shift of the buckling from around the middle line of bolts to the fourth line of bolts region (Figs.4.6-4.8). The opposite behaviour observed in the 400°C wall. For the 800°C wall, it was observed that the buckling failure occurred in the troughs around the middle of the wall along the middle line of bolts, similar to the un-heated wall. There was a decrease in the maximum compressive strength or load capacity of the wall after exposure to elevated temperatures.

20°C 400°C 600°C 800°C

Figure 4.6- SSWs after failure (left view) for control, 400°C, 600°C and 800°C

20°C 400°C 600°C 800°C

Figure 4.7- SSWs after failure (front view) for control, 400°C, 600°C and 800°C

The SSW's up to 400°C retained the same maximum load capacity as those at ambient temperature (Table 4.1, Fig.4.9). This observation makes sense due to the fact that steel sheeting has relatively the same properties for the yield strength at both temperatures. The experimental load capacity at each temperature (N_{et}) is compared to the experimental load capacity observed at ambient temperature (N_{e20}) by using relative load carrying capacity (N_{et}/N_{e20}). The maximum load capacity of the SSW's at 600°C and 800°C was reduced by 12% and 61%, respectfully (Fig. 4.9). The greatest reduction in maximum load capacity was observed between 600°C and 800°C, which was similar to the behaviour of the yield strength reduction of the steel sheeting observed from experimentation.

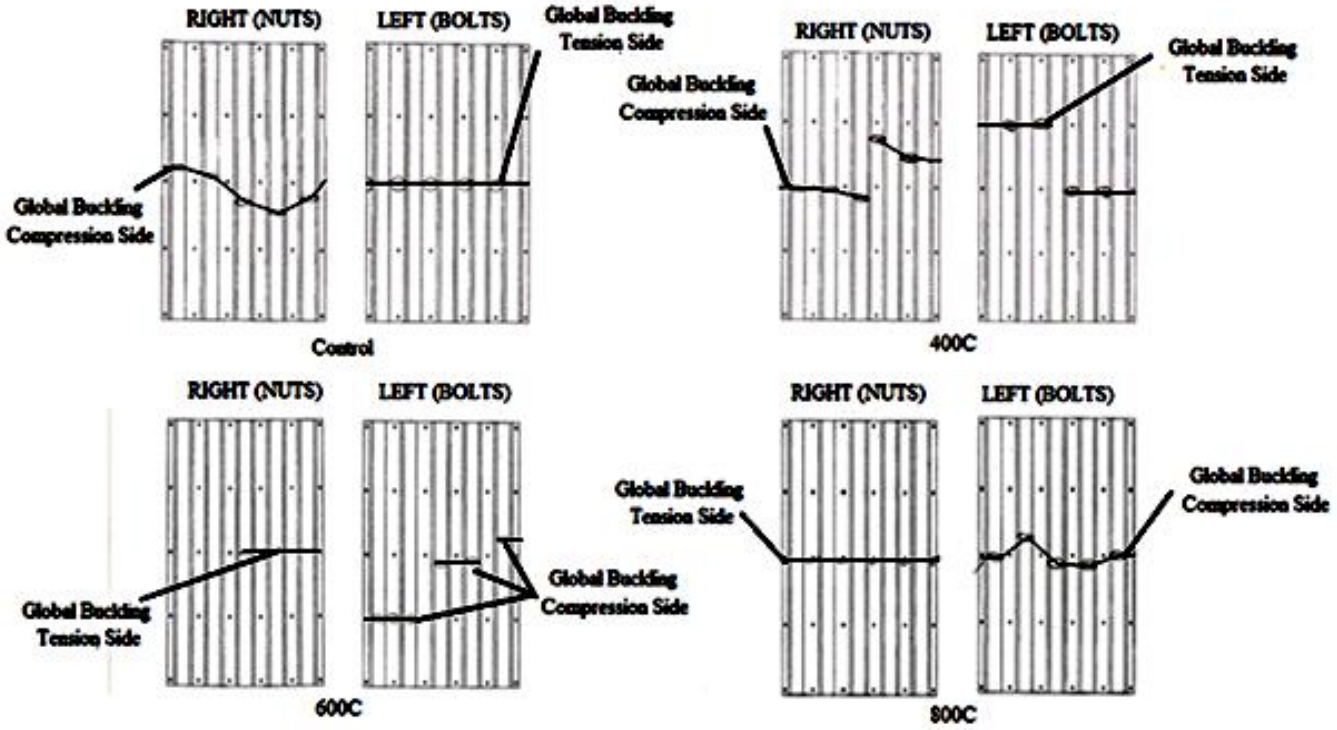

Figure 4.8- Steel sheeting wall failure diagram for Control, 400°C, 600°C and 800°C

Table 4.1- Experimental load capacity for steel sheeting walls exposed to elevated temperatures

Temperature (°C)	20	400	600	800
N_e (kN)	131	132	116	52
Relative Load Capacity (N_{et}/N_{e20})	1.00	1.01	0.88	0.39

N_e – experimental load capacity of wall, N_{et}- experimental load capacity of the wall at a given temperature, N_{e20}- experimental load capacity of the wall at 20°C

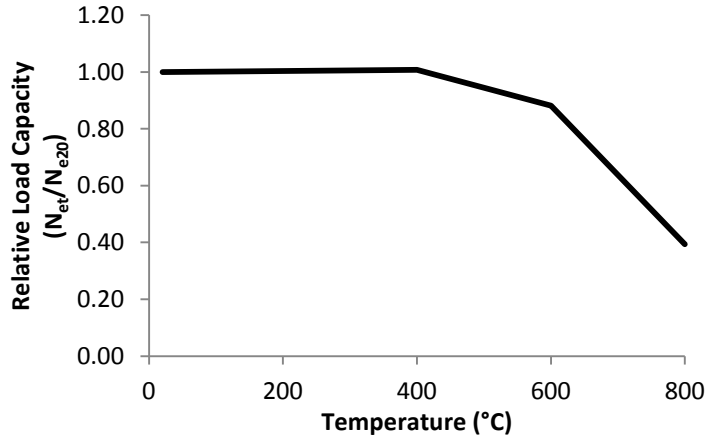

Figure 4.9- Reduction in load capacity of steel sheeting walls exposed to elevated temperatures

4.2.4 Axial Load-Deformation Response and Stiffness/Ductility of the Steel Sheeting Walls

The axial load-deformation response of the SSWs subjected to elevated temperatures is compared in Fig.4.10. The unheated (control) wall and the heated walls behaved in a similar manner showing similar constant initial stiffness (slope of the ascending branch of the axial load-deformation response). The experimental value for the initial stiffness at each temperature (K_{et}) was compared to the experimental value for the initial stiffness observed at ambient temperature (K_{e20}) using relative stiffness (K_{et}/K_{e20}) in Table 4.2 and Fig.4.11.The initial stiffness (K_e) of the SSWs decreased at elevated temperatures. It was observed that the greatest decrease (79% to 22%) in the initial stiffness occurred between 400°C and 600°C, and then decreased to only 12% (about 88% reduction) at 800°C (Fig.4.11). This reduction in initial stiffness is attributed to the decrease in modulus of elasticity and the slight loosening of the nuts on the bolted connections. This loosening was caused by the thermal expansion and contraction of the steel sheeting during heating between 400°C and 600°C and sequential cooling.

Table 4.2- Stiffness and ductility of steel sheeting wall at elevated temperatures

TEMPERATURE (°C)	20	400	600	800
Initial stiffness (K_e) (kN/mm)	59.4	47.1	12.9	7.2
Relative Initial Stiffness (K_{et}/K_{e20})	1.00	0.79	0.22	0.12
$\Delta_{\text{peak load}}$ (mm)	2.21	2.60	9.00	7.31
$\Delta_{0.75\ \text{peak load}}$ (mm)	2.52	2.94	10.00	9.00
K'_e (kN/mm) (Eq.4.1)	105.7	97.1	28.9	7.6
Relative Ductility (K'_{e20}/K'_{et})	1.00	1.09	3.66	13.85

K_e- experimental initial stiffness of the wall, K_{et}- experimental initial stiffness of the wall at a given temperature, K_{e20}- experimental initial stiffness of wall at 20°C, $\Delta_{\text{peak load}}$- the experimental axial deformation of the wall at peak load, $\Delta_{0.75\ \text{peak load}}$- the experimental axial deformation of the wall at 75% peak load, K'_e- experimental post-peak stiffness of the wall, K'_{et}- experimental post-peak stiffness of the wall at a given temperature, K'_{e20}- experimental post-peak stiffness of wall at 20°C

The post-peak ductility of each wall was determined by using the slope of the post-peak descending branch of the axial load-axial deformation response (K'_e), for each wall (Table 4.2).

The slope of the post-peak descending branch of each wall was calculated by determining the slope between the peak load and 75% of peak load using Eq.4.1.

$$K_e' = \left| \frac{P_{peak}(1-0.75)}{\Delta_{peak\ load} - \Delta_{0.75\ peak\ load}} \right| \qquad \text{[Eq.4.1]}$$

where P_{peak} is the maximum axial load capacity of the wall, $\Delta_{peakload}$ is the maximum axial deformation at the peak load, and $\Delta_{0.75\ peak\ load}$ is the axial deformation at 75% of peak load after peak load has been reached.

The relative ductility (K'_{e20}/K'_{et}) of the wall presented in Table 4.2 is defined as the ratio of the post-peak ductility at ambient temperature (K'_{e20}) to the ductility at temperature t°C (K'_{et}).

It was observed that for the unheated (control) wall and the wall heated to 400°C, there was a sharp decrease in load immediately after the peak load showing a descending branch with a high negative slope (Fig.4.10). This indicates an unstable post-peak behaviour with low ductility. This low ductility can be attributed to the commencement of buckling before yielding. The failure was sudden and associated with global buckling at the middle of the wall.

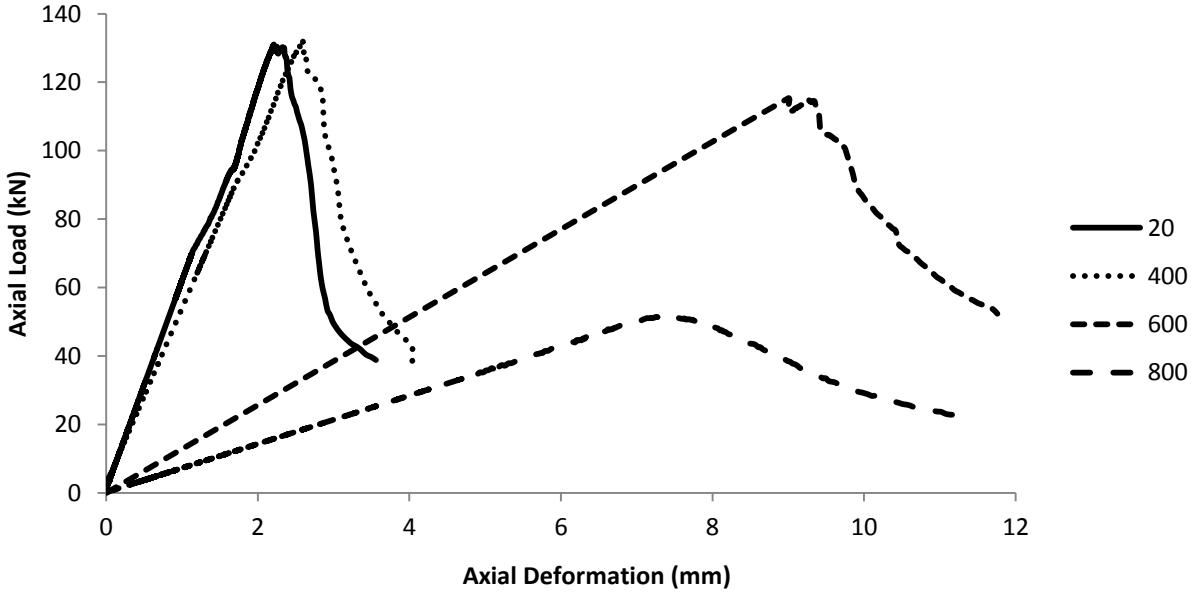

Figure 4.10- Axial load-deformation behaviour for SSWs at elevated temperatures (°C)

The post-peak ductility of the wall increased with the increase of temperature (Fig.4.12). At 600°C, the ductility of the wall increased by a factor of 3.66 compared to ambient temperature. This increased ductility is caused by the steel sheet being softened particularly around the bolt connections, which allowed more post-peak deformation inducing ductile failure. At 800°C, the ductility was increased by a factor of 13.85 compared to ambient temperature and produced an even flatter descending branch. This increased ductility is caused by softening of the entire steel sheet, including around the bolt connections.

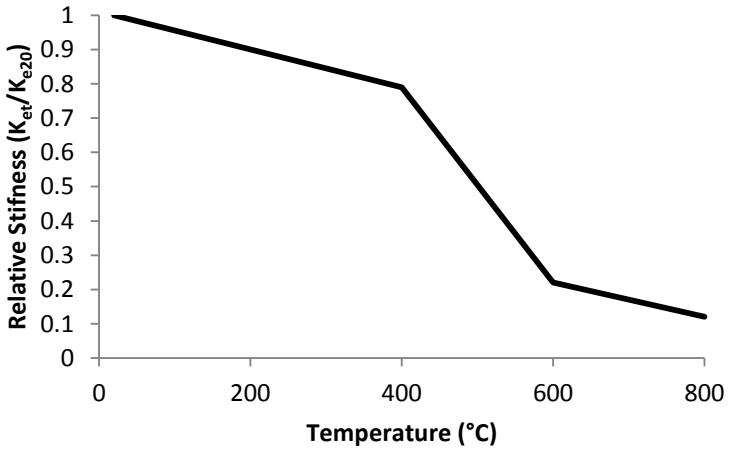

Figure 4.11- Reduction in initial stiffness of steel sheeting walls exposed to elevated temperatures

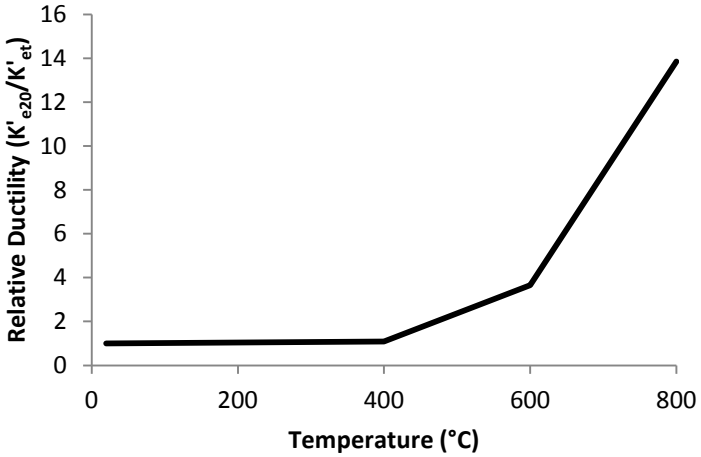

Figure 4.12- Relative ductility of steel sheeting walls at elevated temperatures

4.2.5 Axial Load-Strain Behaviour of the Steel Sheeting Wall

The axial load-strain response at the mid-section of the steel sheet walls are presented in Fig. 4.13. For the unheated (control) wall, the compressive strain at the middle continued to increase until failure. This was also observed for the SSWs heated to 400°C and 800°C. For wall subjected to 600°C, the compressive strain at the middle continued to increase up to about 88 kN (76% of total load capacity) and at that point compressive strain was relaxed due to buckling of the other steel sheet. In all cases, yielding of steel sheeting never occurred at the middle of the wall because the compressive strain at the middle of the wall never reached the yield strain (Y.S.) of the steel. Buckling of the steel sheeting occurred just below the middle of the wall (just below the position of the strain gauge). Therefore the steel sheet walls in all cases were unable to reach yield stress.

The strain at failure observed at the middle of the wall, as well as the percentage of yield strain, is shown in Table 4.3 for all elevated temperatures. The percentage of yield strain can also be taken as the ratio of the buckling stress observed to the yield stress of the steel sheeting. It is found that the developed maximum strain at the middle of the wall ranged between 81 and 90% of the yield strain. In general, strain at failure decreased with the increase of temperature.

Table 4.3- Strain data for steel sheeting walls at elevated temperatures

Temperature	Strain at Failure (Middle)		Strain at Failure (Top)		Y.S.
(°C)	(μ strain)	(% of Y.S.)	(μ strain)	(% of Y.S.)	(μ strain)
Control	2550	89	1662	58	2860
400	1577	81	1101	56	1950
600	1387	90	1099	71	1540
800	1486	86	642	37	1727

Y.S. – the yield strain of the steel sheeting

The axial compressive strain development at the top of the wall for the un-heated (control) SSW and the other heated walls is shown in Fig.4.14. In all cases, yielding of steel sheet never occurred at the top of the wall. The compressive strain at the top of the wall in all cases was less than that observed at the middle. This indicates that load transfer throughout the steel sheeting was not uniform and the middle of the wall was subjected to more stress. This was due to the larger effective length of profiled steel sheet segments between intermediate fasteners at the middle than the top of the wall. The developed maximum strain at the top ranged between 37 and 71% of the yield strain (Table 4.3). In general, maximum failure strain decreased with the increase of temperature.

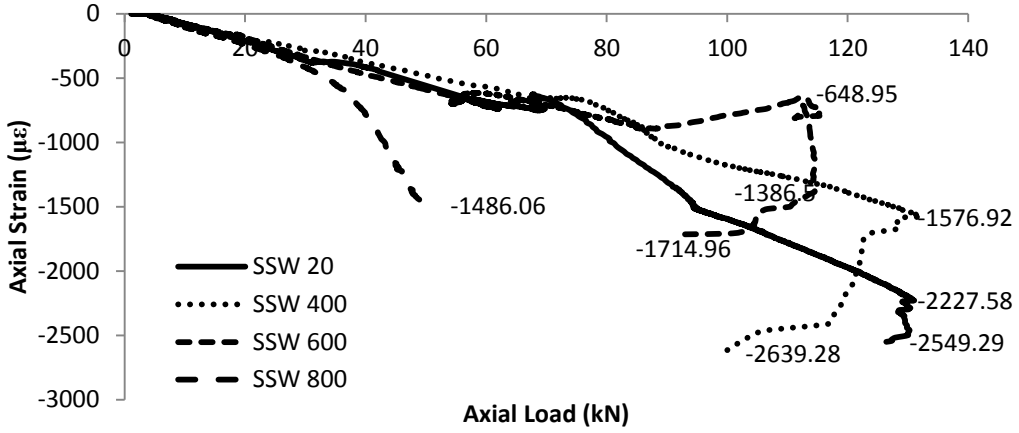

Figure 4.13- Axial load-strain behaviour of steel sheeting walls at elevated temperatures (°C) at the middle

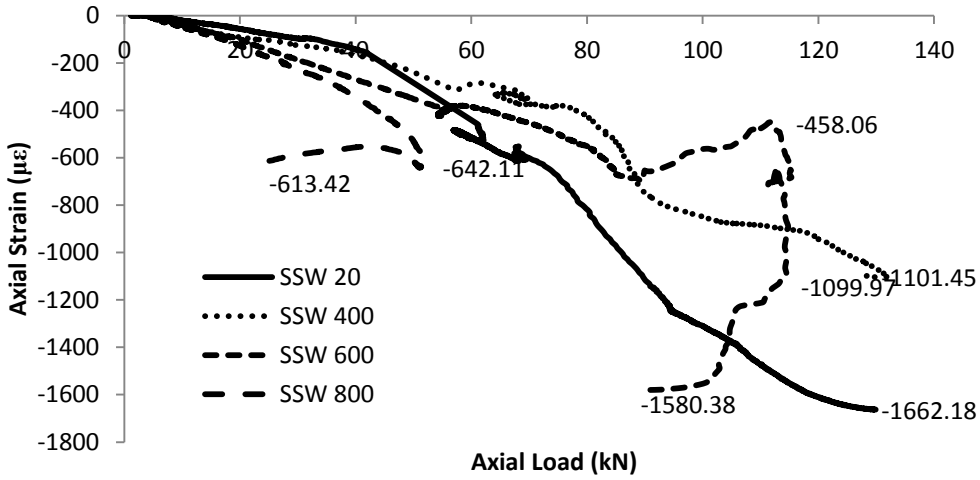

Figure 4.14- Axial load-strain behaviour for steel sheeting walls at elevated temperatures (°C) at the top

4.3 Behavior of Profiled Concrete Wall Exposed to Elevated Temperatures

4.3.1 Sample Preparations and Testing Methodology

Profiled Concrete Walls (PCWs) specimens having overall dimensions of 540mm x 320 mm, containing no profiled steel sheeting, as shown in Fig.4.15, were cast. The PCWs were cast by placing the concrete in between two profiled steel sheeting sheets, used in this case as temporary formwork, as well as timber formwork at the sides and at the bottom as shown in Fig.4.16. In the casting assembly, the wall was braced laterally in the middle by a steel channel to maintain wall verticality as well as to act as lateral support for the hydrostatic pressure of the fresh concrete. In addition, levelling and verticality of the walls were insured by the use of levels and plumb bobs. Additional lateral support in the form of timber members were provided at the top and bottom quarter points of the wall for resisting the fresh concrete pressure. All lateral support, timber and steel sheeting formworks were removed after one day of casting. The walls were then air cured at room temperature until tested (at least 28 days).

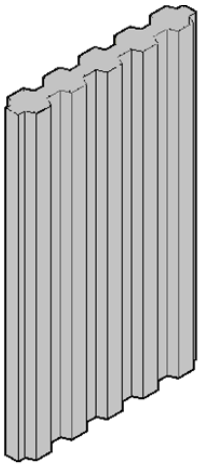

Figure 4.15- Profiled concrete wall

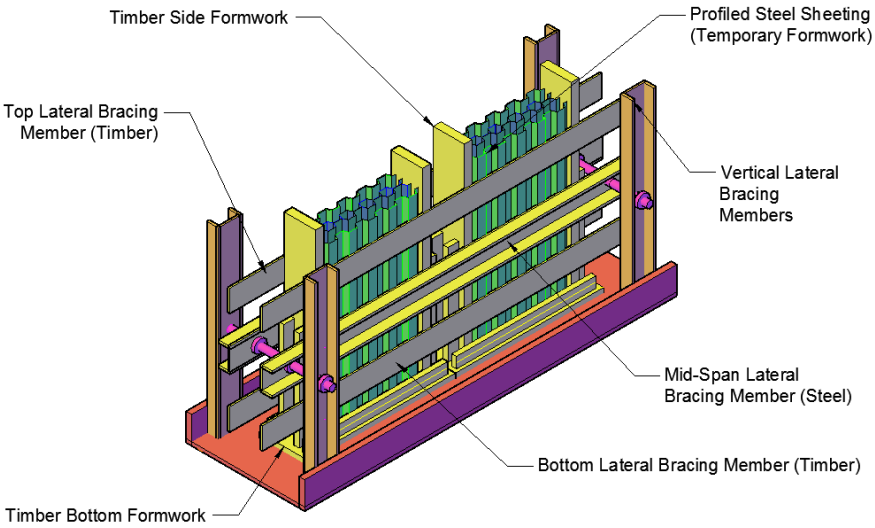

Figure 4.16- Casting setup for profiled concrete walls

The profiled concrete walls (PCWs) were heated at a rate of 2.5°C/min in a kiln up to the steady state temperatures of 400°C and 600°C for SCC and UHPC walls; and 400°C and 500°C for the ECC walls; and were sustained at the respective steady state temperature for two hours (one hour

for ECC) before being cooled down naturally to ambient temperature. ECC walls were heated differently due to lab constraints. This rate was chosen to correspond to the rate used in the material testing of the different concrete types. However, the rate of heating is significantly lower than the standard fire rate of temperature rise specified by ASTM E 119a (2000), which is about 600°C in the first 6.7 min. This was due to the limitations of the kiln. Heating and cooling regimes are presented in Fig.4.4 for SCC/UHPC and Fig.4.17 for ECC. These PCW heated specimens along with the non-heated (control) specimens were then tested in an axial compression testing machine as shown in Fig.4.5. Strain gauges were installed on the crests at the top and the middle of the heated walls (after being cooled) and control walls as shown in Fig.4.2. During testing axial load-deformation response and axial strain development were monitored using a computer aided data-acquisition system. The PCWs were loaded at a gradual rate of 50 kN/ min until failure.

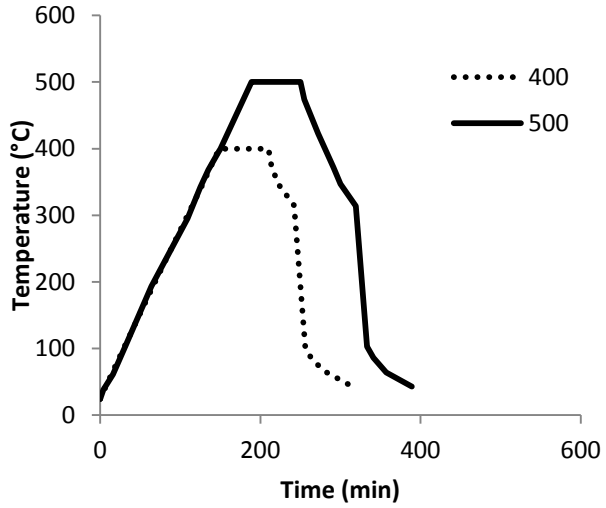

Figure 4.17- Heating-cooling curves for profiled concrete walls composed of ECC

4.3.2 Physical Changes of the Profiled Concrete Walls after Exposure to Elevated Temperatures

The SCC PCWs experienced no spalling of the concrete at all temperatures up to 600°C. No visible cracking was observed in both SCC walls up to 600°C and ECC walls up to 500°C, as shown in Fig.4.18. The reason for the different behaviour of these walls compared to the

cylinders heated in Chapter 3 is the surface area of the concrete and the thickness of the concrete. Due to the greater surface area, the unbounded and bounded water that evaporates has greater ability to escape before resulting in cracking of the concrete. Also, due to the reduced thickness (distance from center to outside layer of concrete) the thermal gradient between the center and outside of the concrete is less than that of the cylinder (100 mm in the cylinder compared to 47 mm in the wall), and therefore the thermal stresses are less there is no cracking.

However, this was not the case for the UHPC wall. There was damage in the form of extensive cracking on the UHPC wall when subjected to 400°C, as shown in Fig.4.19. This cracking was caused by explosive spalling of concrete due to vapour pressure buildup. Portions of the wall broke off suddenly and loud sounds of explosion were heard from within the kiln. The explosive spalling was mostly found on some of the crests and on the exterior edges of the wall. The reason why these areas were more open to explosive spalling is due to the temperature differential between the crests and troughs of the concrete due to the varying thickness and also due the fact that the vapour pressure buildup is observed to be higher in the middle of the concrete then on the outside. This phenomenon was also observed in some of the UHPC cylinders exposed to 400°C. The same reason is also valid for the exterior edges. Therefore, the UHPC PCWs are not suitable for exposure to high temperatures above 400°C. Due to the compromised integrity and damage of this wall, it was not possible to conduct compressive axial test on these walls after exposure to elevated temperatures.

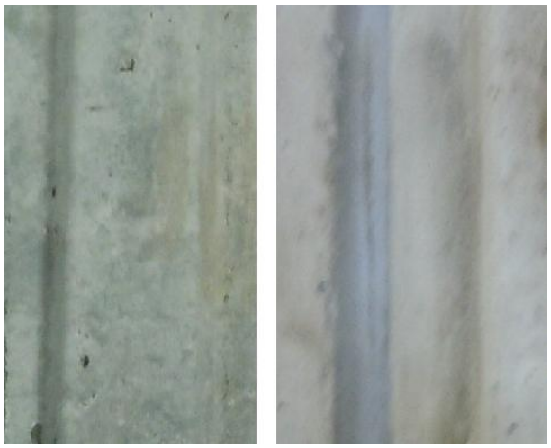

SCC 600°C ECC 500°C

Figure 4.18- Physical changes observed in ECC and SCC profiled concrete walls exposed to elevated temperatures

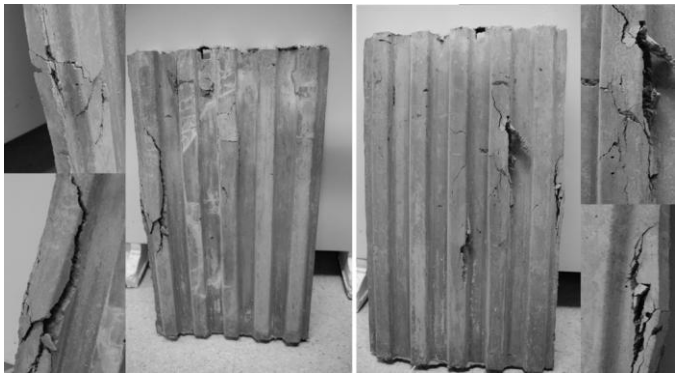

Figure 4.19- Failure of UHPC walls exposed to 400°C

4.3.3 Axial Load Capacity and Failure Modes of the Profiled Concrete Walls

Failure modes of the unheated and heated PCWs subjected to post-fire axial loading are presented in Figs.4.21-4.22. Failure of SCC and ECC non-heated and heated walls subjected to axial compression loading occurred due to the formation of vertical cracking along the wall which led to the crushing of concrete at the top. For the UHPC un-heated wall, the ultimate failure was crushing of the concrete at the top followed by the formation of vertical cracking propagating downwards along the wall.

The SCC unheated wall exhibited the formation of a main vertical crack just prior to failure which ran down the entire wall at the trough in the center web followed by crushing of concrete occurred at the top, as shown in Fig.4.21. Failure occurred first in the trough due to the change in thickness between the crest and through of the webs in the PCWs, which caused an increased stress concentration in the troughs when compared to the crests. The failure at this region occurred as the shear failure between the planes of concrete on either side of the failure. At the plane of failure, bond failure was observed between mortar and coarse aggregates, as shown in Fig.4.20. There was no failure in the coarse aggregates. The specimen also exhibited some areas where concrete broke or spalled off.

The ECC unheated wall exhibited the formation of a main vertical crack at one side of the wall in the trough at the moment of ultimate failure. Failure occurred first in the trough, in a similar manner as SCC. At the plane of failure, it was observed that failure occurred as tearing of

portions of concrete from both sides, as if the concrete in this region was pulling away from each other in the vertical direction, as shown in Fig.4.20. The failure was observed to have a rougher shear plane compared to SCC, which had a smoother shear plane. There was also horizontal cracking along the bottom, where portions of the concrete broke off (Fig.4.21-4.22).

For the UHPC unheated wall, crushing of concrete at the top at the moment of failure was the primary cause of failure. Vertical cracking downwards along the wall did not occur until after the main failure and transpired (Figs.4.21-4.22). This is attributed to the ability of the steel fibers to better control internal cracking and prevent crack propagation until failure (Koksal et al. 2008). There was evidence of vertical cracking with portions of the concrete that broke off, or spalled concrete.

Figure 4.20- Failure in SCC (left) and ECC (right) walls ambient temperature

In general, formation of both downward vertical cracking and the crushing of concrete at the top were sudden and occurred at the ultimate load. As a result, the PCWs were unable to carrying any additional load after the ultimate load had been reached. In all cases, this resulted in portions of concrete breaking off, concrete spalled of in some areas, and separation of vertical portions of concrete from the rest of the core via vertical cracking in the troughs. Therefore, all walls exhibited unstable post-cracking behaviour and post-cracking load carrying capacity should not be considered in the design.

The behaviour of both the SCC and ECC walls subjected to 400^{o}C were similar (Figs.4.21-4.22). Both walls experienced vertical cracks that ran down the entire wall on both sides along the troughs which formed at the moment of failure, and led to the crushing of concrete at the top. Similar to the ambient temperature, there was bond failure between mortar and the coarse aggregates in the SCC, and there was failure due to tearing of portions of the concrete in ECC; and the failure plane of SCC was smoother and was not as rough as what was observed in ECC.

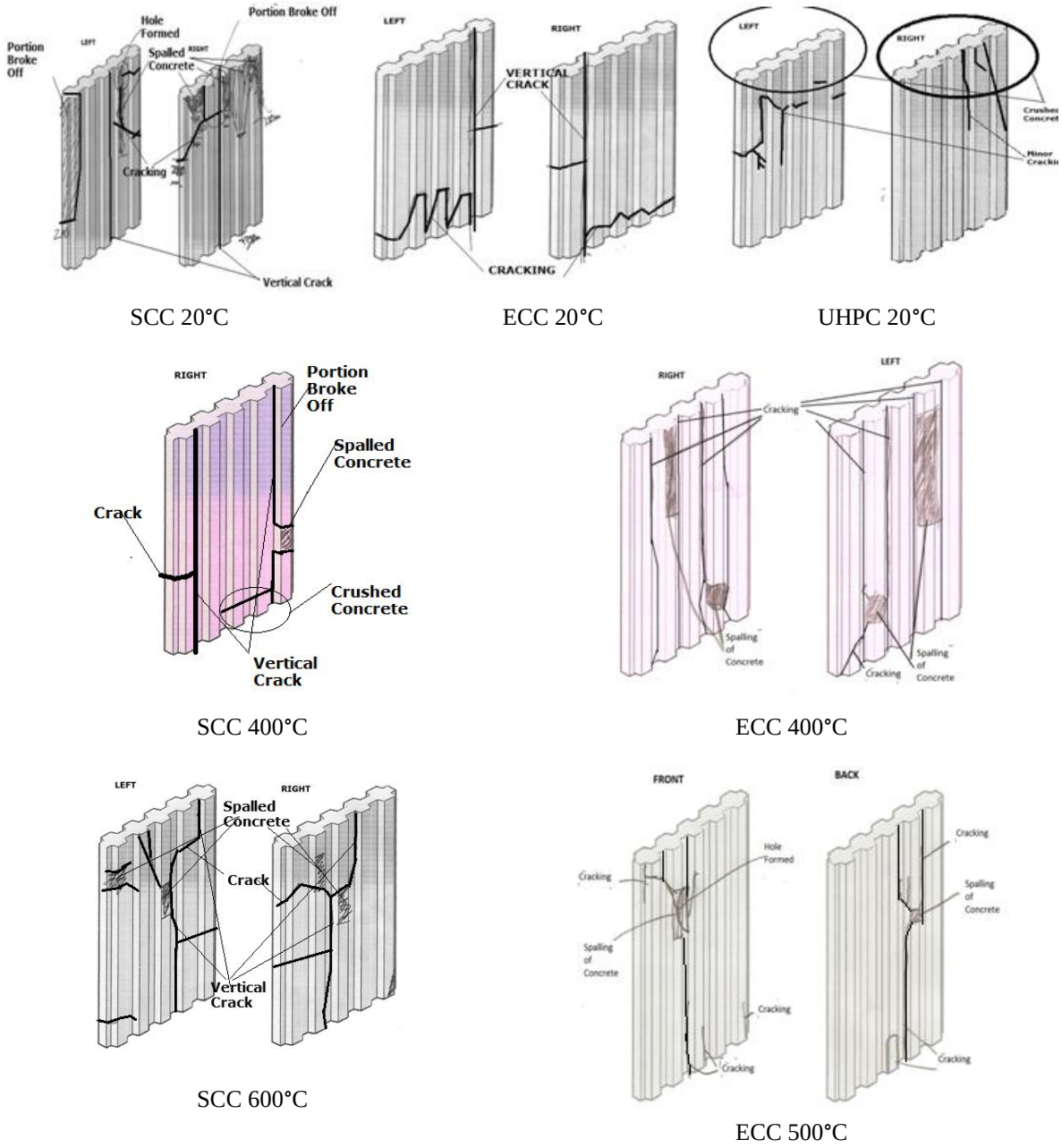

SCC 20°C ECC 20°C UHPC 20°C

SCC 400°C ECC 400°C

SCC 600°C ECC 500°C

Figure 4.21- Failure diagrams for heated and non-heated profiled concrete walls

SCC Control SCC 400°C SCC 600°C

ECC Control ECC 400°C ECC 500°C

UHPC Control

Figure 4.22- Failure modes of profiled concrete walls

There was also evidence of melted fibres in the plane of failure, which lead to increased porosity (Sahmaran et al. 2010). There were also areas of broken and spalled off concrete. The failure observed in ECC walls subjected to 500°C was almost identical to that observed at 400°C

(Figs.4.20-4.21). The performance of the SCC wall at 600°C was different than those at lower temperatures. The top portion of the wall failed in a v-shaped cracking pattern, instead of a pure vertical failure like the other walls.

The experimental maximum load capacity at each temperature (N_{et}) was compared to the experimental maximum load capacity observed at ambient temperature (N_{e20}) by using relative load capacity (N_{et}/N_{e20}). Table 4.4 shows the load capacities of the PCWs at different elevated temperatures. In general, axial load capacity of PCWs decreased with the increase of temperature. In the case of SCC, the value for the maximum load capacity of unheated wall over performed by 35% and therefore the reduction of the SCC walls at elevated temperatures were compared to SCC control wall value with a reduction of 74%. The maximum load capacity of the PCWs composed of SCC at 400°C and 600°C was reduced by 42% and 70%, respectively; and the maximum load capacity of the PCWs composed of ECC at 400°C and 500°C was reduced by 30% and 42%, respectively. It was observed that the reduction in load capacity due to exposure to elevated temperatures was greater in SCC than in ECC (Fig.4.23). This result is in line with the fact the softening of ECC due to fire degradation caused at elevated temperatures is lesser than that observed in SCC. No results were available for the UHPC walls exposed to elevated temperatures due to failure of the wall during the heating which prevented these walls from being tested under axial load.

Table 4.4- Experimental load capacity for profiled concrete walls exposed to elevated temperatures

	SCC			ECC			UHPC		
TEMPERATURE (°C)	20	400	600	20	400	500	20	400	600
Axial load capacity (N_e) (kN)	476	205	104	330	229	192	832	*	*
Relative Load Capacity (N_{et}/N_{e20})	1.35	0.58	0.30	1.00	0.70	0.58	1.17	*	*

N_e – experimental load capacity of wall, N_{et}- experimental load capacity of the wall at a given temperature, N_{e20}- experimental load capacity of the wall at 20°C, *- No values available due to failure of wall during heating

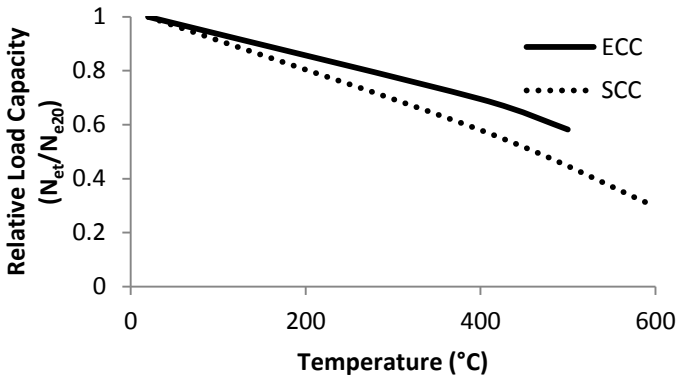

Figure 4.23- Reduction in load capacity of profiled concrete walls exposed to elevated temperatures

4.3.4 Axial Load-Deformation Response and Stiffness/Ductility of the Profiled Concrete Walls

The axial load-deformation behaviour of the PCWs (at ambient and elevated temperatures) for all concrete types is compared in Fig.4.26. It was observed that the SCC/ECC/UHPC unheated and heated walls behaved in a similar manner at the beginning of the testing, having a constant initial stiffness (slope of ascending branch of the axial load- deformation response). The initial stiffness (K_e) of both SCC and ECC concrete core walls decreased at elevated temperatures, as shown in Table 4.5. The experimental value for the initial stiffness at each temperature (K_{et}) was compared to the experimental value for the initial stiffness observed at ambient temperature (K_{e20}) using relative stiffness (K_{et}/K_{e2o}). It was observed that the initial stiffness of the SCC walls decreased at a faster rate than those composed of ECC (Fig.4.24, Fig.4.26, and Table 4.5). This is obvious since the stiffness of the wall is related to the modulus of elasticity, and the modulus of elasticity of SCC decreases at a faster rate than the modulus of elasticity of ECC. At 600°C, the initial stiffness of the SCC walls was reduced by 92% and at 500°C, the initial stiffness of the ECC walls was reduced by 33%.

The slope of the descending branch (post-peak stiffness K'_e) and the relative ductility (K'_{e20}/K'_{et}) of each wall were calculated in the same manner as the steel sheeting walls using Eq.4.1. The post-peak stiffness and relative ductility values are tabulated in Table 4.5.

Axial load-deformation response of SCC walls (Fig.4.26) had a sharp decrease in load after the peak followed by descending branch with high negatives slope. This indicates that the PCWs composed of SCC have a very low ductility. This low ductility is due to the brittleness and low strain hardening capacity of SCC. However, ECC unheated wall had a gradual decrease in load after the peak followed by rebound peak before decreasing again at a gradual rate (Fig. 4.26). This is an indication of higher ductility of ECC walls, around 77 times more than SCC. This observation is in agreement with the higher ductility of ECC over SCC due to the action of the PVA fibers as confirmed from previous research studies (Li 1993; Fischer & Li 2003; Wang & Li 2007; and Sahmaran et al. 2010). Axial load-deformation response of UHPC walls also show ductile with a single peak and gradual post peak descending branch (Fig.4.26). The ductility of the UHPC control wall was observed to be 46 times higher than the ductility of the SCC control wall but 66% lower than the ductility of the ECC control wall.

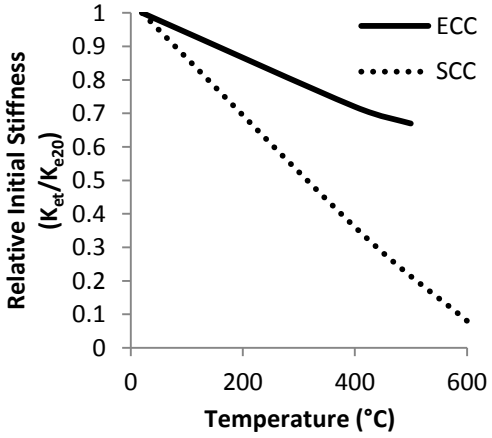

Figure 4.24- Reduction in initial stiffness of PCWs exposed to elevated temperatures

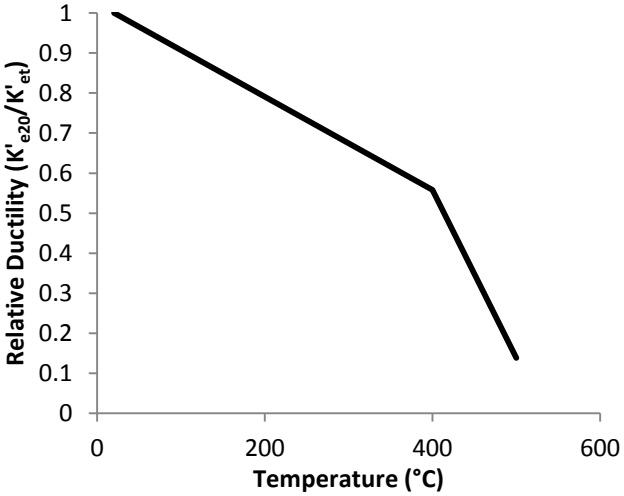

Figure 4.25- Ductility of PCWs composed of ECC at elevated temperatures

At 400°C, ECC walls have higher ductility than SCC walls, around 18% more ductile, which again is due to the inherent ductility of ECC. Between ambient temperature and 400°C, it would appear that softening of the SCC has occurred, which has reduced stiffness and increased post-failure ductility to around 37 times more than observed in SCC at ambient temperature.

Whereas, ECC at 400°C has also underwent softening, so it would be expected that the ductility would increase, but the added ductility provided to ECC in the beginning at ambient temperature

comes in the form of PVA fibers which have since melted. The melting of these fibers has now caused the ECC to begin to revert back to its initial properties of the concrete matrix itself and has become more brittle and caused the ductility of ECC to reduce by 44% at 400°C. At 500°C the ductility of the ECC wall was further reduced to 86% of ductility observed at the ambient temperature (Fig.4.25). In general, ductility decreased with the increase of temperature for ECC and increased with the increase of temperature for SCC, as shown in Table 4.5.

Table 4.5- Stiffness and ductility of profiled concrete walls at elevated temperatures

	SCC			ECC			UHPC		
TEMPERATURE (°C)	20	400	600	20	400	500	20	400	600
Initial stiffness (K_e) (kN/mm)	256.2	92.4	20.0	142.7	102.2	95.2	96.2	*	*
Relative Initial Stiffness (K_{et}/K_{e20})	1.00	0.36	0.08	1.00	0.72	0.67	1.00	*	*
$\Delta_{peak\ load}$ (mm)	1.97	2.25	3.91	2.84	2.24	2.14	8.92	*	*
$\Delta_{0.75\ peak\ load}$ (mm)	2.00	2.72	-	4.44	2.86	2.27	11.35	*	*
K'_e (kN/mm) (Eq.4.1)	3966	109	-	51.5	92.3	373.3	85.6	*	*
Relative Ductility (K'_{e20}/K'_{et})	1.00	36.34	-	1.00	0.56	0.14	1.00	*	*

K'_{e20}/K'_{et} – the relative ductility of the wall, K_e- experimental initial stiffness of the wall, K_{et}- experimental initial stiffness of the wall at a given temperature, K_{e20}- experimental initial stiffness of wall at 20°C, $\Delta_{peak\ load}$- the experimental axial deformation of the wall at peak load, $\Delta_{0.75\ peak\ load}$- the experimental axial deformation of the wall at 75% peak load, K'_e- experimental post-peak stiffness of the wall, K'_{et}- experimental post-peak stiffness of the wall at a given temperature, K'_{e20}- experimental post-peak stiffness of wall at 20°C, *- No values available due to failure of wall during heating

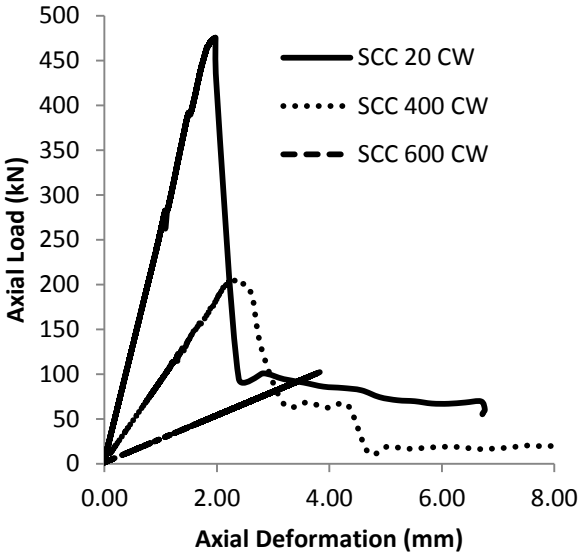

SCC

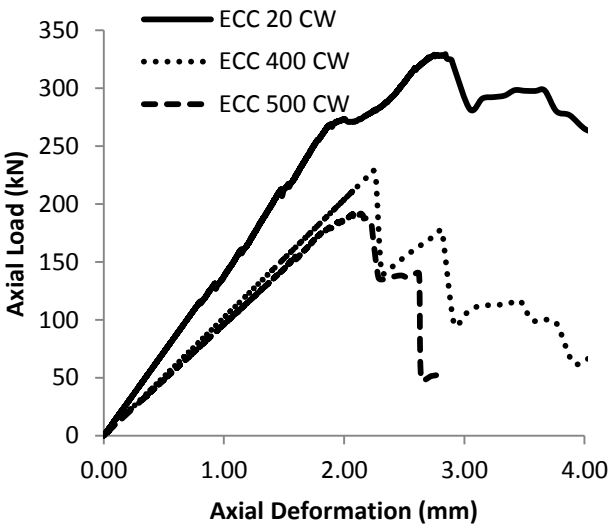

ECC

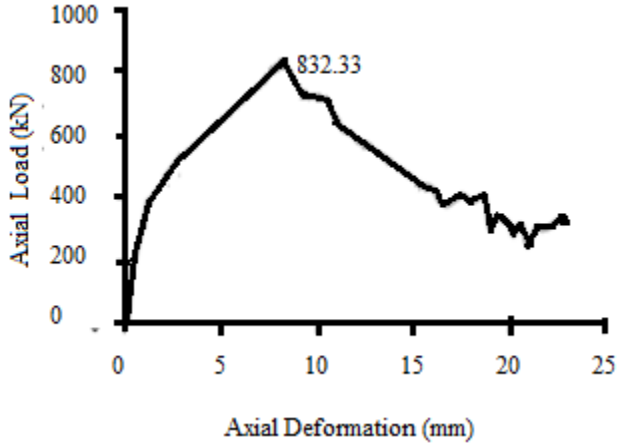

UHPC

Figure 4.26- Axial load-deformation behaviour for profiled concrete walls at elevated temperatures (°C)

4.3.5 Axial Load-Strain Behaviour of the Profiled Concrete Wall

The axial load-strain curves for the PCWs for all three concrete types at the middle are depicted in Figs.4.27- 4.29 and at the top are depicted in Figs.4.30-4.31. The strain values at failure of the unheated and heated walls are summarized in Table 4.6.

For both the heated (control) and un-heated walls, it was observed that as the wall was loaded, the strain at the middle and the top of the wall continued to increase in magnitude as compressive strain until ultimate failure.

For SCC unheated wall, at failure, the compressive strain at the middle was less than that at the top. This indicates that there was higher stress concentrations at the top and bottom of the walls compared to the middle confirming unequal load distribution throughout the height of the wall. Similar behaviour was also observed in the ECC unheated wall. For UHPC unheated walls, the strain at the middle and the top are found to be very close, indicating a better load transfer throughout the wall. It was observed that the compressive strain observed at the top for ambient walls in all cases reached equal or very close to the maximum compressive strain (M.C.S.) of the respective concrete type. Therefore all the walls did reach the full compressive strength of the concrete at ambient temperature (Table 4.6).

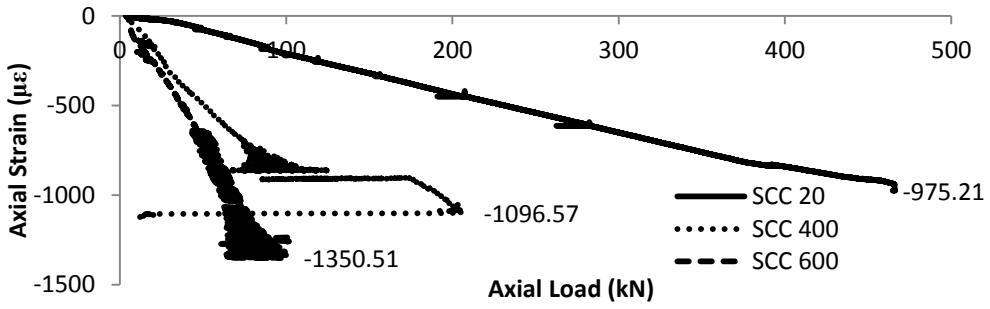

Figure 4.27- Axial load-strain behaviour for SCC profiled concrete walls exposed to elevated temperatures (°C) at the middle

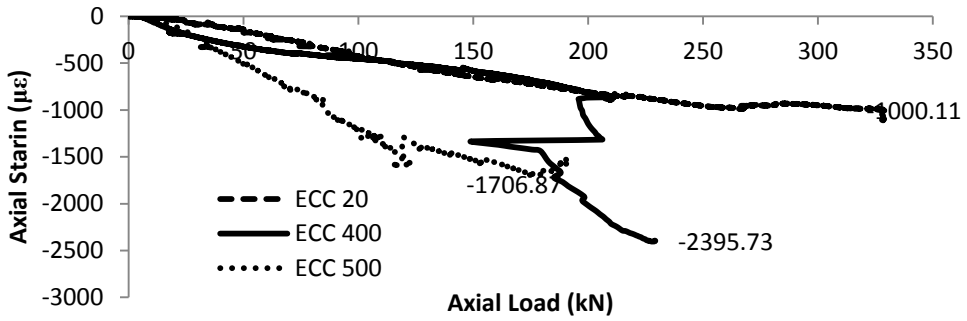

Figure 4.28- Axial load-strain behaviour for ECC profiled concrete walls at elevated temperatures (°C) at the middle

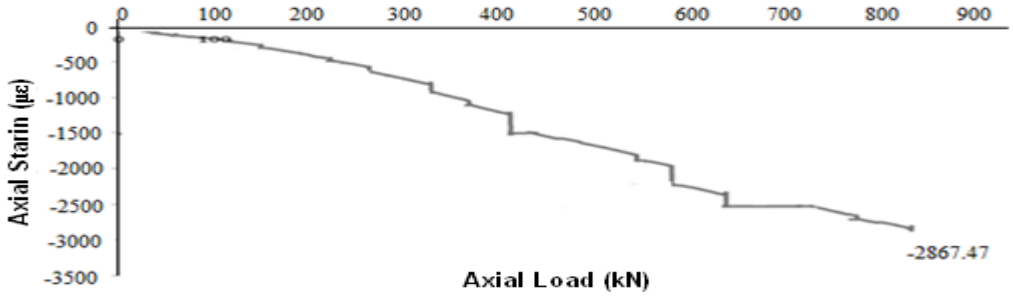

Figure 4.29- Axial load-strain behaviour for UHPC profiled concrete walls at ambient temperature at the middle

Table 4.6-Strain data for profiled concrete core walls at elevated temperatures

Temperature	Strain at Failure (Middle)		Strain at Failure (Top)		M.C.S.
(°C)	(μ strain)	(% of M.C.S.)	(μ strain)	(% of M.C.S.)	(μ strain)
SCC Control	975	54	1783	98	1820
SCC 400	1097	60	532	29	1820
SCC 600	1351	74	-	-	1820
ECC Control	1000	36	2696	97	2779
ECC 400	2396	86	1494	54	2779
ECC 500	1707	61	989	36	2779
UHPC 20	2867	108	2766	104	2655

M.C.S.- the maximum compressive strain of the concrete

For SCC wall at 400°C, the maximum compressive strain at failure at the middle was higher than the strain reached at the top. This indicates that there was higher stress concentrations located at

the center of the wall, than at the top and bottom indicating unequal load distribution throughout the wall. This behaviour is the opposite of what was observed in the SCC and ECC control walls and was also observed in the ECC 400°C wall. It was observed that the maximum strain at the middle for the 400°C wall for both SCC and ECC did not reach the maximum compressive strain of the respective concrete type. It was observed that strain at the center of the ECC wall at 400°C was closer to its respective maximum strain, than SCC. This observation makes sense because elevated temperatures have a greater affect on the softening of SCC, than ECC. Therefore ECC is better suited to reach the full compressive strength of the concrete, over SCC, but in both cases a further reduction should be applied to the maximum compressive capacity to account for this softening behaviour. The behaviour of ECC at 500°C and the effect of SCC at 500°C are similar to behaviour of both concrete types at 400°C.

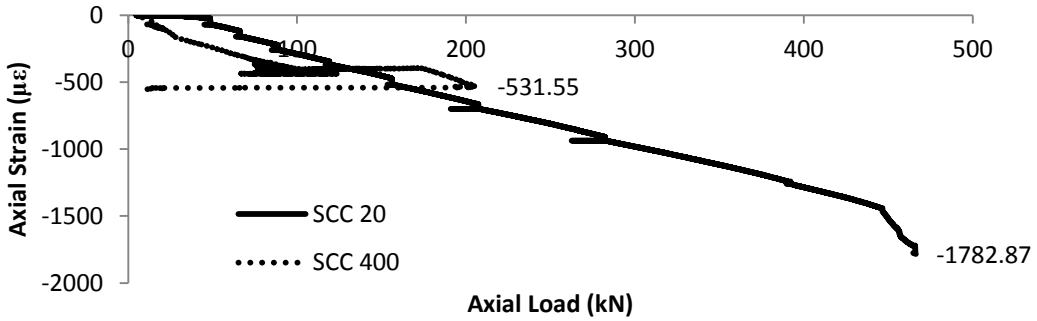

Figure 4.30- Axial load-strain behaviour for SCC profiled concrete walls exposed to elevated temperatures (°C) at the top

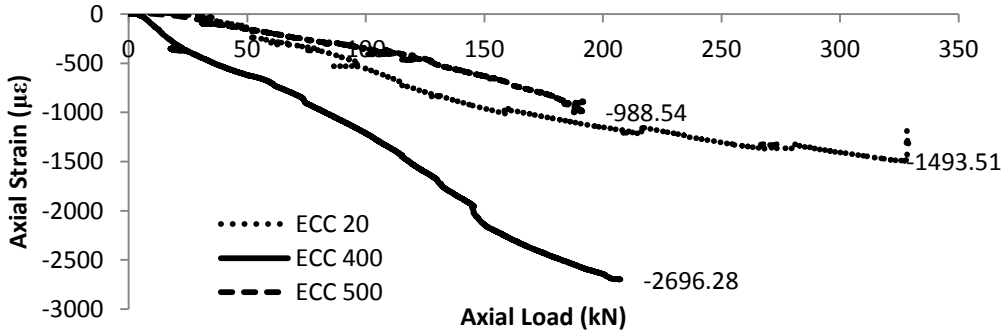

Figure 4.31- Axial load-strain behaviour for ECC profiled **c**oncrete **w**alls at **e**levated **t**emperatures (°C) at the top

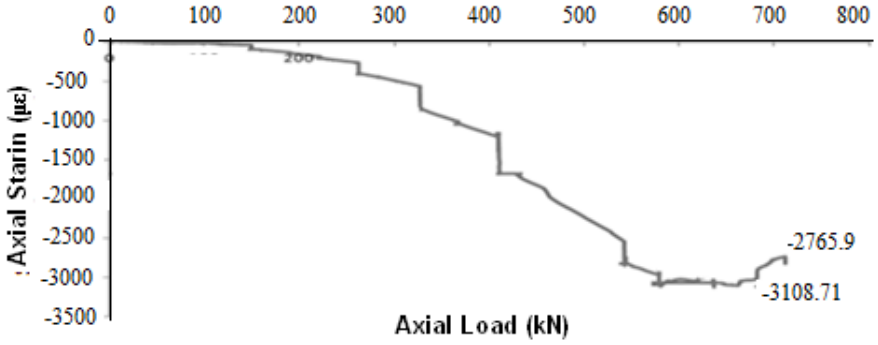

Figure 4.32- Axial load-strain behaviour for UHPC profiled concrete walls at ambient temperature at the top

4.4 Chapter Conclusion

In this chapter experimental results of steel sheeting walls (SSWs) and profiled concrete walls (PCWs) composed of three different types of high performance concretes (HPC): Self-Consolidating Concrete "SCC", Engineered Cementitious Composite "ECC", and Ultra High Performance Concrete "UHPC" subjected to elevated temperatures of up to 800^{o}C were presented. It was observed that heated SSWs under axial loading failed due to global buckling in and around the middle of the wall before yielding. Residual axial load capacity and initial stiffness decreased with the increase of temperature. The failure was sudden and the wall was unable to carrying any additional load after the ultimate load and the wall exhibited unstable post-buckling behaviour. However, the ductility of the SSWs was observed to increase at elevated temperatures due to the softening of the steel sheeting around the bolted connections, followed by overall softening of the steel sheet.

Heated PCWs subjected to axial loading composed of SCC and ECC failed due to development of cracks along the height of the wall associated with crushing of the concrete at the top. UHPC concrete wall subjected to higher temperature of up to 400^{o}C damaged severely and lost structural integrity to carry loads. Axial load capacity and stiffness of SCC and ECC PCWs decreased with the increase of temperature. SCC walls exhibited higher decrease in both axial load capacity and initial axial stiffness than the ECC PCWs. The ductility of SCC PCWs increased at elevated temperatures while the ductility of ECC PCWs decreased.

CHAPTER 5

Double Skin Composite Walls Exposed to Elevated temperatures

5.1 Introduction

In this chapter, experimental results on the axial load behaviour of double skin composite walls (DSCWs) subjected to elevated temperatures is presented. The DSCWs are composed of a pair of profiled light-gauge cold-formed steel sheets having a thickness of 0.61mm and concrete in-fill composed of three types of high performance concrete (HPC): Self-Consolidating Concrete (SCC), Engineered Cementitious Composite (ECC), and Ultra High Performance Concrete (UHPC). The performance of the walls is described based on post-fire residual axial load capacity or strength, axial load-deformation response, stiffness/ductility, load-strain characteristics and failure modes. The walls were tested after being exposed to elevated temperatures of up to 800°C (500°C for ECC).

5.2 Behavior of Double Skin Composite Walls Exposed to Elevated Temperatures

5.2.1 Sample Preparations and Testing Methodology

Double skin composite wall (DSCWs) having an overall dimensions of 540 x 320 mm, were constructed by attaching two profiled light-gauge cold-formed steel sheets of thickness 0.61 mm by using intermediate fasteners at each trough in five rows at spacing of 110 mm at the top and bottom and 140 mm at the center (Figs.5.1-5.3). Shear interaction between the steel sheeting and concrete was improved through the use of steel hooks used as shear connectors that were placed in the crests, at the top and bottom of the wall, which were attached to the steel sheeting by riveted connections to the profiled steel sheeting (Figs.5.1-5.3).

The DSCWs were cast by placing the concrete (SCC, ECC and UHPC) in between two profiled steel sheeting sheets, which acted as permanent formwork, as well as timber formwork at the sides and at the bottom as shown in Fig.5.4., in the casting assembly. The wall was braced laterally in the middle by a steel channel to maintain wall verticality as well as to act as lateral support for the hydrostatic pressure of the fresh concrete. In addition, levelling and verticality of the walls were insured by the use of levels and plumb bobs. All lateral support and timber formwork were removed after one day of casting. The walls were then air cured at room temperature until tested (at least 28 days).

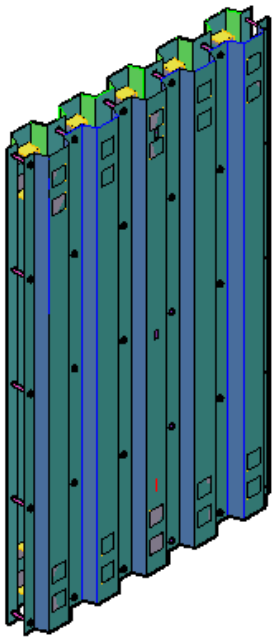

Figure 5.1- Double skin composite wall (before in-fill of concrete)

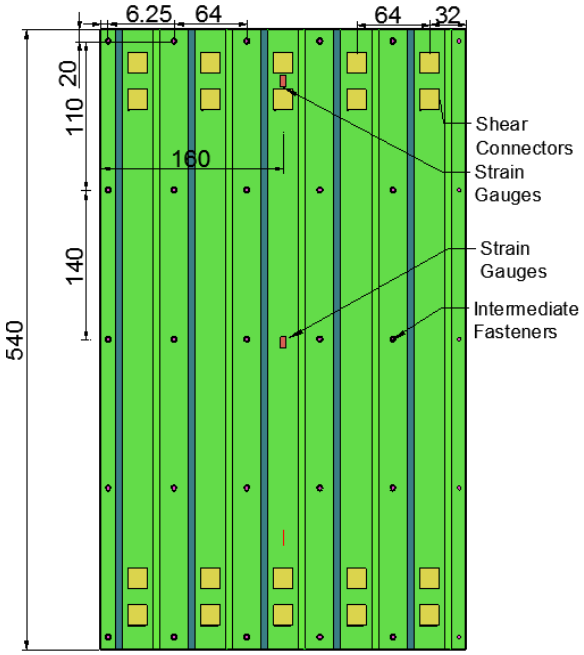

Figure 5.2- Dimensions of double skin composite wall (dimensions in mm)

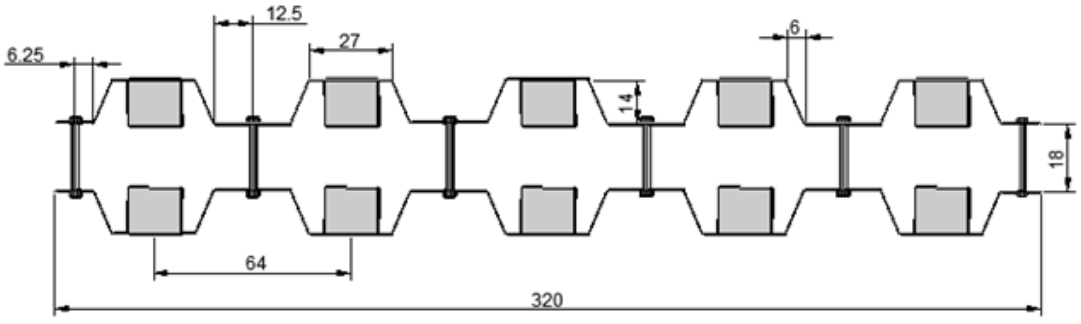

Figure 5.3- Cross section of double steel skin composite wall (dimensions in mm)

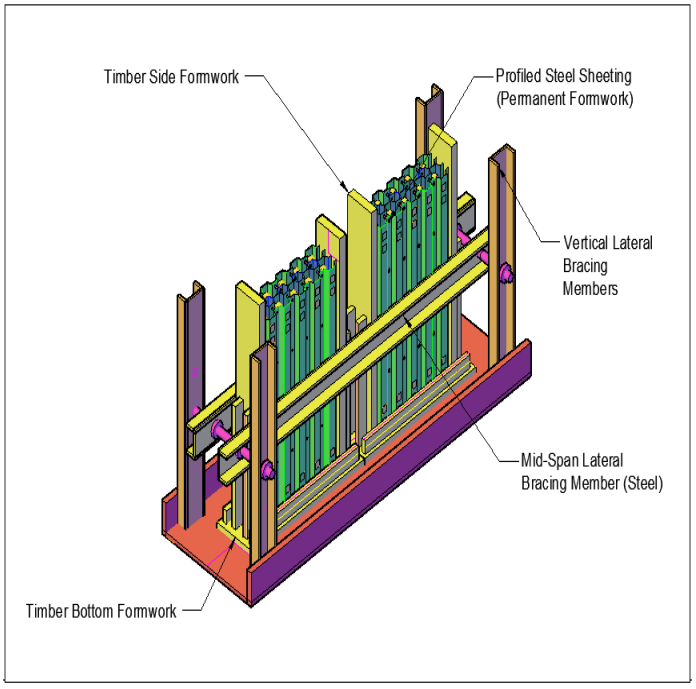

Figure 5.4 - Casting setup for double skin composite walls

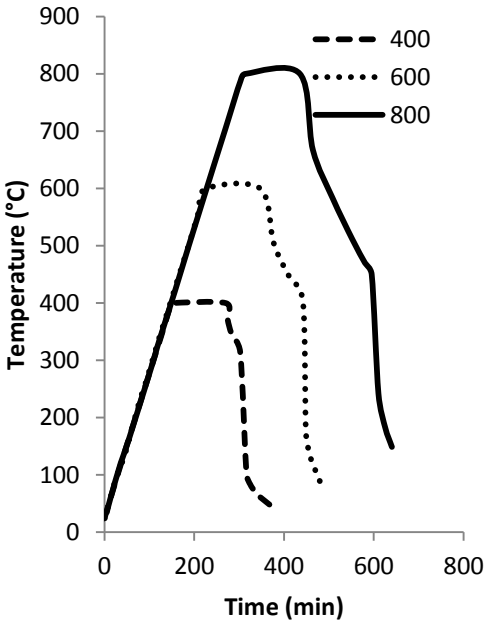

Figure 5.5- Heating-cooling curve for double skin composite wall composed of SCC and UHPC

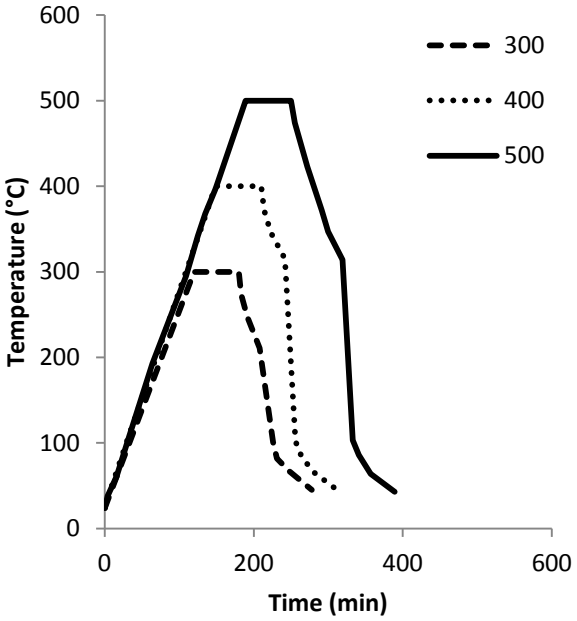

Figure 5.6- Heating-cooling curve for double skin composite wall composed of ECC

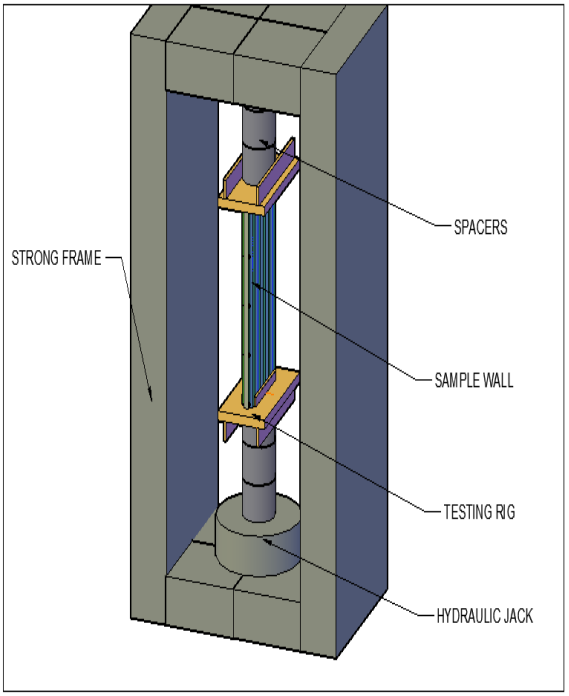

Figure 5.7- Axial load testing setup for double skin composite walls

The DSCW specimens were heated at a rate of 2.5°C/min in a kiln up to the given temperatures of 400°C, 600°C and 800°C, for SCC/UHPC and 300°C, 400°C and 600°C for ECC; and sustained at the respective steady state temperatures for two hours for SCC/UHPC and one hour for ECC, before being cooled down to room temperatures. ECC walls were heated differently due to lab constraints. This rate was chosen to correspond to the rate used in the steel sheeting and concrete cylinder samples as well as steel sheeting and profiled concrete walls. The heating and cooling curves for each temperature are presented in Figs.5.5-5.6. Heated and unheated (control) DSCWs were then tested in an axial compression testing machine until failure as shown in Fig.5.7. Strain gauges were placed on the crests at the top (65 mm from the top) and the middle, as shown in Fig.5.2. During testing axial load-deformation response and axial strain development were obtained using data-acquisition system. The double skin composite walls were loaded at a loading rate of 50 kN/min until failure.

5.2.2 Physical Changes of the Double Skin Composite Walls after Heating

No discolouration or damage of the exterior surface of the steel was observed up to 400°C in all walls (Figs.5.8-5.10). At 600°C, minor greyish discoloration was observed on the steel only on the very top layer as a form of dust or powder. At 800°C, the discoloration observed on the steel was a mixture of black and brown, and instead of being a fine dust or powder, the burnt portions of the steel peeled or flaked off, indicating a greater extent of damage compared to those samples elevated at 600°C. No physical damaged was observed on any of the steel sheeting on the walls heated to elevated temperatures. This behaviour is similar to what was observed on the profiled steel sheeting walls and steel sheeting samples exposed to elevated temperatures.

The DSCWs composed of all three concrete types experienced no spalling of the concrete at all temperatures up to 800°C for SCC/UHPC and 500°C for ECC. There were no visible signs of cracking on the sides, top, or bottom of the wall in both the SCC and UHPC walls, but cracking was observed on the sides of the ECC walls after they were heated between 400°C to 500°C. A thin layer of dust was observed on the sides of the wall composed of ECC and SCC at 500°C and 800°C, respectively. At a temperature of 800°C a total breakdown of the integrity of the

aggregates and the cement paste was observed, as well as the bond between the two was weakened.

At a temperature of 400°C, there was minor sheet separation in all walls composed of each concrete type. This sheet separation was less than the thickness of the steel sheeting itself (~0.30 mm). This separation was caused by the breakdown of chemical bond between the steel sheeting and the concrete due to heat. At a temperature of 500°C for ECC and 600°C for SCC and UHPC walls, the sheet separation had increased further (~0.61 mm) due to combination of steel sheet-concrete debonding and differential thermal expansion between the steel sheeting and the concrete. At a temperature of 800°C for both SCC and UHPC walls, the sheet separation had increased to about two times the thickness of the steel sheeting (~1.2mm). This separation was caused mostly due to differential higher thermal expansion between the steel sheeting and the concrete compared to lower temperatures.

The DSCWs composed of UHPC showed shown no visible damage in the form of explosive spalling in the concrete due to vapour pressure buildup. The confinement of the steel sheeting had the effect of containing the concrete in such a way that it prevented explosive concrete spalling of the concrete. This was contradictory to the behaviour of the profiled concrete core wall composed of UHPC. However, it should be noted that the relative small thickness and small aspect ratio of the wall may have contributed to this behaviour and that walls with different geometric properties may not behave in a similar manner. Similar to SCC and ECC, there was minor cracking in the UHPC behind the steel sheeting caused by thermal stress, but the cracked confined concrete after the heating to elevated temperatures could still resist applied axial load at a diminished capacity.

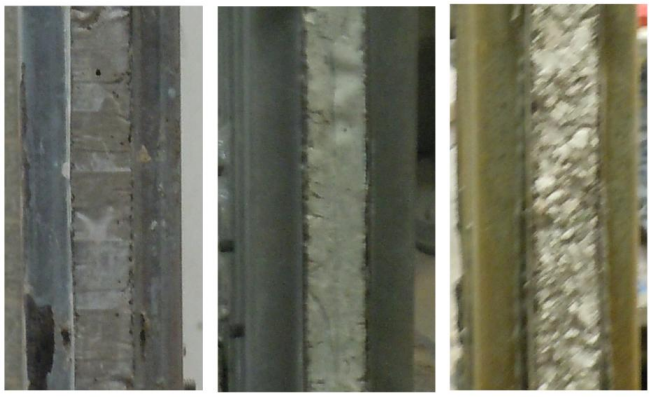

Figure 5.8- Physical changes observed in SCC double skin composite walls exposed to elevated temperatures

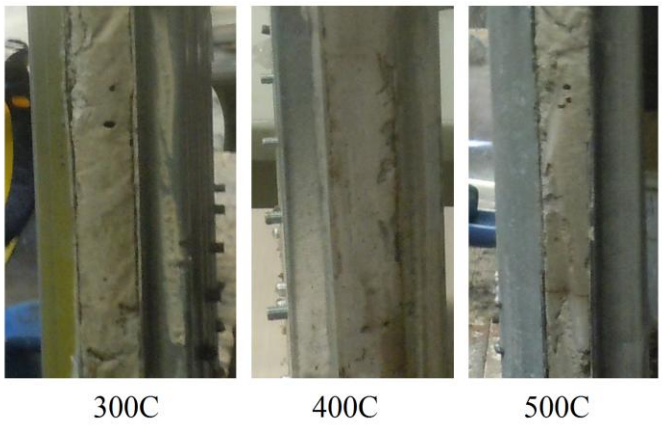

Figure 5.9- Physical changes observed in ECC double skin composite walls exposed to elevated temperatures

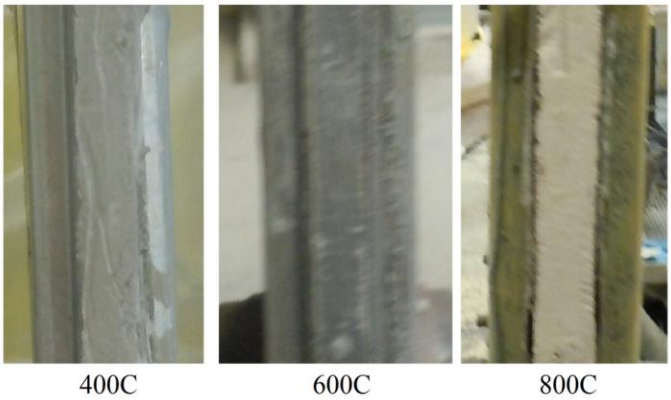

Figure 5.10- Physical changes observed in UHPC double skin composite walls exposed to elevated temperatures

5.2.3 Axial Load Capacity and Failure Modes of the Double Skin Composite Walls

The failure modes of heated (400°C, 600°C and 800°C, for SCC/UHPC and 300°C, 400°C and 600°C for ECC) and unheated DSCWs subjected to axial loading are presented in Figs.5.11-5.17.

5.2.3.1 Failure Modes of the Un-heated Control Walls

The failure of the un-heated (control) SCC DSCWs occurred due to concrete crushing at the top of the wall as well as local buckling of the steel sheeting in the same region, similar to the behaviour observed by Hossain (2000). At the ultimate load, failure occurred in the concrete in-fill first with signs of crushing of the concrete and small portions of concrete being observed to break off from the top, as shown in Figs.5.11-5.17. This result indicates that the concrete was loaded to the maximum compressive stress of this material. After which the steel sheeting was forced to carry the entire load at once and quickly buckled, seconds after the initial failure of the concrete in-fill. The buckling of the steel sheeting on both sides began with plastic hinges forming around the second line of bolts, followed by outwards deflection of the steel sheeting away from the concrete. Based on research conducted by Hossain (2000) and failure observed in the profiled concrete core walls, it is plausible to assume that cracking occurred along down the troughs of the concrete. Unfortunately due to the amount of intermediate spacers present and the shear connectors at the bottom, the steel sheeting was not able to be removed to view the crack pattern. There was no evidence of tearing of the sheet from the concrete at the second line of bolts and both components still remained intact with minor separation after the test. There was however evidence of tearing of the sheet at the first line of bolts near the top. The region of failure of the SCC control wall was confined to the portion of the wall between the first and second line of bolts, as shown in Figs.5.11-5.17.

In comparison to the steel sheeting walls (SSWs), global buckling of the steel sheeting did not occur at the middle of the wall with global lateral deflection of both sheets in the same direction, but instead local buckling occurred at the top where sheet buckled outwards from the concrete in different directions. This result indicates that the additional stiffness provided by the in-fill of concrete deterred the ability of the steel sheeting to buckle globally. Buckling did not occur until

concrete was no longer able to carry load in the upper region of the wall. The region of buckling failure was confined to the region in which concrete had failed. The rest of the wall, other than minor sheet separation, was unaffected by the buckling in the upper portion of the wall (Figs.5.11-5.17).

In comparison to the profiled concrete walls (PCWs), ultimate failure did not occur due to vertical cracking along the troughs, even though vertical cracking of the troughs still occurred. The confinement of the concrete in-fill by the steel sheeting allowed the cracked portions to remain together, instead of breaking off, and continued to resist the compressive load, albeit at a diminished capacity when compared to pre-cracking strength, until crushing of the concrete occurred. This result indicates that the additional confinement provided by the steel sheeting aids in the ability of the in-fill concrete to resist compressive loads after cracking occurs in the troughs of the concrete. The region of crushing failure of the concrete was confined to the region in which the steel sheeting had buckled afterwards. The rest of the wall did not experience any crushing of concrete, but it is assumed that vertical cracking along the troughs occurred throughout the wall (Figs.5.11-5.17).

For ECC unheated wall, the crushing of concrete at the top occurred at a much slower rate when compared to the SCC unheated wall, due to the higher ductility of ECC over SCC (Figs.5.11-5.17). The buckling of the steel sheeting occurred at around the same time as the crushing of the concrete, which is different from what was observed in SCC, and therefore both components failed together with the steel sheeting gradually taking more load and the concrete gradually taking less load, until failure of the concrete followed by failure in the steel sheeting. As the concrete failed more gradually, the steel sheeting was able to begin buckling at the same time as crushing of the concrete and therefore there was no immediate load transfer from the whole wall to just the steel sheeting, as was the case for SCC wall. There was no evidence of tearing of the sheet at the first line of bolts near the top in ECC wall, unlike what was observed in SCC wall. However there was crimping of the steel sheeting around some of the bolt connections in the first line of bolts. This was due to no immediate stress being placed on the sheet-bolt-concrete interface at the top.

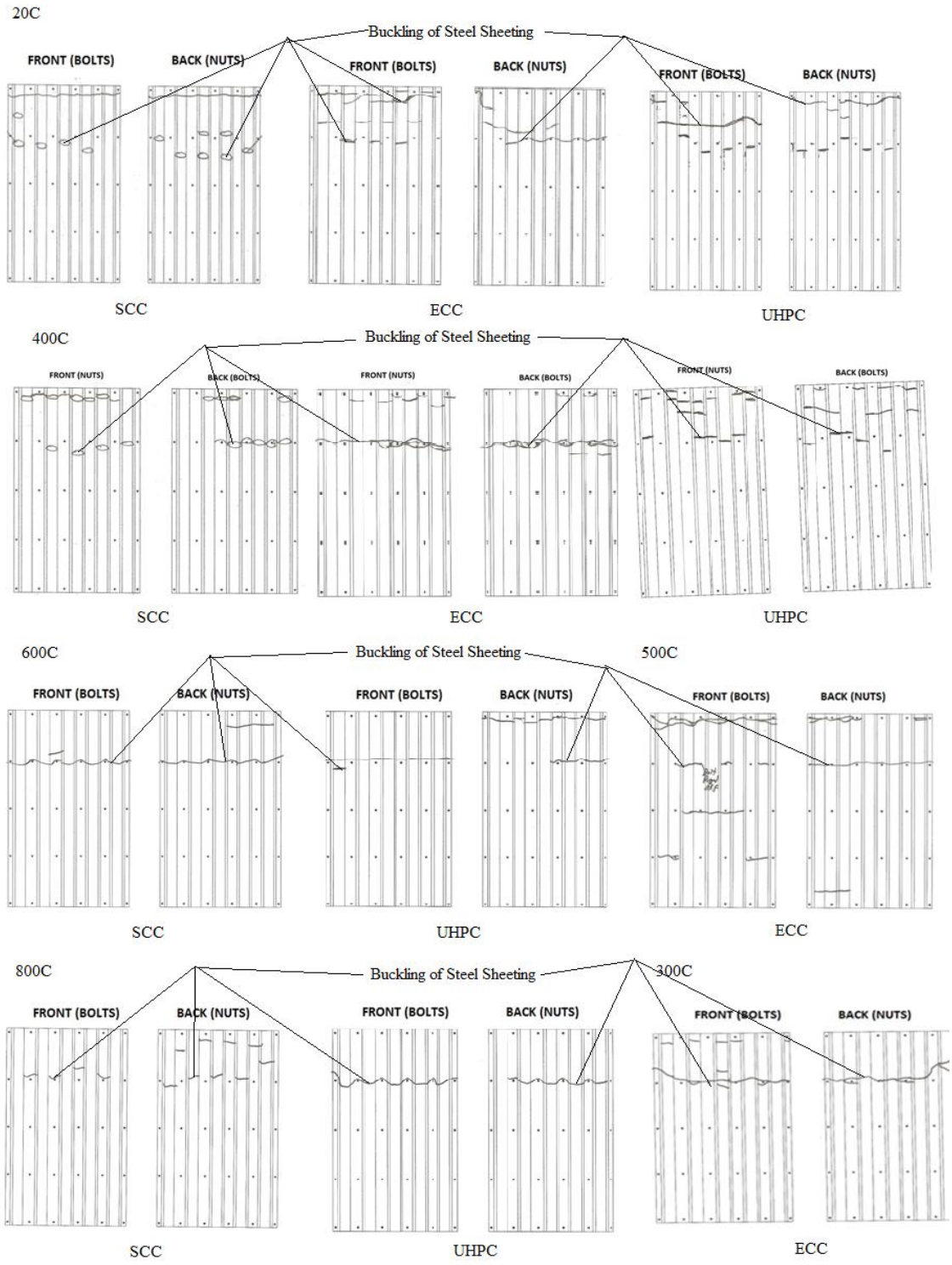

Figure 5.11- Failure diagram of double skin composite walls

For UHPC unheated wall, the crushing of the concrete at the top occurred at a slower rate compared to the SCC control wall, but at a faster rate than the ECC control wall. Under compression, the steel fibers in UHPC aid in the concrete ductility although (Figs.5.11-5.17). ECC wall has overall higher ductility due to PVA fibers. Similar to ECC, the buckling of the steel sheeting occurred at around the same time as the crushing of the concrete in UHPC walls. There was no evidence of tearing of the sheet at the first line of bolts near the top in UHPC wall, similar to what was observed in the behaviour of the ECC wall. There was also crimping of the steel sheeting around some of the bolted connections in the first line of bolts.

Figure 5.12- SCC double skin composite wall failure (back view) for control, 400°C, 600°C, and 800°C

Figure 5.13- ECC double skin composite wall failure (back view) for control, 300°C, 400°C, and 500°C

Figure 5.14- UHPC double skin composite wall failure (back view) for control, 400°C, 600°C, and 800°C

Figure 5.15- SCC double skin composite wall failure (left and right view) for control, 400°C, 600°C, and 800°C

Figure 5.16- ECC double skin composite wall failure (left and right view) for control, 300°C, 400°C, and 500°C

Figure 5.17- UHPC double skin composite wall failure (left and right view) for control, 400°C, 600°C, and 800°C

5.2.3.2 Failure Modes of Walls Subjected to Elevated Temperatures

The mode of failure observed in the SCC unheated wall during post-fire conditions was also observed in the 400°C, 600°C, and 800°C SCC wall and the ECC unheated wall, 300°, 400°C, and 500°C walls with slight variations (Figs.5.11-5.17). The UHPC unheated wall and 400°C, 600°C, and 800°C walls experienced a different failure mode in which the ultimate failure occurred due to cracking of concrete with minor local crushing at the top that led to the buckling of the steel sheeting in the same region. Based on the PCWs, it is plausible to assume that no major cracking occurred along the troughs of the concrete. Therefore the general mode of failure is unaffected by exposure to elevated temperatures for UHPC walls.

The crushing of the concrete at the top for SCC DSCWs at elevated temperatures occurred at a much faster rate with each increasing interval of temperature, indicating that elevated temperatures had a softening effect on the concrete that reduced in-fill concrete stiffness at elevated temperatures. It was also noted that crushing of the concrete and buckling of steel sheet occurred at the same time at temperatures higher than 400°C. (Figs.5.11, 5.12, & 5.15)

The crushing of concrete in ECC DSCWs at elevated temperatures occurred at the top at a similar rate during all intervals of temperature indicating that at elevated temperatures the softening effect on the concrete was is counteracted by the melted PVA fibers which had-reduced the overall ductility of ECC. It should also be noted that plastic hinges also formed on

the middle and fourth lines of bolts, in addition to the second line of bolts. (Fig5.11, 5.13., & 5.16)

For UHPC DSCWs at elevated temperatures, the crushing of the concrete occurred at the top at a similar rate during all intervals of temperature indicating that at elevated temperatures the softening effect is counteracted by the steel fibers preserving the stiffness of the UHPC. (Figs.5.11, 5.14, & 5.17)

5.2.3.3 Axial Load Capacity

The experimental axial load capacities at various temperature "t" (N_{et}) are compared with the axial load capacity observed at ambient temperature (N_{e20}) in Table 5.1. In general, residual axial capacity of DSCWs decreased with the increase of temperature as confirmed from relative load capacity (N_{et}/N_{e20}) (Fig.5.18 and Table 5.1). The maximum load capacity of the DSCWs composed of SCC at 400°C, 600°C, and 800°C was reduced by 23%, 43%, and 82%, respectively; for ECC wall the maximum load capacity at 300°C, 400°C, and 500°C was reduced by 28%, 36%, and 40%, respectively and for UHPC walls at 400°C, 600°C, and 800°C was reduced by 32%, 51%, and 80%, respectively (Figure 5.18). It was observed that the reduction in load capacity due to exposure to elevated temperatures was the same for both DSCWs composed of UHPC and ECC, which was greater than the reduction observed in SCC.

Table 5.1- Axial load capacity of double skin composite walls at elevated temperatures

	SCC				ECC				UHPC			
TEMP. (°C)	20	400	600	800	20	300	400	500	20	400	600	800
N_e (kN)	453	348	260	81	473	388	302	284	745	505	362	151
N_{et}/N_{e20}	1.00	0.77	0.57	0.18	1.00	0.82	0.64	0.60	1.00	0.68	0.49	0.20

N_e- axial load capacity of the wall, N_{et}/N_{e20}- relative load capacity

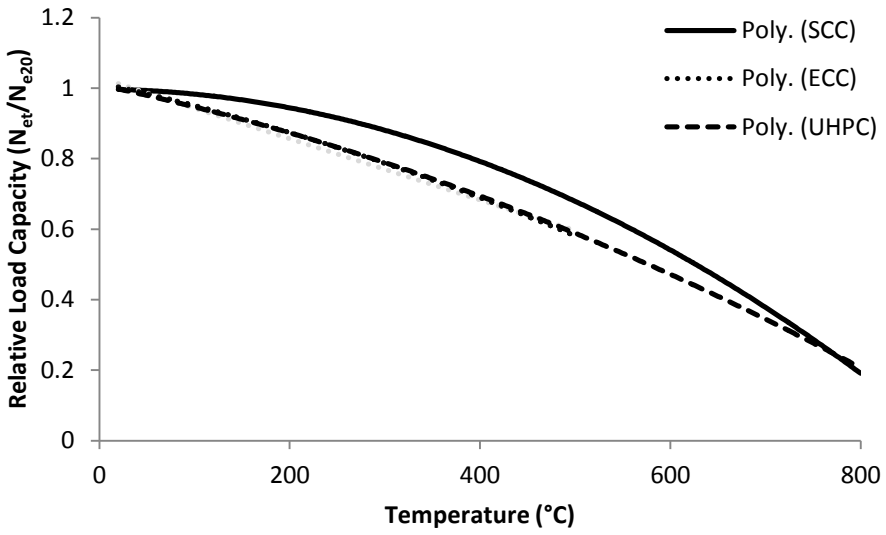

Figure 5.18- Reduction in load capacity of double skin composite walls exposed to elevated temperatures

5.2.4 Axial Load-Deformation Response of the Double Skin Composite Walls

The axial load-deformation response of the DSCWs, for all concrete types, exposed to elevated temperatures is depicted in Fig.5.19. The unheated (control) DSCW for each concrete type behaved in a similar manner showing more or less constant initial stiffness (slope of the ascending branch of the axial load-deformation response). Axial load-deformation response of wall subjected to elevated temperatures had an ascending branch (with an initial stiffness) until peak load. Post peak axial load-deformation response was characterized by a descending branch followed by a flat branch at failure. The experimental values for the initial stiffness of the wall at each temperature "t" (K_{et}) were compared to the experimental value for the initial stiffness observed at ambient temperature (K_{e20}) in Table 5.2. The relative stiffness (K_{et}/K_{e20}) are also computed to illustrate stiffness degradation with temperature and presented in Table 5.2 and Figure 5.20.

The initial stiffness (K_e) of the DSCWs decreased with elevated temperatures (Table 5.2 and Fig. 5.20). Initial stiffness for SCC, ECC and UHPC was decreased by 91%, 81% and 93%, respectively when temperature was increased to 800^{o}C for SCC and UHPC and to 500^{o}C for ECC.

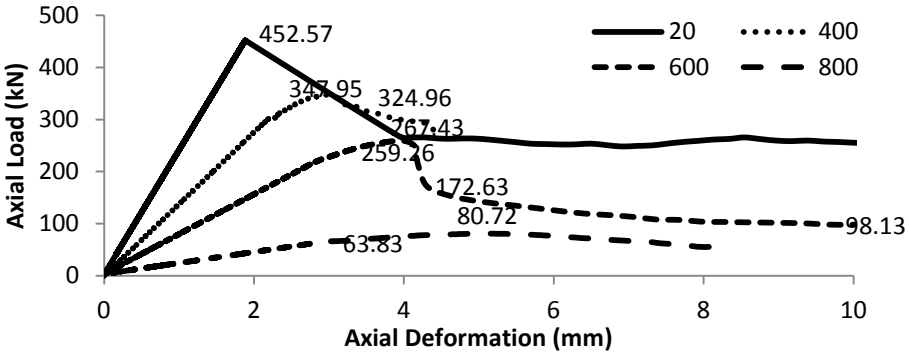

SCC

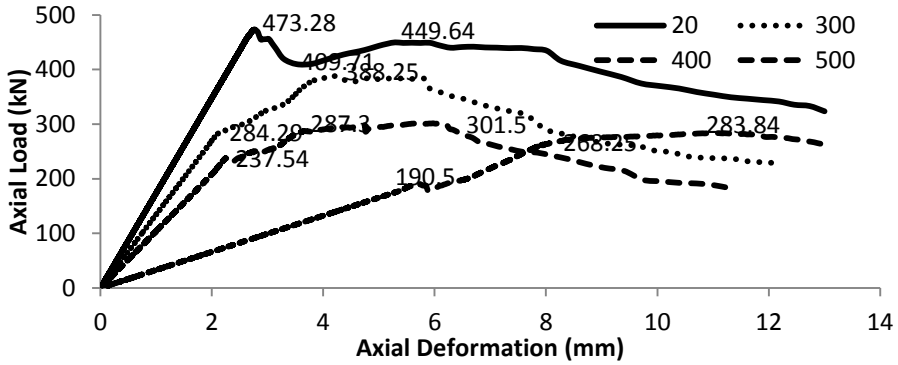

ECC

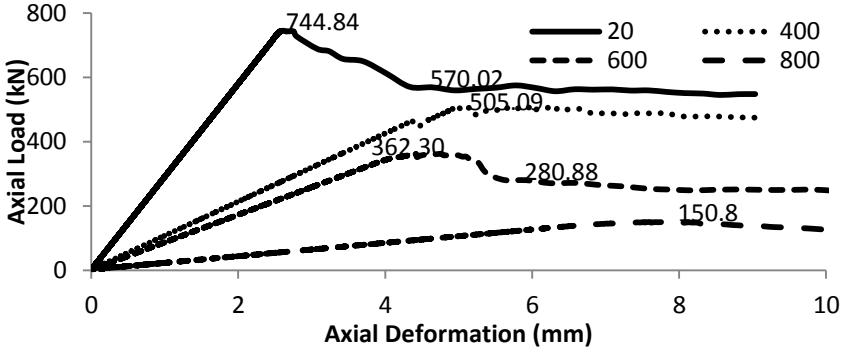

UHPC

Figure 5.19- Axial load-deformation behaviour for double skin composite walls exposed to elevated temperatures (°C) composed of SCC, ECC, and UHPC

The reduction in initial stiffness of the DSCWs composed of all three concrete types was similar up to 400°C. Between 400°C and 500°C, the initial stiffness of ECC walls dropped dramatically due to loss (melting) of PVA fibers and cracking due to thermal stresses. Cracking in SCC was not as extensive in UHPC and as a result the stiffness reduction is smaller in SCC, than in UHPC walls.

The post-peak ductility of each wall was determined by using the slope (post-peak stiffness) of the descending branch of the axial load-deformation response (K'_e) between peak load and 75% of post peak load as per Eq, 4.1 presented in Chapter 4. The relative ductility (K'_{e20}/K'_{et}) of the wall presented in Table 5.2 and Fig. 5.21 is defined as the ratio of the ductility at ambient temperature (K'_{e20}) to the ductility at temperature t^{o}C (K'_{et}).

It was observed in the unheated (control) SCC DSCW that after peak load there was a sharp decrease in load or a descending branch with a high negatives slope, as shown in Fig.5.19 and 5.21, indicating a low ductility. However, the ECC unheated wall showed a gradual decrease in post peak load with a rebound peak indicating a higher ductility than SCC. The ECC unheated wall was found to be 6 times more ductile than SCC as indicated by the relative ductility and post-peak stiffness (Table 5.2). This higher ductility can be attributed to the high strain hardening capacity of ECC compared to SCC. The ductility of the UHPC unheated wall was also higher than SCC by 9% due to the effect of cracking control provided by the steel fibers and lower than ECC by a factor of 5.6 (Table 5.2). This result indicated that the ECC provided better ductility in DSCWs at ambient temperature than SCC and UHPC. This result is similar to that of the PCWs at ambient temperature; except for the fact the addition of steel sheeting to the concrete had increased the ductility of both the SCC and ECC DSCWs by a factor of 44 and 3.5. However the ductility of the UHPC DSCW did not change.

Overall, the post-peak ductility of SCC DSCWs remained higher compared to UHPC/ECC DSCWs up to a temperature of 600^{o}C. The ductility of SCC/UHPC DSCWs increased up to about 11 and 7 times the ductility at ambient temperature, respectively, with the increase of temperature up to 800^{o}C (Table 5.2), while ECC DSCWs showed a decrease in ductility up to half the ductility at ambient temperature, with the increase of temperature up to 500^{o}C (Table

5.2 and Fig.5.21). The ductility of the SCC DSCWs was higher than the ECC/UHPC DSCWs due to the breakdown of bond between the aggregates and cement paste at 800°C. The steel fibers in the UHPC do not melt at this temperature and remain intact to aid in crack control of the concrete and therefore the stiffness reduces less and causes the increase in ductility to be lower than in SCC walls. The reduced ductility of ECC can be associated with increased porosity due to the melting of PVA fibers. It was observed that the post-peak ductility of the DSCWs is very similar to the ductility observed in the SSWs indicating that the steel sheeting plays a greater role in the post-peak ductility of DSCWs than the in-fill concrete, especially at temperatures greater than 600°C.

Table 5.2- Initial stiffness and ductility of DSCWs at elevated temperatures

	SCC				ECC				UHPC			
TEMP. (°C)	20	400	600	800	20	300	400	500	20	400	600	800
K_e	240	138	78	22	173	135	104	33	299	108	86	21
K_{et}/K_{e20}	1.00	0.57	0.33	0.09	1.00	0.78	0.60	0.19	1.00	0.36	0.30	0.07
$\Delta_{peak\ load}$	1.9	3.0	4.0	5.2	2.8	4.3	6.0	11.0	2.6	6.0	4.7	7.9
$\Delta_{0.75\ peak\ load}$	3.1	4.4	4.3	7.7	10.9	8.0	8.8	-	4.8	-	6.2	10.8
K'_e	91	64	191	8	15	26	27	-	84	-	62	13
K'_{e20}/K'_{et}	1.00	1.43	0.48	11.3	1.00	0.56	0.54	-	1.00	-	1.36	6.60

K'_{e20}/K'_{et} – the relative ductility of the wall, K_e- experimental initial stiffness of the wall in kN/mm, K_{et}- experimental initial stiffness of the wall at a given temperature, K_{e20}- experimental initial stiffness of wall at 20°C, $\Delta_{peak\ load}$- the experimental axial deformation of the wall at peak load in mm, $\Delta_{0.75\ peak\ load}$- the experimental axial deformation of the wall at 75% peak load in mm, K'_e- experimental post-peak stiffness of the wall (Eq.4.1) in kN/mm, K'_{et}- experimental post-peak stiffness of the wall at a given temperature, K'_{e20}- experimental post-peak stiffness of wall at 20°C

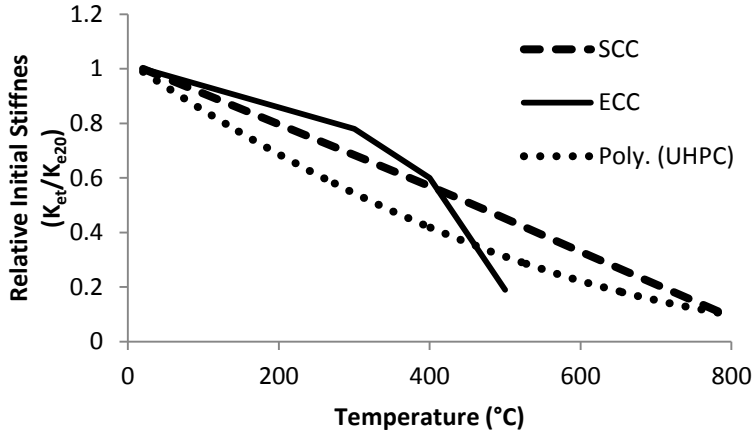

Figure 5.20- Reduction in initial stiffness of double skin composite walls exposed to elevated temperatures

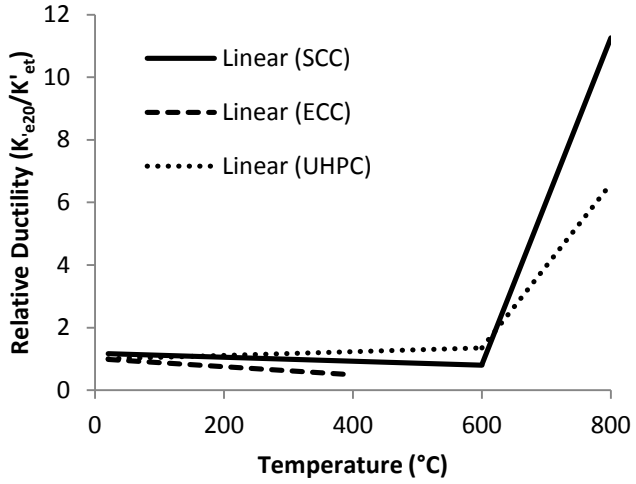

Figure 5.21- Relative ductility of DSCW walls exposed to elevated temperatures

5.2.5 Axial Load-Strain Behaviour of the Double Skin Composite Walls

The axial load-strain curves for the DSCWs at the middle and top are depicted in Figs.5.22 and 5.23 and a summary of strain characteristics is provided in Table 5.3. For the unheated walls, the strain at the middle/top of SCC/ECC/UHPC continued to increase with the increase in load until ultimate failure. Similar trend of strain variation was observed by Wright (1998) and Hossain (2000).

The walls were subjected predominantly to compressive strain with the exception of UHPC walls at higher temperatures develop tensile strain at the top (Fig.5.23) possibly due to localized buckling of the steel sheet. It was observed for the composite walls that the middle of the wall did not reach yield strain (Y.S.) at ambient temperature or at 400°C for SCC, 300°C for ECC, 400°C for UHPC but did reach yield strain at 600°C and 800°C for SCC, 400°C and 500°C for ECC, and 600°C and 800°C for UHPC. In most cases, the strain at the top did not reach yield strain. ECC walls developed higher strain compared to SCC/UHPC walls at respective temperatures. The small strain results were also observed in composite walls tested by Wright (1998).

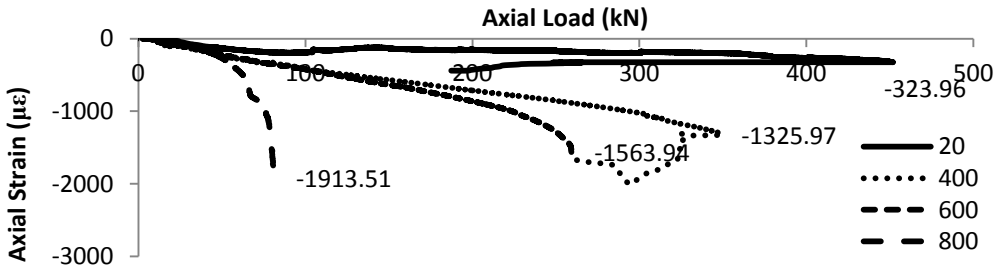

SCC

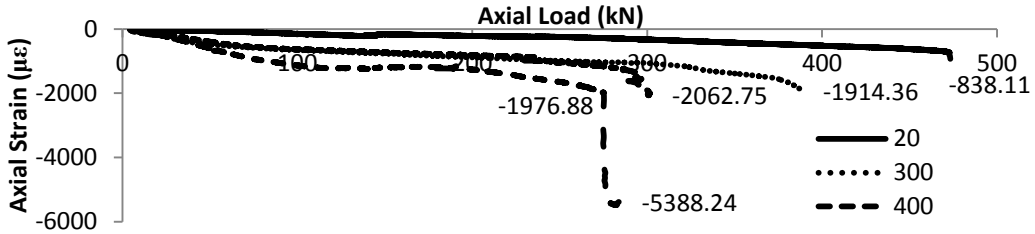

ECC

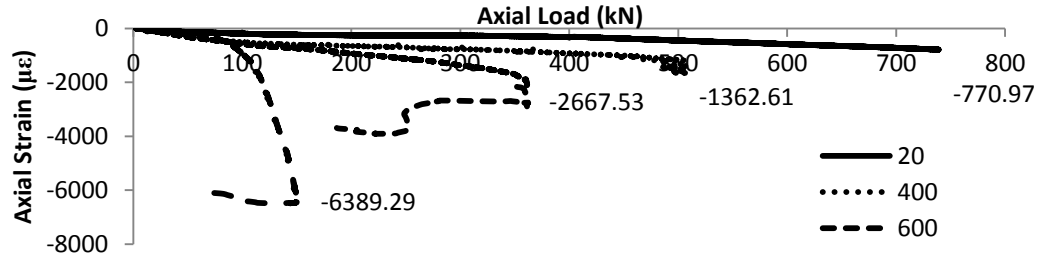

UHPC

Figure 5.22- Axial load-strain behaviour for SCC/ECC/UHPC double skin composite walls exposed to elevated temperatures **(°**C**)** at the middle

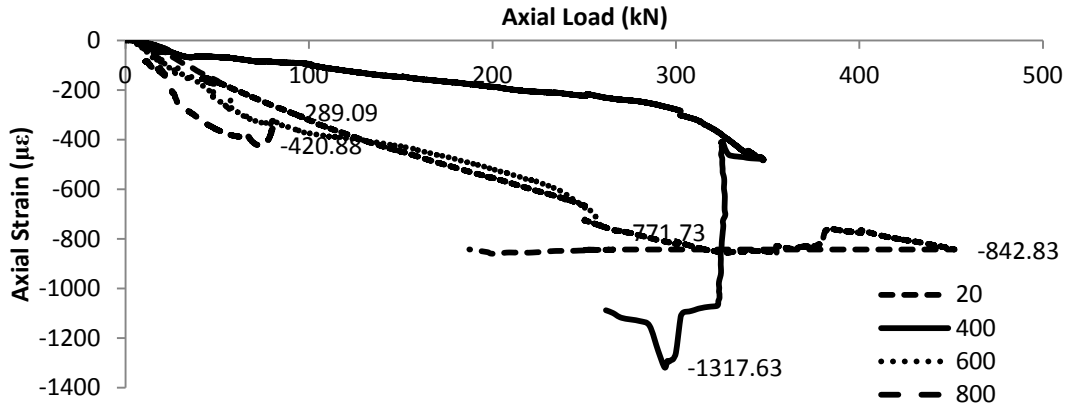

SCC

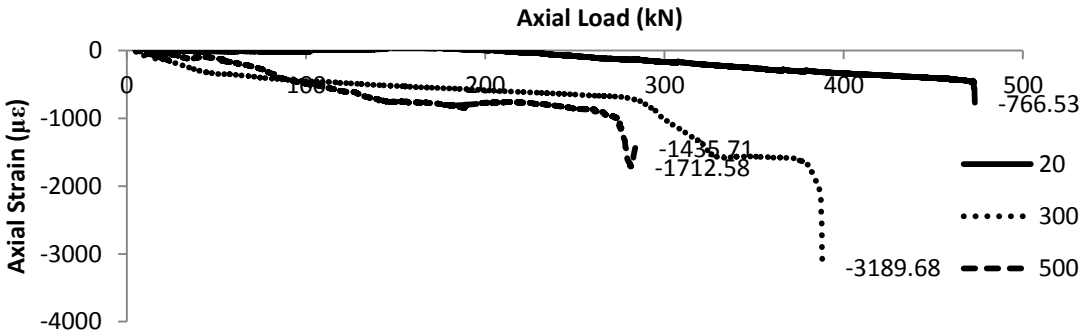

ECC

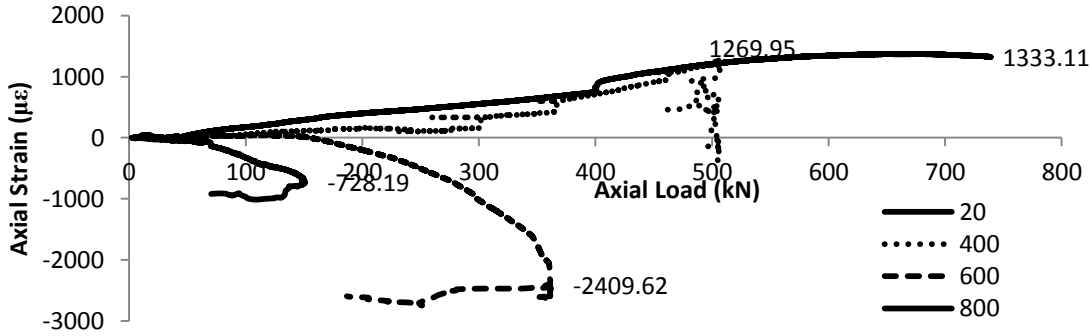

UHPC

Figure 5.23- Axial load-strain behaviour for SCC/ECC/UHPC double skin composite walls exposed to elevated temperatures (°C) at the top

Table 5.3-Strain data for double skin composite walls at elevated temperatures

Temperature	Strain at Failure (Middle)		Strain at Failure (Top)		Y.S.
(°C)	(μ strain)	(% of Y.S.)	(μ strain)	(% of Y.S.)	(μ strain)
Control SCC	324	11	843	29	2860
Control ECC	838	29	767	27	2860
Control UHPC	771	27			2860
300 ECC	1914	93	3190	156	2051*
400 SCC	1326	68	1318	68	1950
400 ECC	2063	106	-	-	1950
400 UHPC	1363	70			1950
500 ECC	5388	309	1713	98	1741*
600 SCC	1564	102	772	50	1540
600 UHPC	2668	173	2410	156	1540
800 SCC	1914	111	421	24	1727
800 UHPC	6389	370	728	42	1727

Y.S.- the yield strain of the steel sheeting, *- These values of yield strain were computed by interpolation of yield strain values obtain from experimentation.

5.3 Chapter Conclusion

Experimental results on the axial load behaviour of double skin composite walls (DSCWs) after exposure to elevated temperatures of up to 800^{o}C are presented and discussed. The effect of elevated temperatures on the failure modes, strength, stiffness, ductility and stress development of DSCWs composed of SCC, ECC, and UHPC is described.

For all SCC/ECC/UHPC DSCWs, failure due to global buckling was not observed in and around the middle of the wall as was the case for steel sheeting walls (SSWs). Instead the buckling was localised to the region between the first and second line of bolts (served as sheet-concrete connectors) and such localized buckling occurred just before or simultaneously with the crushing of the concrete in the same region. The major failure occurred due to crushing of the concrete at the top of the wall. It was not possible to remove the steel sheeting. It was reasonable to conclude

that vertical cracking along the troughs developed. The steel confinement allowed the cracked concrete in-fill to carry the load until crushing of concrete at the top occurred at ultimate load. Overall axial strength and stiffness of the SCC/ECC/UHPC DSCWs decreased with the increase of temperatures. Strain development in the walls remained predominantly compressive until failure in heated/non-heated control walls.

CHAPTER 6

Analytical Models for Double Skin Composite Walls Subjected to Elevated Temperatures

6.1 Introduction

In this chapter, an analytical model for post-fire residual axial load capacity of double skin composite walls (DSCWs) subjected to elevated temperatures of up to 800^{o}C is presented in addition to models for its components: steel sheeting walls (SSWs) and profiled concrete walls (PCWs). The analytical models are developed based on experimental results on the post-fire (i) material properties of the steel sheeting and high performance concrete (HPC) (described in Chapter 3), (ii) axial load behaviour of SSWs and PCWs (described in Chapters 4) and (iii) axial load behaviour of DSCWs (described in Chapter 5). The performance of the analytical models is described based on experimental results.

6.2 Analytical Model for Axial Load Capacity of Steel Sheeting Walls (SSWs) subjected to Elevated Temperatures

The development of a model for the post-fire axial load capacity of the SSWs began with the assumption that the walls fabricated for the experimentation would yield first before local/global buckling would occur. This assumption was made due to the use of adequate number of intermediate fasteners (bolts) throughout the wall (to connect the sheets) in order to reduce the effective length of buckling from the entire wall height to the distance between the rows of bolts. It was assumed that spacing of intermediate fasteners would be sufficient to deter global buckling until after yielding of the steel sheet had occurred. Therefore, the model presented in Eq. 2.6 (Chapter 2) was modified by removing the concrete component to derive the axial load capacity of SSWs as presented in Eq. 6.1:

$$N_s = 0.75 f_y \beta A_s \quad \text{[Eq. 6.1]}$$

where N_s is the axial load capacity of the unheated SSWs, f_y is the yield strength of the steel sheeting, ß is the ratio of the buckling stress to yield stress of the wall, and A_s is the cross-sectional area of the profiled steel sheets. The ß can be obtained from Eq. 6.1a (Hossain 2000):

$$\beta = 3.9846(10)^{-0.01(b/T)} \quad \text{[Eq 6.1a]}$$

where T is the thickness of the steel sheeting and b is the smallest flange thickness presented in the profiled steel sheeting (Fig.6.1).

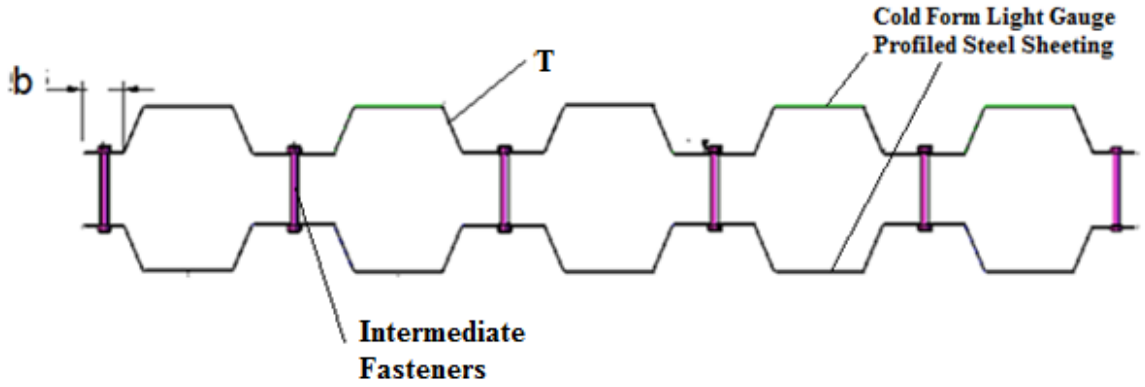

Figure 6.1- Cross-section of profiled steel sheeting wall

The model presented in Eq.6.1 was further modified for heated SSWs by introducing a fire degradation/reduction factor ($ß_s$), to take into account the effect of elevated temperatures on the yield strength of the steel sheeting. The modified equation for the axial load capacity (N_s) of SSWs is presented in Eq.6.2:

$$N_s = 0.75 f_y \beta A_s \beta_s \quad \text{[Eq. 6.2]}$$

The fire degradation/reduction factor for the yield strength of steel sheeting was obtained through experimental investigation conducted on the steel sheeting, as discussed in Chapter 3.

The models fire degradation/reduction factors for the maximum yield strength of the steel sheeting for various temperature (t) ranges are presented in Eqs.6.3a-b:

$ß_s = -0.00012t + 1.0024$ for $20\ °C \leq t \leq 400\ °C$ ($r^2 = 1.0$) [Eq.6.3a]

$ß_s = -2.605(10)^{-6}t^2 + 1.688(10)^{-3}t + 0.696$ for $400°C < t < 800\ °C$ ($r^2 = 1.0$) [Eq.6.3b]

The experimental axial load capacities (N_e) of profiled SSWs at various elevated temperatures were determined from tests. Table 6.1 summarizes experimental and analytical axial load capacities of SSWs at various elevated temperatures.

Table 6.1- Maximum load capacity of steel sheeting walls

Geometric and material properties				
b = 12.5mm	T = 0.61 mm	b/T = 20.49	f_y = 393.57 MPa	
Temperature (°C)	20	400	600	800
ß (Eq.6.1a)	1.0	1.0	1.0	1.0
$ß_s$ (Eq.6.3a-b)	1.00	0.95	0.77	0.38
N_s (Eq.6.2) (kN)	147.59	140.84	113.79	55.98
N_e (kN)	131.03	131.99	115.50	51.59
N_e / N_s	0.89	0.94	1.02	0.92
Ratio buckling to yield Strain	0.89	0.81	0.90	0.86
N_s (corrected) (kN)	131.35	114.08	102.41	48.14
$N_e / N_{s(corrected)}$	1.00	1.16	1.13	1.07

ß the ratio of buckling to yield stress of the wall, $ß_s$ – fire degradation reduction factor for steel, N_s – analytical load capacity of the wall, N_e – experimental load capacity of the wall

The fire degradation/reduction factors were calculated using Eq.6.3a-b and are shown in Table 6.1. The analytical values for axial load capacity (N_s) were calculated using Eq.6.2 and were compared to the experimental axial load capacity (N_e) from Chapter 4 as the ratio of experimental to analytical load (N_e/N_s). This ratio shows that the experimental values were less than the analytical values, where the model somewhat over predicted the load capacity (Table

6.1). It is found from the review of the load-strain behaviour of these walls, as shown in Table 6.2, that none of the walls tested at each temperature reached yielding of steel, as was assumed. Therefore in order to check the analytical model prediction against the experimental results, the yield strength of the steel sheeting in the model was reduced by a factor equal to the percentage of yield strain (Y.S.) observed in the experimental walls at each temperature.

Table 6.2- Strain data for profiled steel sheeting walls at elevated temperatures

Temperature	Strain at Failure (Middle)		Strain at Failure (Top)		Y.S.
(°C)	(μ strain)	(% of Y.S.)	(μ strain)	(% of Y.S.)	(μ strain)
Control	2550	89	1662	58	2860
400	1577	81	1101	56	1950
600	1387	90	1099	71	1540
800	1486	86	642	37	1727

Y.S. – the yield strain of the steel sheeting

The maximum buckling effective length of the sheet in the wall was 140 mm, located above and below the middle line of bolts. This is the location at which buckling failure had occurred in the walls. Buckling stress of steel sheeting was around 88 percent of the yield strain (Y.S) (Table 6.2). It was observed that by reducing the yield strength by a factor (ratio of buckling to yield strength), the model safely predicted the maximum load capacity of SSWs at each temperature ($N_e/N_{s\text{-}corercted}$ >1.0) as shown in Table 6.1. Therefore, the analytical model (Eq. 6.2) can still be used to predict the maximum load capacity of SSWs.

6.3 Analytical Model for Axial Load Capacity of Profiled Concrete Walls (PCWs) Subjected to Elevated Temperatures

The model for the post-fire axial load capacity of the profiled concrete walls (PCWs) was developed by modifying Eq. 2.6 (removing the steel sheeting contribution) and presented as Eq. 6.4:

$$N_C = 0.63 f_c' a A_c \quad \text{[Eq. 6.4]}$$

where N_c is the axial load capacity of the PCWs, f'_c is the compressive cylinder strength of the different concrete types, A_c is the cross-sectional area of the wall and α is a reduction factor to take into account the extent of void created by the profiling on the compressed edge of the wall determined as per Eq.6.4a (Hossain 2000):

$$\alpha = 1 - ((D * P) - A_{cp})/2A_{cp} \quad \text{[Eq 6.4a]}$$

where D is the overall thickness of the wall, P is the pitch of the profiles in the wall and A_{cp} is the cross-section area of the concrete in one pitch of the wall (Fig.6.2).

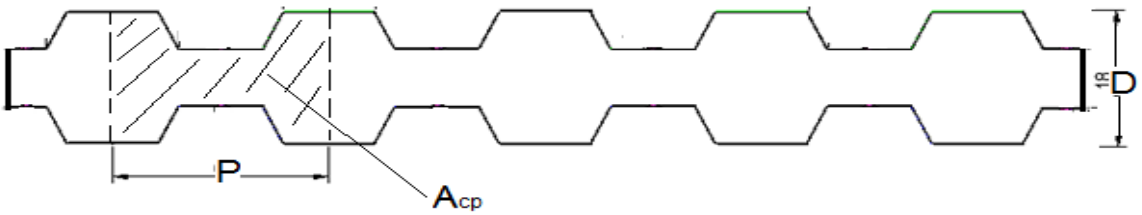

Figure 6.2- Cross-section of in-fill concrete

The model presented in Eq.6.4 was further modified to Eq.6.5 by introducing a softening reduction factor due to the fire degradation of the concrete ($ß_{cs}$) into the existing model. This factor takes into account the reduction of SCC/ECC compressive strength after exposure to elevated temperatures due to softening of the concrete, in which the stresses observed at cracking (when concrete reaches maximum compressive strain) is less than the compressive strength of the concrete. The fire softening/reduction factors ($ß_{cs}$) for of SCC and ECC as a function of temperature (t) are presented in Eqs, 6.6a and 6.6b, respectively.

$$N_C = 0.63 f_c' a A_c \beta_{cs} \quad \text{[Eq. 6.5]}$$

β_{cs} = -0.000000102t^2 - 0.00111t + 1.03 for 20 °C ≤ t ≤ 800 °C (r^2 = 0.98) [Eq.6.6a]

β_{cs}= -0.00000062t^2 - 0.000316t + 1.01 for 20 °C ≤ t ≤ 500 °C (r^2 = 1.00) [Eq.6.6b]

The experimental (N_e) and analytical (N_c) axial load capacities of the PCWs subjected to various elevated temperatures are compared in Table 6.3. It was calculated based on the dimensions of the PCWs, that there is a reduction of 23% in strength due to the extent of void created by the profiling in the wall, corresponding to a α value of 0.77, as shown in Table 6.3.

Table 6.3- Maximum load capacity of profiled concrete walls

Geometric and material properties											
D = 47.2 mm P = 64 mm A_{cp} = 2076 mm^2											
SCC: f'_c = 61.5 MPa ECC: f'_c = 60.3 MPa UHPC: f'_c = 119.6 MPa											
	SCC				ECC				UHPC		
Temp. (°C)	20	400	600	800	20	300	400	500	20	400	600
α	0.77	0.77	0.77	0.77	0.77	0.77	0.77	0.77	0.77	0.77	0.77
$ß_{cs}$	1.00	0.57	0.33	0.08	1.00	0.86	0.78	0.70	1.00*	**	**
N_c (kN)	310	176	101	24	304	261	240	197.	602	**	**
N_e (kN)	476	205	104	-	330	-	230	192	832	**	**
N_e / N_c	1.54	1.16	1.03	-	1.09	-	0.95	0.97	1.38	**	**

α - the reduction factor due to profiled concrete void (Eq.6.4a), $ß_{cs}$ – softening reduction factor for concrete (Eq.6.6a-b), N_c – analytical load capacity of the wall (Eq.6.5), N_e – experimental load capacity of the wall, *- no equation derived for UHPC, but at control temperature this factor is equal to 1.00, **- no values available due to failure of wall during heating

The fire degradation/reduction factors calculated using Eq.6.6a-b and are shown in Table 6.3. The analytical values for axial load capacity (N_s) were calculated using Eq.6.5 and were compared to the experimental axial load capacity (N_e) from Chapter 4 as the ratio of experimental to analytical load (N_e/N_s). This ratio showed that the analytical model predicted the axial load capacity of the wall reasonably well and is safe. It was discovered after a review of the load-strain behaviour of these walls, as shown in Table 6.4, that all of the walls tested at ambient temperature reached full compressive load capacity of the wall. The walls that were heated did not reach full compressive load capacity and therefore ,the maximum compressive strain observed in these heated walls was less than the compressive strain at maximum load of each type of concrete (S.M.L.). This was caused by softening of the concrete due to fire degradation,

which is taken into account when using the softening reduction factors due to the fire degradation of each type of concrete ($ß_{cs}$).

Table 6.4-Strain data for profiled concrete walls at elevated temperatures

Temperature	Strain at Failure (Middle)		Strain at Failure (Top)		M.C.S.
(°C)	(μ strain)	(% of M.C.S.)	(μ strain)	(% of M.C.S.)	(μ strain)
SCC Control	975.21	54	1782.87	98	1820
SCC 400	1096.57	60	531.55	29	1820
SCC 600	1350.51	74	-	-	1820
ECC Control	1000.11	36	2696.28	97	2779
ECC 400	2395.73	86	1493.51	54	2779
ECC 500	1706.87	61	988.54	36	2779
UHPC 20	2867.47	108	2765.9	104	2655

M.C.S.- the maximum compressive strain of the concrete

6.4 Analytical Model for Axial Load Capacity of Double Skin Composite Walls Subjected to Elevated Temperatures

The analytical model (presented as Eq.6.7) for the post-fire axial load capacity of the DSCWs (N_w) is developed based on Eq.2.6 by introducing a fire degradation/reduction factor ($ß_{s,}$) for steel and each type of concrete ($ß_c$) to take into account the effect of exposure to elevated temperatures on the steel yield strength and concrete maximum compressive strength. These reduction factors for the steel sheeting and each type of concrete were obtained through experimental investigation as discussed in Chapter 3. The fire degradation/reduction factors for the steel sheeting is presented in Eqs.6.3a-b, and the fire degradation/reduction factors for all three types of concrete are presented in Eqs.6.8a-c.

$$N_w = 0.75 f_y ß A_s \beta_s + 0.63 f_c' \alpha A_c \beta_c \quad \text{[Eq. 6.7]}$$

where N_w is the axial load capacity of the DSCWs, f_y is the yield strength of the steel sheeting, f'_c is the maximum compressive cylinder strength of the different concrete types, α is a reduction factor to take into account the extent of void created by the profiling on the compressed edge of the wall, as shown in Eq.6.4a, ß is the ratio of buckling to yield stress of the steel sheet, as shown in Eq.6.1a, and A_s, A_c are the cross-sectional area of the wall steel sheeting and concrete core, respectively.

SCC

$ß_c = -0.0000012t^2 + 0.000196t + 1.002 \leq 1.00$ for 20 °C $\leq t \leq$ 800 °C ($r^2 = 0.99$) [Eq. 6.8a]

ECC

$ß_c = -0.00000206t^2 + 0.000525t + 0.99 \leq 1.00$ for 20 °C $\leq t \leq$ 500 °C ($r^2 = 0.99$) [Eq. 6.8b]

UHPC

$ß_c = -0.000000963t^2 - 0.0002581t + 0.996$ for 20 °C $\leq t \leq$ 800 °C ($r^2 = 0.99$) [Eq. 6.8c]

The fire degradation/reduction factors for both steel sheeting and each concrete type were calculated using Eq.6.3a-b and Eq.6.8 a-c., respectively, which are also presented in Table 6.6.

The analytical values for axial load capacity (N_s) were calculated using Eq.6.7 and were compared to the experimental axial load capacity (N_e) from Chapter 5 as the ratio of experimental to analytical load (N_e/N_s). This ratio was calculated for comparison.

Generally at elevated temperatures, Eq. 6.7 over predicts the axial load capacity of the walls and does not accurately model the reduction in axial load capacity. The reason for this difference is that the model does not take into account the reduction of load as a result of decrease in interaction between concrete core and steel sheets at elevated temperatures. Therefore, using the ratio of the experimental to analytical load termed as interaction reduction factor ($ß_i$), the model in Eq.6.7 is modified. This new model with a further reduction of 10% (for a margin safety and imperfections in the wall) is presented in Eq.6.9.

The interaction reduction factors for the double skin composite wall calculated using Eq.6.10a-c are presented in Table 6.5. Table 6.5 also compares modified analytical (N_{wm}) and experimental (N_e) axial load capacity of DSCWs at various elevated temperatures. The ratio of modified analytical and experimental loads (N_e/N_{wm}) was greater than 1.0 (ranging between 1.03 and 1.20) which suggests that Eq. 6.9 can accurately and safely predict the post-fire residual axial load capacity of DSCWs at elevated temperatures and can be used as a guideline for future design consideration.

Table 6.5- Axial load capacity of double skin composite walls

	SCC				ECC				UHPC			
Temp. °C)	20	400	600	800	20	300	400	500	20	400	600	800
ß	1.0	1.0	1.0	1.0	1.0	1.0	1.0	1.0	1.0	1.0	1.0	1.0
α	0.77	0.77	0.77	0.77	0.77	0.77	0.77	0.77	0.77	0.77	0.77	0.77
$ß_s$	1.00	0.95	0.77	0.38	1.00	0.97	0.95	0.89	1.00	0.95	0.77	0.38
$ß_c$	1.00	0.89	0.68	0.38	1.00	0.96	0.87	0.74	1.00	0.74	0.49	0.17
N_w (kN)	457	415	325	175	451	435	407	340	749	585	411	160
N_e (kN)	453	376	259	89	473	388	301	284	745	505	362	151
N_e / N_w	0.99	0.91	0.80	0.51	1.05	0.89	0.74	0.84	0.99	0.86	0.88	0.94
$ß_i$	1.00	0.93	0.77	0.52	1.00	0.86	0.79	0.72	1.00	0.93	0.90	0.87
N_{wm} (kN)	411	348	226	82	406	335	288	230	674	492	334	126
N_e / N_{wm}	1.10	1.08	1.15	1.09	1.17	1.16	1.05	1.23	1.10	1.03	1.08	1.20

α - reduction factor due to profiled concrete void (Eq.6.4a), ß - the ratio of buckling to yield stress of steel (Eq.6.1a), $ß_s$ – fire degradation reduction factor for steel (Eq.6.3a-b), $ß_c$ – fire degradation reduction factor for concrete (Eq.6.8a-c), $ß_i$ – interaction reduction factor for wall (Eq.6.10a-c), N_w – analytical load capacity of the wall (Eq. 6.7), N_e – experimental load capacity of the wall, N_{wm} – modified analytical load capacity of the wall (Eq. 6.9).

$$N_{wm} = \beta_i\left[0.675 f_y b A_s \beta_s + 0.567 f_c^{'} a A_c \beta_c\right] \quad \text{[Eq. 6.9]}$$

SCC

$\beta_i = -1.104(10^{-6})t^2 + 2.959(10^{-4})t + 0.991 < 1.00$ for 20°C < t < 800°C ($r^2 = 0.99$) [Eq. 6.10a]

ECC

$\beta_i = -3.098(10^{-7})t^2 - 4.304(10^{-4})t + 1.013$ for 20°C < t < 500°C ($r^2 = 0.91$) [Eq. 6.10b]

UHPC

$\beta_i = -1.55(10^{-4})t + 0.996$ for 20°C < t < 800°C ($r^2 = 0.96$) [Eq. 6.10c]

6.4.1 Analysis of Modified Analytical Model for Axial Load Capacity

Eq. 6.9 is used to compute axial load (L) capacity of SCC/ECC/UHPC composite wall, concrete core (1st term of the Eq.6.9) and steel sheeting (2nd term of the Eq.6.9) and presented as function time (t) in Fig.6.3. Eq. 6.9 is found to closely predict the reduction in axial load capacity with temperature compared to experimental values (Fig.6.3).

The sheet-concrete interaction in of DSCWS is analyzed for each concrete type at elevated temperatures by comparing the load resisted by the steel sheeting and the concrete core independently to the load resisted by the composite wall by using Fig.6.3.

It was observed in all cases that the reduction in load carried by the steel sheeting did not significantly reduce until after 400°C (Fig.6.3). This result conforms with experiments conducted on both the steel sheeting coupon samples and the profiled SSWs which produced very little difference in yield strength and maximum load capacity, respectively, when exposed to temperatures below 400°C. The effect of reduction in the load carried by the concrete core was observed in all cases to be the significant factor in the overall reduction of the composite wall load capacity, especially in the region between ambient temperature and 400°C. This is evident in Fig.6.3 where the trend of the reduction in load capacity of the composite wall is similar to the trend of concrete core.

The rate of load decrease carried by the double skin composite wall for each concrete type was analysed by taking the first derivative (dL/dt) of the load (L)-time (t) curve presented in Fig.6.3. The rate of load decrease, is found to increase proportionally with the increase of temperature (Table 6.6 and Fig. 6.4). This is expected as temperature increases there is degradation in both the steel sheeting and in-fill concrete and a reduction in interaction between the two. This general

trend of strength/interaction degradation is found similar, regardless of concrete type. UHPC walls is found to experience the highest rate of load decrease, followed by ECC and SCC as shown in Fig.6.3 and Table 6.6.

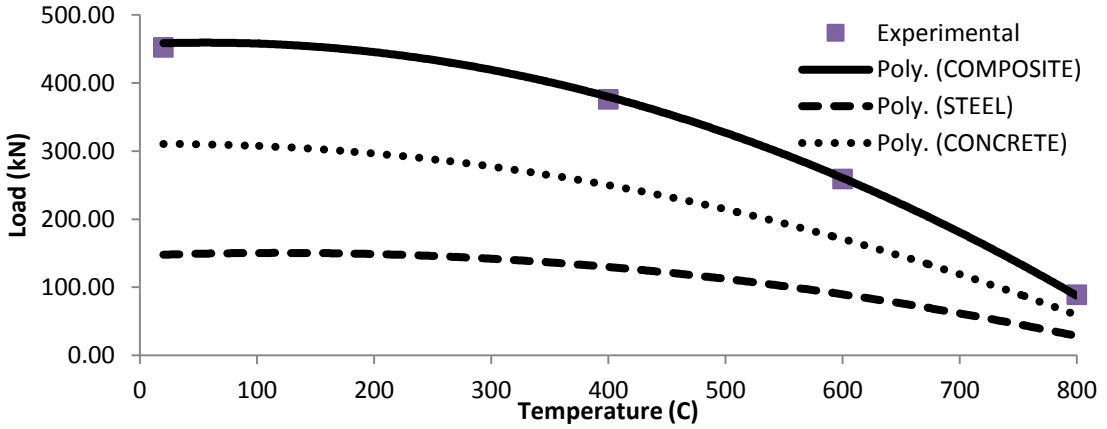

SCC

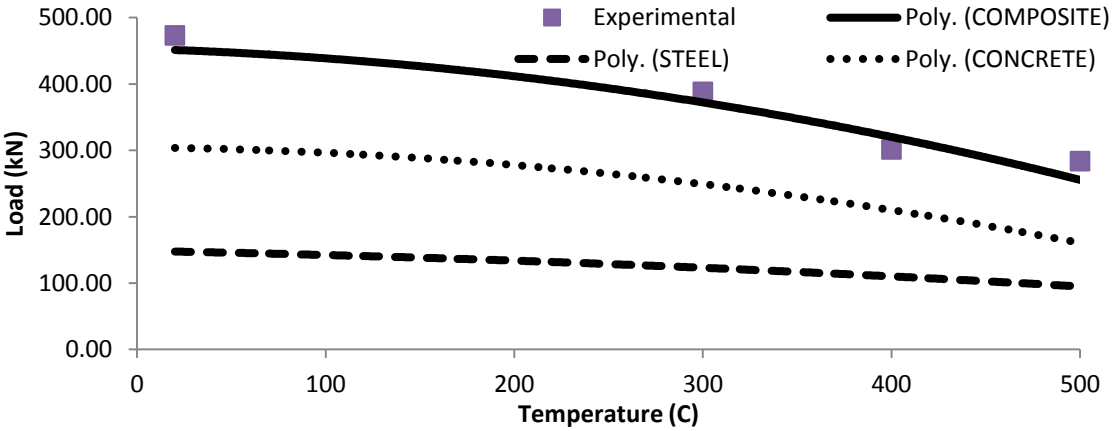

ECC

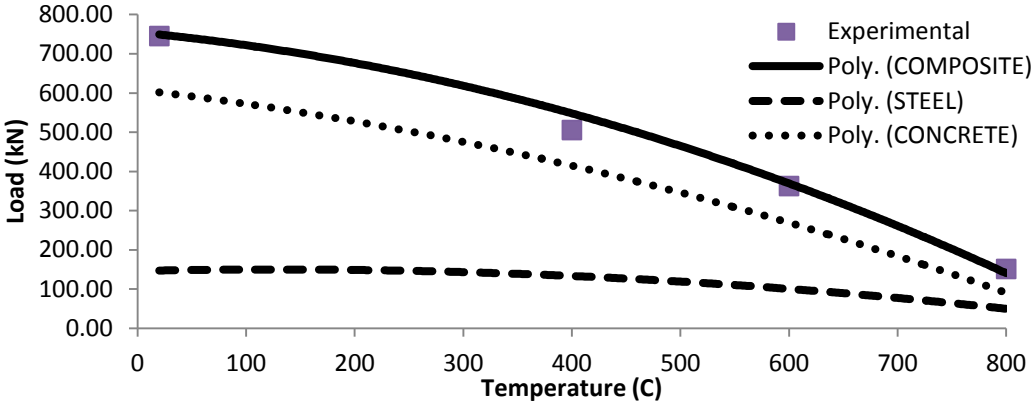

UHPC

Figure 6.3- Load interaction of double skin composite walls at elevated temperatures

The second derivative of load with respect to temperature was taken (d^2L/dt^2) for each concrete type to determine the effect of elevated temperatures on the change in the rate of load decrease (second rate of load decrease). It was observed that the second rate of load decrease for the composite wall was similar in all cases with an average value of 0.0013 kN/ °C^2. This same behaviour was observed in the steel sheeting and concrete in-fill with average values of 0.0004 kN/ °C^2 and 0.0009 kN/ °C^2, respectively. As expected, the second rate of load decrease is affected more by the decrease in concrete load capacity which was 70% of the double skin composite wall load capacity compared to 30% of steel sheeting. This explains why in every case the failure of the double skin composite wall began with failure in the in-fill concrete, followed by failure in the steel sheeting. This second rate of load decrease is also found to be the same regardless of the concrete type. Therefore, the type of concrete has no effect on the second rate of load decrease for the steel sheeting, concrete core, and the composite wall. This rate is based on the structural failure of the double skin composite wall.

Table 6.6- The rate of load decrease of double skin composite walls at elevated temperatures

Temperature (°C)	20	400	600	800
SCC (kN/°C)	0	-0.4846	-0.7646	-1.0446
UHPC (kN/°C)	-0.2896	-0.7456	-0.9856	-1.2256
Temperature	20	300	400	500
ECC (kN/°C)	-0.1057	-0.4417	-0.5617	-0.6817

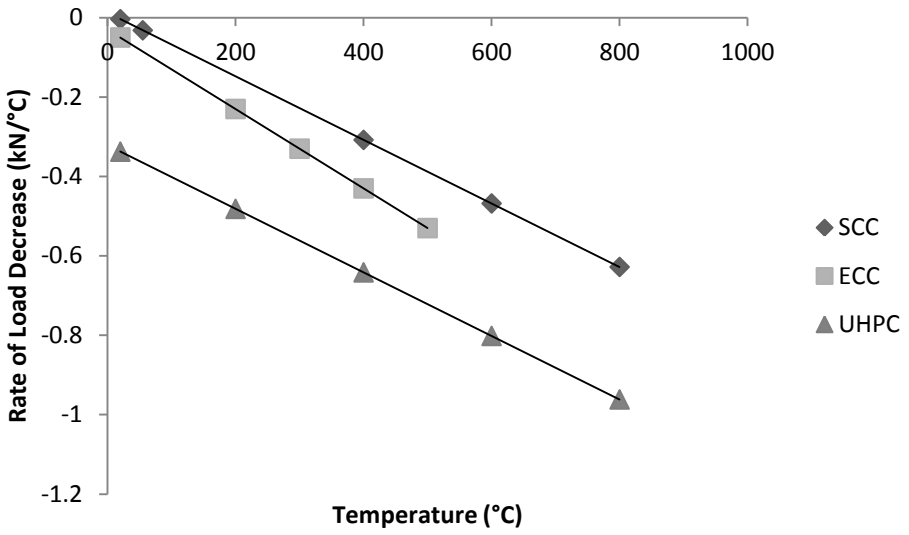

Figure 6.4- The rate of load decrease of double skin composite walls at elevated temperatures

6.5 Chapter Conclusion

In this chapter, analytical models for post-fire residual axial load capacities of SSWs, PCWs, and DSCWs subjected to elevated temperatures of up to 800°C are presented. The performance of these models are validated through experimental results. The models take into account strength degradation or softening of steel and concrete as well as sheet-concrete interaction through incorporating various temperature dependent strength reduction/softening factors (for steel and concrete) and interaction reduction factors.

Models are presented for the SSW and the PCW to predict the post-fire residual axial load capacity at elevated temperatures. It was found that the model accurately predicted the axial load capacity for the SSW, when compared to experimental results, once the steel yield capacity is reduced by the axial strain observed in experiments to take into account the buckling of the steel sheet. Otherwise the model overestimated slightly due to the average buckling load being 88 percent of the yield load. Therefore, further research is required on determining the effect of the buckling effective length (by varying the distance between the intermediate fasteners) on the ratio of buckling load to the yield load at failure for these types of walls.

It was found that the model for the PCW accurately predicted the post-fire residual axial load capacity compared to experimental results. At ambient temperature, all walls reached full compressive axial load capacity of the wall.

A model was presented for the DSCWs to predict the post-fire residual axial load capacity of the wall subjected to elevated temperatures. The model introduces a fire degradation/reduction factor to the yield strength of the steel sheeting, a softening reduction factor to the compressive strength of the concrete core and a steel sheet-concrete interaction reduction factor to take into account interaction degradation. The model is found to predict the axial load capacity of the DSCWs with good degree of accuracy.

CHAPTER 7

Conclusions and Recommendations

7. 1 Conclusions

This research investigated analytically and experimentally the post-fire behaviour of double skin composite walls (DSCWs) comprising of profiled steel sheeting with an infill of concrete and its components: steel sheeting walls (SSWs) and profiled concrete walls (PCWs) exposed to steady state elevated temperatures of up to 800^{o}C and for a duration of up to 2 hours. In addition, the post-fire material properties of cold formed light-gauge profiled steel sheeting and three different types of high performance concrete (HPC) infill namely Self-Consolidating Concrete (SCC), Engineered Cementitious Composites (ECC), and Ultra High Performance Concrete (UHPC) exposed to elevated temperatures. The post-fire axial load behaviour of DSCWs, SSWs and PCWs were described based on axial load-deformation response, axial strength, initial stiffness, post-peak ductility, stress-strain characteristics, concrete cracking, steel sheet buckling, steel sheet-concrete interaction and overall failure modes. Analytical models were developed to predict residual strength and modulus of elasticity of steel sheet and HPCs subjected to elevated temperatures. Finally, analytical models for residual strength of DSCWS, SSWs and PCWs at various elevated temperatures are developed and performance validated through experimental results. The conclusions drawn from this research are summarized in the following sections.

7.1.1 Profiled Steel Sheeting and HPC Material

- The cold formed light-gauge profiled steel sheeting used during the experimentation performed better than the nominal steel illustrated in Eurocode 4 (2005) and previous research studies in terms residual yield strength (f_y); and modulus of elasticity (E_s). At 800°C, the residual yield strength of profiled steel sheet was reduced to 38% (compared to about 10% of nominal steel as per Eurocode) and the residual modulus of elasticity

was reduced to 84% (compared to about 10% of nominal steel as per Eurocode) of ambient temperature properties.

- Both SCC and ECC performed better than the normal strength concrete (NSC) described in Eurocode 4 (2005). At 800°C, the compressive strength of SCC was reduced to 41%, and at 500°C, ECC strength was reduced to 74% of the compressive strength at ambient temperature (20^{o}C). UHPC compressive strength was reduced to 18% at 400^{o}C. UHPC's tendency towards explosive spalling at elevated temperatures goes against the use of this type of concrete in fire conditions. Overall, the reduction in compressive strength was the same for both SCC and ECC up to 400°C, and the reduction in modulus of elasticity was lower in ECC compared to SCC.
- The equations proposed for residual yield strength and modulus of elasticity of cold form light-gauge profiled steel sheeting as well as for residual compressive strength and modulus of elasticity of SCC/ECC/UHPC as a function of temperature showed good performance and were utilized to develop analytical models for residual axial load capacity (strength) of axial strength of SSWs, PCWs and DSCWs.

7.1.2 Steel Sheeting Walls (SSWs)

- The failure of all un-heated and heated SSWs under axial loading was due to global buckling and steel strain development did not show any yielding. The greatest reduction in axial load capacity was observed between 600°C and 800°C with a reduction of 61% at 800°C compared to un-heated walls.
- In general, axial load capacity and initial stiffness decreased with the increase of temperature. The greatest reduction in initial stiffness was observed between 400°C and 800°C with a reduction of 88% at 800°C. The greatest increase in post-peak ductility was observed between 600°C and 800°C – up to 13.85 times higher than that at ambient temperature.

7.1.3 Profiled Concrete Walls (PCWs)

- The failure for all un-heated and heated SCC/ECC PCWs under post-heat axial load was due to the formation of vertical cracking in the profile troughs followed by concrete crushing at the top. UHPC walls failed only due to crushing of concrete at the top.
- In general, axial strength and initial stiffness decreased with the increase of temperature for all PCWs. With respect to axial load capacity, ECC walls performed better than those walls composed of SCC, with a reduction of 30% at 600°C and 42% at 500°C, respectively. The reduction in initial stiffness of the ECC walls was less than that observed in walls composed of SCC, 33% at 500°C and 92% at 600°C, respectively.
- The greatest increase in post-peak ductility was observed in SCC which had a post-peak ductility at 400°C around 36 times the ductility at ambient temperature. Overall, the reduction in axial load capacity and initial stiffness is less in ECC than in SCC, therefore, ECC is more suitable concrete for profiled concrete walls.
- Strain results indicated that all the walls reached maximum compressive strength/strain of the concrete at ambient temperatures, but failed before this strength at elevated temperatures due to the softening of the concrete. The UHPC walls suffered extensive damage at temperatures above 400°C and showed the highest axial strength and stiffness degradation.

7.1.4 Double Skin Composite Walls (DSCWs)

- The failure for all SCC/ECC/UHPC DSCWs (un-heated and heated) under axial loading was due to crushing of concrete and local buckling of the steel sheeting at the top. With respect to axial load capacity, both SCC and ECC walls performed better than those walls composed of UHPC.
- In general, residual axial strength and initial stiffness of DSCWs decreased with the increase of temperature. The axial load capacity of the DSCWs composed of SCC, ECC and UHPC was reduced by 82% (at 800°C), 40% (at 500°C) and 80% (at 800°C), respectively. The reduction in residual initial stiffness of the ECC walls was less than

that observed in SCC/UHPC walls. At 800°C, both UHPC and SCC DSCWs had almost the same reduction in initial stiffness, 91% and 93%, respectively.

- The post-peak ductility was observed to be the highest in SCC, followed by UHPC and ECC. The ECC walls developed higher strain than the SCC/UHPC walls, but none of the walls reached yield strain in the steel sheeting.

7.1.5 Analytical Models

- Analytical models are proposed for the post-fire residual axial load capacity of SSWs, PCWs and DSCWs as a function of temperature by incorporating various temperature dependent strength reduction/softening factors (for steel and concrete) and steel sheet-concrete interaction reduction factor. The empirical equations for determining such factors are provided based on experimental results.
    - The analytical models for SSWs and PCWs accurately predicted the post-fire residual axial load capacities compared with experimental results.
    - The analytical model for the double skin composite walls (DSCWs) accurately predicted the post-fire residual axial strength with the ratio of analytical to experimental values ranging between 1.03 and 1.20. Analytical model may safely be used for design purposes to predict the residual axial load capacity of DSCWs at elevated temperatures. However, it should be noted that the analytical models are developed based on small-scale tests and their performance needs to be validated through full-scale tests on DSCWs, SSWs, and PCWs.

7.1.6 General

Double skin composite walls (DSCWs) have shown great potential to be used as axial and lateral load resisting elements in building. Current research has contributed to the better understanding of the degradation of material properties of cold formed profiled steel sheeting and HPCs subjected to elevated temperatures. The results of this research on fire resistance/durability of DSCWs made of HPCs will aid in the future design of external fire protection measures when such walls are used in buildings. The proposed models will be useful for post-fire strength

prediction of DSCWs in which fire proofing/protection measures have been compromised. The proposed models can also be used with post-fire field investigation to assess residual strength and extent of damage and hence, to determine the appropriate rehabilitation measures for DSCWs.

7.2 Recommendations for Further Research

The following recommendations are made:

- Since this research focused on the behaviour of DSCWs after subjected to elevated temperatures, further research should be conducted by simultaneously heating and loading the walls.
- Research should be conducted on the in-plane monotonic and cyclic shear behaviour of DSCWs exposed to elevated temperatures.
- Investigation should be conducted on the application of fire protection measures for the DSCWs. This should include determining the appropriate fire proofing material and thickness required to maintain a fire rating of at least two to four hours.
- Modeling of the behaviour of DSCWs exposed to elevated temperatures using finite element (FE) programs can be very useful in validating the results of current research studies for post-fire behaviour, as well as performance during fire loading (not investigated in this research). Also development of finite element models to simulate fire resistance of DSCWs will allow further parametric studies to study the effect of the geometric and steel sheet-concrete fastener characteristics on the post-fire structural behaviour.
- Currently guidelines for fire resistance/fire protection of DSCWs are not available and future research should focus in that direction.

REFERNCES

ACI 318 (2011), "Building Code Requirements for Structural Concrete and Commentary", Farmington Hills, Missouri, U.S.

ASTM A820 (2011), "Standard Specification for Steel Fibers for Fiber-Reinforced Concrete", Annual Book of ASTM Standards, West Conshohocken, Pennsylvania, U.S.

ASTM C39 (2012), "Standard Test Method for Compressive Strength of Cylindrical Concrete Specimens", Annual Book of ASTM Standards, West Conshohocken, Pennsylvania, U.S.

ASTM C192 (2007), "Standard Practice for Making and Curing Concrete Test Specimens in the Laboratory", Annual Book of ASTM Standards, West Conshohocken, Pennsylvania, U.S.

ASTM C494 (2011), "Standard Specification for Chemical Admixtures for Concrete", Annual Book of ASTM Standards, West Conshohocken, Pennsylvania, U.S.

ASTM C1116 (2010), "Standard Specification for Fiber-Reinforced Concrete", Annual Book of ASTM Standards, West Conshohocken, Pennsylvania, U.S.

ASTM E8 (2011), "Standard Test Methods for Tension Testing of Metallic Materials", Annual Book of ASTM Standards, West Conshohocken, Pennsylvania, U.S.

ASTM E119 (2012), "Standard Test Methods for Fire Tests of Building Construction and Materials", Annual Book of ASTM Standards, West Conshohocken, Pennsylvania, U.S.

Ametrano, D. (2010), "Development length of GFRP bars in ultra high strength concrete", MASc Thesis, Dept. of Civil Engineering, Ryerson University, Jan 2011 (completed).

Annerel, E., Taerwe, L., and Vandevelde, P. (2007), "Assessment of temperature increase and residual strength of SCC after fire exposure", *5th International RILEM Symposium on SCC*, RILEM Publications S.A.R.L., Ghent, Belgium, September 5-7 2007, 715–720.

Bandula Heva, D. (2009), "Behaviour and design of cold-formed steel compression members at elevated temperatures", *PhD thesis, Queensland University of Technology*, Brisbane, Australia.

Bastami, M., Chaboki-Khiabani, A., Baghbadrani, M., and Kordi, M. (2011), "Performance of high strength concretes at elevated temperatures", *Scientia Iranica* , (18) 1028-1036.

Behnood, A., and Ghandehari, M. (2009), “Comparison of compressive and splitting tensile strength of high-strength concrete with and without polypropylene fibers heated to high temperatures”, *Fire Safety Journal*, 44(8) 1015–1022.

Behnood, A., and Ziari, H. (2008), “Effects of silica fume addition and water to cement ratio on the properties of high-strength concrete after exposure to high temperatures”, *Cement and Concrete Composites*, 30(2) 106–112.

Bouzoubaâ, N. and Lachemi, M. (2001), “Self-Compacting Concrete Incorporating High Volumes of Class F Fly Ash: Preliminary Results”, *Cement and Concrete Research*, 31(3) 413–420.

Bradford, M. A., Wright, H.D. and Uy, B. (1998). “Short and long term behaviour of axially loaded composite walls”, *Proceedings of the Journal of Structures and Buildings, ICE*, 128(1) 26-37.

Çavdar, A. (2012), “A study on the effects of high temperature on mechanical properties of fiber reinforced cementitious composites”, *Composites: Part B*, 43(5) 2452-2463.

Chan, S. Y., Luo, X., and Sun, W. (2000a), “Effect of high temperature and cooling regimes on the compressive strength and pore properties of high performance concrete”, *Construction and Building Materials*, 14(5) 261-266.

Chan, S.Y., Luo, X., and Sun, W. (2000b), “Compressive strength and pore structure of high-performance concrete after exposure to high temperatures up to 800 degrees”, *Cement and Concrete Research*, 30(2) 247-251.

Chan, S.Y., Peng, G., and Anson, M. (1999a), "Residual strength and pore structure of high-strength concrete and normal-strength concrete after exposure to high temperatures", *Cement and Concrete Composites*, 21(1) 23-27.

Chan, S.Y., Peng, G., and Anson, M. (1999b), "Fire behaviour of high-performance concrete made with silica fume at various moisture contents", *ACI Materails Journal*, 96(3) 405-411.

Chen, B., and Liu, J., (2004), “Residual strength of hybrid-fiber-reinforced high-strength concrete after exposure to high temperatures, *Cement and Concrete Research*, 34(6) 1065–1069.

Chen, J., and Young, B., (2004), "Mechanical properties of cold-formed steel at elevated temperatures", *Proceedings of the 17th International Specialty Conference on Cold-formed Steel Structures*, 437–465, University of Missouri-Rolla, Orlando, Florida, USA, Nov. 4th to 5th.

CSA A23.3 (2004), "Design of Concrete Structures", Toronto, Ontario, Canada.

CSA A3001 (2008), "Cementitious Materials Compendium", Toronto, Ontario, Canada.

El-Dieb, A.S., (2009), "Mechanical, durability and microstructural characteristics of ultra-high-strength self-compacting concrete incorporating steel fibers", *Materials and Design*, 30 (10), 4286–4292.

European Committee for Standardisation (CEN) (2005), "Eurocode 4 — Design of composite steel and concrete structures: Part 1-2: General rules — Structural fire design", BS EN 1994-1-2:2005, Brussels, Belgium.

Fares, H., Noumowe, A., and Remond, S. (2009), "Self-consolidating concrete subjected to high temperature Mechanical and physicochemical properties", *Cement and Concrete Research*, 39(12) 1230–1238.

Fischer, G., and Li, V. C. (2003), "Deformation Behavior of Fiber-Reinforced Polymer Reinforced Engineered Cementitious Composite (ECC) Flexural Members under Reversed Cyclic Loading Conditions", *ACI Structural Jounrnal*, 100(1) 25-35.

Felicetti, R., and Gambarova, P.G. (1998), "Effects of high temperature on the residual compressive strength of high-strength siliceous concretes", *ACI Materials Journal*, 95(4) 395–406.

Grainger, B.N. (1980), "Concrete at High Temperatures", *Central Electricity Research Laboratories*, UK, 1980.

Hammer, T.A., (1995), "High strength concrete phase 3- compressive strength and e-modulus at elevated temperatures", SP 6 Fire Resistance, Report 6.1, *SINTEF Structures and concretes*, STF 70 A95023.

Hayakawa, M.; Matsuoka, Y. and Shindoh, T. (1993), "Development and Application of super Workable Concrete," *Proceeding of an International RILEM Workshop on special concrete: Workability and Mixing*, Scotland, pp.183–190.

Hertz, K.D. (1984), "Heat-induced explosion of dense concretes". Report No.166, *Institute of Building Design*, Technical University of Denmark, Lyngby.

Hertz, K.D. (1992), "Danish investigations on silica fume concretes at elevated temperatures", *ACI Materials Journal*, 89(4) 345–347.

Hossain, K.M.A. (2000), "Axial Load Behaviour of Pierced Profiled Composite Walls," *IPENZ Transactions*, (27) 1 1–7.

Hossain, K.M.A. (1999a), "Fire resistance of Light weight Volcanic pumice concrete", *Proceedings of 24th OWICS Conference, "21st century concrete and structures",* 25-26 August, 1999, Singapore, Vol. XVIII, pp. 201-208 (ISBN 981-04-1540-0).

Hossain, K.M.A. (1999b), "Fire Durability of light weight volcanic pumice concrete with special reference to thin walled filled sections", *Durability of Building Material and Components 8, Canadian Institute for Scientific and Technical Information (CISTI)*, NRC Research Press, NRC No. 42738, Volume 1-4: PP. 149-158, 1999. (ISBN 0-660-17737-4).

Hossain, K.M.A. (2001), "Performance of Volcanic Pumice based Thin Walled Composite Columns" *Proceedings of International Conference on Composite Engineering 8 (ICCE/8),* pp. 367-368, August 5-11, Canary Islands, Spain, 2001

Hossain, K.M.A. (2003a), "Behaviour of volcanic pumice based thin walled composite filled columns under eccentric loading", *Structural Engineering and Mechanics- International Journal*, (16) 1 63-82.

Hossain, K.M.A. (2003b), "Behaviour of Thin walled composite Columns under Axial loading", *Composites – Part B: Engineering- an International Journal*, 34(8) 715-725.

Hossain, K.M.A. (2006), "High strength blended cement concrete incorporating volcanic ash: Performance at high temperatures", Cement and Concrete Composites, 28(6) 535-545.

Hossain, K.M.A. and Lachemi M. (2003a), "Behaviour of steel-concrete composite filled columns under axial and fire loading" *Proceedings Response of structures to extreme loading Conference*, 3-6 August 2003, Toronto, Canada.

Hossain, K.M.A. and Lachemi M. (2003b), "Torsional behaviour of thin walled filled composite elements", *Proceedings of the 10th International conference on composites/nano engineering*, (ICCE 10), July 20-26, 2003, New Orleans, USA.

Hossain, K.M.A., Lachemi M., and Wright, H.D. (2005), "Steel-concrete interaction in double skin profiled composite walls: development of finite element models" 33rd *Annual General Conference of the Canadian Society for Civil Engineering*, Toronto, Ontario, Canada, June 2-4, 2005.

Hossain, K.M.A. and Lachemi M. (2007), "Mix design, strength, durability and fire resistance of lightweight concrete with pumice aggregate", *ACI Materials Journal,* 104(5) 449-457.

Hossain, K.M.A. and Lachemi M. (2010), "Fresh, mechanical, and durability characteristics of self-consolidating concrete incorporating volcanic ash", *ASCE Journal of Materials in Civil Engineering,* 22(7) 651-657.

Hossain, K.M.A., Mak, C., and Ametrano, D. (2012), "GFRP reinforced UHPC composites for sustainable bridge construction", *Canadian Civil Engineer*, Spring (29.1) 2012, 12-15.

Hossain, K. M. A., and Wright, H. D. (1995), "Composite walling with special reference to the stabilization of building frames, *Proceedings of the Nordic Steel Construction Conference,* Malmo, Sweden, 19-21 June 1995, pp. 531-538.

Hossain, K.M.A. and Wright, H.D. (1998a), "Shear Interaction between Sheeting and Concrete in Profiled Composite Construction", *Proceedings of the Australasian Structural Engineering Conference*, Auckland, Vol. 1, pp. 181–188.

Hossain, K.M.A. and Wright, H.D. (1998b), "Performance of Profiled Concrete Shear Panels", *Journal of Structural Engineering, ASCE,* 124(4) 368–381.

Hossain, K.M.A. and Wright, H.D. (2004a), "Behaviour of Composite Walls Under Monotonic and Cyclic Shear Loading", *Structural Engineering and Mechanics,* 17(1) 69–85.

Hossain, K.M.A. and Wright, H.D. (2004b), "Design Aspect of Double Skin Profiled Composite Framed Shear-Walls in Construction and Service Stages", *ACI Structural Journal*, 101(1) 94–102.

Hossain, K.M.A. and Wright, H.D. (2004c), "Experimental and Theoretical Behaviour of Composite Walling Under In-plane Shear", *Journal of Constructional Steel Research,* 60(1) 59–83.

Hossain, K.M.A. and Wright, H.D. (2004d), "Performance of Double Skin Profiled Composite Shear walls – Experiments and Design Equations", *Canadian Journal of Civil Engineering*, 31(2) 204–217.

Hossain, K.M.A. and Wright, H.D. (2004e), "Bending and shear behaviour of double skin profiled composite elements", *Structural Engineering and Mechanics - An International Journal*, 4(2) 113-132.

Kankanamge, N. D., and Mahendran, M. (2011), "Mechanical properties of cold-formed steels at elevated temperatures",*Thin-Walled Structures*, 49(1) 26–44.

Khatib, J. M. (2008), "Performance of self-compacting concrete containing fly ash", *Construction and Building Materials*, 22(9) 1963–1971.

Khayat, K.H. (1999), "Workability, Testing, and Performance of Self-Consolidating Concrete," *ACI Materials Journal*, 96(3) 346–35.

Khayat, K. H., Paultre, P., and Tremblay, S. (2001), "Structural performance and in-place properties of self-consolidating concrete used for casting highly reinforced columns", *ACI Materials Journal*, 98(5) 371–378.

Khoury, G.A. and Anderberg, Y. (2000), ''Concrete spalling review'', *Report Submitted to the Swedish National Road Administration.*

Kodur, V. (1999), "Performance-based fire resistance design of concrete-filled steel columns", *Journal of Constructional Steel Research* , 51(1) 21–36.

Koksal, F., Altun, F., Yigit, I., and Sahin, Y. (2008), "Combined effect of silica fume and steel fiber on the mechanical properties of high strength concretes", *Construction and Building Materials*, 22(8) 1874-1880.

Kolarkar, P. (2006), Structural and fire behaviour of a new steel stud wall system using composite panels. *PhDthesis,Queensland Universit yof Technology*.

Kunieda, M., and Rokugo, K. (2006), "Recent progress on HPFRCC in Japan: Required performance and applications", *Journal of Advances in Concrete Technology*, 4(1) 19–33.

Lachemi, M.; Hossain, K.M.A.; Lambros, V.B.. and Bouzoubaâ, N. (2003), "Development of Cost-Effective Self-Consolidating Concrete Incorporating Fly Ash, Slag Cement, or Viscosity-Modifying Admixtures", *ACI Materials Journal*, 100(5) 419–425.

Lachemi M., Hossain, K.M.A., and Lambros, V.B.(2006a), "Axial load behaviour of self-consolidating concrete-filled steel tube columns in construction and service stages", *ACI Materials Journal,* 103(1) 38-47.

Lachemi M. , Hossain, K.M.A., and Lambros, V.B. (2006b), "Self-consolidating concrete filled steel tube columns – Design equations for confinement and axial strength", *Structural Engineering and Mechanics – An International Journal,* 22(5) 541-562.

Lee, J.H., Mahendran, M., and Makelainen, P., (2003), "Prediction of mechanical properties of light gauge steels at elevated temperatures", *Journal of Constructional Steel Research,* 59(12) 1517–1532.

Lepech, M. D., and Li, V. C. (2008a),"Large-Scale Processing of Engineered Cementitious Composites", *ACI Materials Journal*, 105(4) 358-366.

Lepech, M. D., Li, V. C., Robertson, R. E., and Keoleian, G. A. (2008b), "Design of Green Engineered Cementitious Composites for Improved Sustainability", *ACI Materials Journal*, 105(6) 567-575.

Li, V.C. (1993), "From micromechanics to structural engineering: the design of cementitious composites for civil engineering applications", *Journal of Structural Mechanics and Earthquake Engineering,* 10(2) 37–48.

Li, V. C. (1995), "New construction materials proliferate in Japan", *Civil Engineering (N.Y.),* 65(8) 38–41.

Li, V. C. (1998), "ECC-tailored composites through micromechanical modeling", *Proceedings on the International Symposium on Fiber Reinforced Concrete: Present and the Future*, CSCE, Montreal, 64–97.

Li, V. C. (2003), "On engineered cementitious composites (ECC)–A review of the material and its applications", *Advances in Concrete Technology*, 1(3) 215–230.

Li, V.C. and Kanda, T. (1998), "Engineered cementitious composites for structural applications", ASCE *Journal of Materials in Civil Engineering*, 10(2) 66-69.

Li, V. C., Wang, S., and Wu, C. (2001), "Tensile strain-hardening behavior of PVA-ECC", *ACI Materials Journal*, 98(6) 483–492.

Lu, H., Zhao, X.-L., and Han, L.-H. (2009), "Fire behaviour of high strength self-consolidating concrete filled steel tubular stub columns", *Journal of Constructional Steel Research,* 65(10-11) 1995-2010.

Mak, C. (2011), "Experimental and theoretical investigations of splice length of GFRP bars in UHPC slabs", MASc Thesis, Dept. of Civil Engineering, Ryerson University, Sept. 2011.

Mecozzi, E., and Zhao, B. (2005), "Development of stress–strain relationships of cold-formed lightweight steel at elevated temperatures", *Proceedings of Eurosteel Conference*, C, 5.1-41–5.1-49, Maastricht, 8 –10 June 2005.

Nawy, E.G. (2008), "Concrete Construction Engineering Handbook," 2ed Edition, Taylor and Francis Group, p. 1884.

Neville, A. (2010), "Properties of Concrete" , 4th Edittion, Pearson- Prentice Hill, .London, p. 844

Nishida, A., Yamazaki, N., Inoue, H., Schneider, U., and Diederichs, U. (1995), "Study on the properties of high strength concrete with short polypropylene fibers for spalling resistance", *Proceedings on the International Symposium. on Concrete Under Severe Environment*, Vol. 2, K. Sakai, N. Banthia, and O. E. Gjorv, eds., 1141–1150.

Outinen, J., (1999), "Mechanical Properties of Structural Steels at Elevated Temperatures, *Licentiate Thesis*, Helsinki University of Technology, Finland, 1999.

Ozawa, K., Maekawa, K., Kunishima, H., and Okamura, H. (1989), "Performance of concrete based on the durability design of concrete structures", *Proceedings on the 2nd East-Asia-Pacific Conference on Structural Engineering and Construction*, Vol. 1, Chiang Mai, Thailand, 445–456.

Peng, G.-F., Yang, W.-W., Zhao, J., Liu, Y.-F., Bian, S.-H., and Zhao, L.-H. (2006), "Explosive spalling and residual mechanical properties of fiber-toughened high-performance concrete subjected to high temperatures", *Cement and Concrete Research*, 36(4) 723-727.

Persson, B. (2004), "Fire resistance of self-compacting concrete, SCC", *Materials and Structures*, 7(10) 575–584.

Petersson, O. (1998), "Application of self-compacting concrete for bridge castings", *Swedish Cement and Concrete Research Institute, Stockholm, Sweden.*

Phan, L.T., and Carino, N.J. (2002), "Effects of test conditions and mixture proportions on behaviour of high-strength concrete exposed to high temperatures, *ACI Materials Journal*, 99(1) 54–66.

Poon, C., Azhar, S., Anson, M., and Wong, Y. (2001), "Comparison of the strength and durability performance of normal and high-strength pozzolanic concretes at elevated temperatures", *Cement and Concrete Research*, Volume 31(9) 1291–1300.

Poon, C. S., and Ho, D. W. S. (2004b), "A feasibility study on the utilization of r-FA in SCC", *Cement and Concrete Research*, 34(12) 2337–2339.

Poon, C., Shui, Z., and Lam, L. (2004a), "Compressive behavior of fiber reinforced high-performance concrete subjected to elevated temperatures", *Cement and Concrete Research* , 34(12) 2215–2222.

Rafiei, S., Hossain, K.M.A., and Lachemi, M. (2009), "Behaviour of a New Form of Composite Shear Wall System under In-plane Monotonic and Cyclic Shear Loadings", *CSCE 2009 Annual General Conference*, St. John's, Newfoundland and Labrador , May 27-30, 2009.

Rafiei, S. (2011), "Behaviour of Double Skin Profiled Composite Shear Wall System under In-plane Monotonic, Cyclic and Impact Loadings", *PhD thesis,* Dept. of Civil Engineering, Ryerson University.

Ranawaka, T., and Mahendran, M. (2009a), "Experimental study of the mechanical properties of light gauge cold-formed steels at elevated temperatures", *Fire SafetyJournal*, 44(2) 219–229.

Ranawaka, T., and Mahendran, M. (2009b), "Distortional buckling tests of cold-formed steel compression members at elevated temperatures",*Journal of Constructional Steel Research*, 65(2) 249-259.

Reis, B.C., Neves, I.C., Tadeu, A.J.B., and Rodrigues, C., (2001), "High-temperature compressive strength of steel fiber high-strength concrete", *Journal of Materials in Civil Engineering*, 13(3) 230–234.

Romero, M. L., Moliner, V., Espinos, A., Ibañez, C., and Hospitaler, A. (2011), "Fire behavior of axially loaded slender high strength concrete-filled tubular columns", *Journal of Constructional Steel Research*, 67(12) 1953–1965.

Sahmaran, M. L., Lachemi, M., and Li, V. C. (2010),"Assessing Mechanical Properties and Microstructure of Fire-Damaged Engineered Cementitious Composites", *ACI Materials Journal*, 107(3) 297-304.

Şahmaran, M., Lachemi, M., Hossain, K.M.A., and Li, V.C. (2009), "Influence of aggregate type and size on the ductility and mechanical properties of ECC", *ACI Materials Journal*, 106(3) 308-316.

Şahmaran, M., and Li, V. C. (2009), "Durability properties of micro-cracked ECC containing high volumes fly ash", *Cement and Concrete Research*, 39(11) 1033–1043.

Şahmaran, M., Özbay,O., Yüce, H.E., Lachemi, M., and Li, V.C. (2011), "Effect of Fly Ash and PVA Fiber on Micro-structural Damage and Residual Properties of Engineered Cementitious Composites Exposed to High Temperatures", *Journal of Materials in Civil Engineering*, December 2011 1735-1745.

Sarshar, R., and Khoury, G.A. (1993), "Material and environmental factors influencing the compressive strength of unsealed cement paste and concrete at high temperatures", *Magazine of Concrete Research*, 45(162) 51–61.

Sarvaranta, L., and Mikkola, E. (1994a), "Fibre mortar composites in fire conditions." *Fire and Materials*, 18(1) 45–50.

Sarvaranta, L., and Mikkola, E. (1994b), "Fibre mortar composites under fire conditions: Effects of ageing and moisture content of specimens", *Materials and Structures*, 27(9) 532–538.

Sidey, M.P., and Teague, D.P., (1988), "Elevated temperature data for structural grades of Galvanised steel", *British Steel (Welsh Laboratories) Report*, UK, 1988.

Tai, Y.-S., Pan, H.-H., and Kung, Y.-N. (2011), "Mechanical properties of steel fiber reinforced reactive powder concrete following exposure to high temperature reaching 800 ◦C", *Nuclear Engineering and Design*, 241(7) 2416-2424.

Taormina, A. and Hossain, K.M.A. (2012), "Behaviour of Profiled Composite Walling System under Elevated Temperatures", *Proceedings of the 3rd International Structural Specialty Conference*, CSCE, Edmonton, Alberta, June 6-9, 2012.

Tolentino, E., Lameiras, F.S., Gomes, A.M., Rigo da Silva, C.A., and Vasconcelos, W.L. (2002), "Effects of high temperature on residual performance of Portland cement concrete", *Materials Research*, (5) 301–307 .

Wang, S. and Li, V.C. (2006), "High-early-strength engineered cementitious composites", *ACI Materials Journal*, 103(2) 97-105.

Wang, S., and Li, V. C. (2007), "Engineered Cementitious Composites with High-Volume Fly Ash", *ACI Materials Journal*, 104(3) 233-241.

Wright, H.D. (1998a), "The Axial Load Behaviour of Composite Walling", *Journal Constructional Steel Research*, 45(3) 353–375.

Wright, H.D. (1998b), "Axial and Bending Behaviour of Composite Walls", *Journal of Structural Engineering, ASCE*, 124(7) 758–764.

Wright, H.D.; Evans, H.R. and Gallocher, S.C. (1992), "Composite walling", *Proceedings of an Engineering Foundation Conference on Composite Construction in Steel and Concrete II*, 783–797, Potosi, Missouri, June 14-19, 1992 .

Wright, H. D., Evans, H. R., and Harding, P. W. (1987), "The use of profiled steel sheeting in floor construction", *Journal of Construction Steel Research*, 7(4) 279-295.

Wright, H.D. and Gallocher, S.C. (1995), "The Behaviour of Composite Walling under Construction and Service Loading", *Journal of Constructional Steel Research*, 35(3) 257–273.

Wright, H.D., Hossain, K.M.A., and Gallocher, S.C. (1994), "Composite walls as shear elements in tall structures", *Proceedings of papers presented at ASCE Structures Congress XII*, Atlanta, GA, USA, April 24-28, pp. 140-145.

Wright, H.D. and Hossain, K.M.A. (1997), "In-Plane Shear Behaviour of Profiled Steel Sheeting", *Thin walled Structures*, 29(1–4) 79–100.

Wright, H.D.; Hossain, K.M.A. and Gallocher, S.C. (1994), "Composite Walls as Shear Elements in Tall Structures", *Proceedings of papers the ASCE Structures Congress XII*, 140–145, *Atlanta, Georgia*, April 24-27, 1994.

Yahia, A., Tanimura, M., Shimabukuro, A., and Shimoyama, Y. (1999), "Effect of rheological parameters on self compactability of concrete containing various mineral admixtures", *Proceedings of the First RILEM International Symposium on Self-Compacting Concrete*, Stockholm, Sweden, September, 1999, pp. 523-535.

Yurugi, M. (1998), "Application of self-compacting concrete in Japan", *Proceedings of the 23th OWICS Conference.*, CI-Premier, Singapore, 29–42.